EFFICIENT COMMUNICATION PROTOCOLS FOR UNDERWATER ACOUSTIC SENSOR NETWORKS

A Thesis
Presented to
The Academic Faculty

by

Dario Pompili

In Partial Fulfillment
of the Requirements for the Degree
Doctor of Philosophy in the
School of Electrical and Computer Engineering

Georgia Institute of Technology
August 2007

EFFICIENT COMMUNICATION PROTOCOLS FOR UNDERWATER ACOUSTIC SENSOR NETWORKS

Approved by:

Professor Ian F. Akyildiz, Advisor
School of Electrical and Computer Engineering
Georgia Institute of Technology

Professor William D. Hunt
School of Electrical and Computer Engineering
Georgia Institute of Technology

Professor Faramarz Fekri
School of Electrical and Computer Engineering
Georgia Institute of Technology

Professor Mostafa H. Ammar
College of Computing
Georgia Institute of Technology

Professor Raghupathy Sivakumar
School of Electrical and Computer Engineering
Georgia Institute of Technology

Date Approved: June 5th, 2007

Ad Alessandra

ACKNOWLEDGEMENTS

The author wishes to thank most sincerely Prof. Ian F. Akyildiz for his continuing guidance in the completion of this work, as well as for his valuable support as advisor during the entire Ph.D. program. His mentorship was paramount in providing a well rounded experience, which I will treasure in my career.

To all the academic members of the Electrical and Computer Engineering Department at the Georgia Institute of Technology, I wish to express my deepest gratitude for excellent advice, constructive criticism, helpful and critical reviews throughout the Ph.D. program.

A special thank goes to Drs. Fekri, Sivakumar, Hunt, and Ammar, who kindly agreed to serve in my Ph.D. Defense Committee.

The author is indebt to his friend and colleague Tommaso Melodia for all the valuable work done together during the completion of the Ph.D. program. As well, the author would like to thank all former and current members of the Broadband and Wireless Networking Laboratory for sharing this learning experience.

Last but not least, the author is grateful to the many anonymous reviewers that with their unselfish comments greatly improved the content of the papers from which this thesis has been partly extracted.

TABLE OF CONTENTS

LIST OF TABLES

LIST OF FIGURES

SUMMARY

Underwater sensor networks find applications in oceanographic data collection, pollution monitoring, offshore exploration, disaster prevention, assisted navigation, tactical surveillance, and mine reconnaissance. The enabling technology for these applications is acoustic wireless networking. UnderWater Acoustic Sensor Networks (UW-ASNs) consist of sensors and Autonomous Underwater Vehicles (AUVs) deployed to perform collaborative monitoring tasks. The objective of this research is to explore fundamental key aspects of underwater acoustic communications, propose communication architectures for UW-ASNs, and develop efficient sensor communication protocols tailored for the underwater environment. Specifically, different deployment strategies for UW-ASNs are studied, and statistical deployment analysis for different architectures is provided. Moreover, a model characterizing the underwater acoustic channel utilization efficiency is introduced. The model allows setting the optimal packet size for underwater communications. Two distributed routing algorithms are proposed for delay-insensitive and delay-sensitive applications. The proposed routing solutions allow each node to select its next hop, with the objective of minimizing the energy consumption taking the different application requirements into account. In addition, a resilient routing solution to guarantee survivability of the network to node and link failures in long-term monitoring missions is developed. Moreover, a distributed Medium Access Control (MAC) protocol for UW-ASNs is proposed. It is a transmitter-based code division multiple access scheme that incorporates a novel closed-loop distributed algorithm to set the optimal transmit power and code length. It aims at achieving high network throughput, low channel access delay, and low energy consumption. Finally, an efficient cross-layer communication solution tailored for multimedia traffic (i.e., video and audio streams, still images, and scalar sensor data) is introduced.

CHAPTER I

INTRODUCTION

1.1 Background

Underwater sensor networks are envisioned to enable applications for oceanographic data collection, pollution monitoring, offshore exploration, disaster prevention, seismic monitoring, equipment monitoring, assisted navigation and tactical surveillance applications. Multiple Unmanned or Autonomous Underwater Vehicles (UUVs, AUVs), equipped with underwater sensors, will also find application in exploration of natural undersea resources and gathering of scientific data in collaborative monitoring missions. To make these applications viable, there is a need to enable underwater communications among underwater devices. Underwater sensor nodes and vehicles must possess self-configuration capabilities, i.e., they must be able to coordinate their operation by exchanging configuration, location and movement information, and to relay monitored data to an onshore station.

Wireless underwater acoustic networking is the enabling technology for these applications. UnderWater Acoustic Sensor Networks (UW-ASNs) consist of a variable number of sensors and vehicles that are deployed to perform collaborative monitoring tasks over a given volume of mater. To achieve this objective, sensors and vehicles self-organize in an autonomous network, which can adapt to the characteristics of the ocean environment.

The above described features enable a broad range of applications for underwater acoustic sensor networks:

- **Ocean Sampling Networks**. Networks of sensors and AUVs, such as the Odyssey-class AUVs, can perform synoptic, cooperative adaptive sampling of the 3D coastal ocean environment. Experiments such as the Monterey Bay field experiment demonstrated the advantages of bringing together sophisticated new robotic vehicles with

advanced ocean models to improve the ability to observe and predict the characteristics of the oceanic environment.

- **Environmental Monitoring.** UW-ASN can perform pollution monitoring (chemical, biological, and nuclear). For example, it may be possible to detail the chemical slurry of antibiotics, estrogen-type hormones and insecticides to monitor streams, rivers, lakes, and ocean bays (*water quality in-situ analysis*) [95]. In addition, UW-ASNs can perform ocean current and wind monitoring, and biological monitoring such as tracking of fish or micro-organisms. Also, UW-ASNs can improve weather forecast, detect climate change, and understand and predict the effect of human activities on marine ecosystems. For example, in [97], the design and construction of a simple underwater sensor network is described to detect extreme temperature gradients (thermoclines), which are considered to be a breeding ground for certain marine microorganisms.

- **Undersea Explorations.** Underwater sensor networks can help detecting underwater oilfields or reservoirs, determine routes for laying undersea cables, and assist in exploration for valuable minerals.

- **Disaster Prevention.** Sensor networks that measure seismic activity from remote locations can provide *tsunami* warnings to coastal areas [79], or study the effects of submarine earthquakes (*seaquakes*).

- **Seismic Monitoring.** Frequent seismic monitoring is of great importance in oil extraction from underwater fields to asses field performance. Underwater sensor networks would allow reservoir management approaches.

- **Equipment Monitoring.** Sensor networks would enable remote control and temporary monitoring of expensive equipment immediately after the deployment, to assess deployment failures in the initial operation or to detect problems.

- **Assisted Navigation.** Sensors can be used to identify hazards on the seabed, locate dangerous rocks or shoals in shallow waters, mooring positions, submerged wrecks, and to perform bathymetry profiling.

- **Distributed Tactical Surveillance**. AUVs and fixed underwater sensors can collaboratively monitor areas for *surveillance*, *reconnaissance*, *targeting*, and *intrusion detection* systems. For example, in [16], a 3D underwater sensor network is designed for a tactical surveillance system that is able to detect and classify submarines, Small Delivery Vehicles (SDVs) and divers based on the sensed data from mechanical, radiation, magnetic, and acoustic microsensors. With respect to traditional radar/sonar systems, underwater sensor networks can reach a higher accuracy, and enable detection and classification of low signature targets by also combining measures from different types of sensors.

- **Mine Reconnaissance**. The simultaneous operation of multiple AUVs with acoustic and optical sensors can be used to perform rapid environmental assessment and detect mine-like objects.

Underwater networking is a rather unexplored area although underwater communications have been experimented since World War II, when, in 1945, an underwater telephone was developed in the United States to communicate with submarines [71]. Acoustic communications are the typical physical layer technology in underwater networks. In fact, radio waves propagate at long distances through conductive salty water only at extra low frequencies $(30 - 300\,\mathrm{Hz})$, which require large antennae and high transmission power. For example, the Berkeley Mica 2 Motes, the most popular experimental platform in the sensor networking community, have been reported to have a transmission range of $120\,\mathrm{cm}$ in underwater at $433\,\mathrm{MHz}$ by experiments performed at the Robotic Embedded Systems Laboratory (RESL) at the University of Southern California. Optical waves do not suffer from

such high attenuation but are affected by scattering. Moreover, transmission of optical signals requires high precision in pointing the narrow laser beams. Thus, links in underwater networks are based on *acoustic wireless communications* [82].

The traditional approach for ocean-bottom or ocean-column monitoring is to deploy underwater sensors that record data during the monitoring mission, and then recover the instruments [69]. This approach has the following disadvantages:

- **No real-time monitoring.** The recorded data cannot be accessed until the instruments are recovered, which may happen several months after the beginning of the monitoring mission. This is critical especially in surveillance or in environmental monitoring applications such as seismic monitoring.

- **No on-line system reconfiguration.** Interaction between onshore control systems and the monitoring instruments is not possible. This impedes any adaptive tuning of the instruments, nor is it possible to reconfigure the system after particular events occur.

- **No failure detection.** If failures or misconfigurations occur, it may not be possible to detect them before the instruments are recovered. This can easily lead to the complete failure of a monitoring mission.

- **Limited Storage Capacity.** The amount of data that can be recorded during the monitoring mission by every sensor is limited by the capacity of the onboard storage devices (memories, hard disks).

Therefore, there is a need to deploy underwater networks that will enable real-time monitoring of selected ocean areas, remote configuration and interaction with onshore human operators. This can be obtained by connecting underwater instruments by means of wireless links based on acoustic communication.

Many researchers are currently engaged in developing networking solutions for terrestrial wireless ad hoc and sensor networks. Although there exist many recently developed

network protocols for wireless sensor networks, the unique characteristics of the underwater acoustic communication channel, such as limited bandwidth capacity and variable delays [70], require very efficient and reliable new data communication protocols.

Major challenges in the design of underwater acoustic networks are:

- The available bandwidth is severely limited;
- The underwater channel is impaired because of multi-path and fading;
- Propagation delay in underwater is five orders of magnitude higher than in Radio Frequency (RF) terrestrial channels, and variable;
- High bit error rates and temporary losses of connectivity (shadow zones) can be experienced;
- Underwater sensors are characterized by high cost because of a small relative number of suppliers (i.e., not much economy of scale);
- Battery power is limited and usually batteries can not be recharged, also because solar energy cannot be exploited;
- Underwater sensors are prone to failures because of fouling and corrosion.

1.2 Organization of the Thesis

This thesis is organized in eight chapters.

In Chapter 2, several fundamental key aspects of underwater acoustic communications are investigated. Different architectures for two-dimensional and three-dimensional underwater sensor networks are discussed, and the underwater channel is characterized. The main challenges for the development of efficient networking solutions posed by the underwater environment are detailed and a cross-layer approach to the integration of all communication functionalities is suggested. Furthermore, open research issues are discussed and possible solution approaches are outlined.

In Chapter 3, different deployment strategies for two-dimensional and three-dimensional communication architectures for UnderWater Acoustic Sensor Networks (UW-ASNs) are proposed, and statistical deployment analysis for both architectures is provided. The objectives of this chapter are to determine the minimum number of sensors needed to be deployed to achieve the optimal sensing and communication coverage, which are dictated by the application; provide guidelines on how to choose the optimal deployment surface area, given a target region; study the robustness of the sensor network to node failures, and provide an estimate of the number of redundant sensors to be deployed to compensate for possible failures.

In Chapter 4, a model characterizing the acoustic channel utilization efficiency is introduced, which allows investigating some fundamental characteristics of the underwater environment. In particular, the model allows setting the optimal packet size for underwater communications given monitored volume, density of the sensor network, and application requirements. Moreover, the problem of data gathering is investigated at the network layer by considering the cross-layer interactions between the routing functions and the characteristics of the underwater acoustic channel. Two distributed routing algorithms are introduced for delay-insensitive and delay-sensitive applications. The proposed solutions allow each node to select its next hop, with the objective of minimizing the energy consumption taking the varying condition of the underwater channel and the different application requirements into account. The proposed routing solutions are shown to achieve the performance targets by means of simulation.

In Chapter 5, the problem of data gathering for three-dimensional underwater sensor networks is investigated at the network layer by considering the interactions between the routing functions and the characteristics of the underwater acoustic channel. A two-phase resilient routing solution for long-term monitoring missions is developed, with the objective of guaranteeing survivability of the network to node and link failures. In the first phase,

energy-efficient node-disjoint primary and backup paths are optimally configured, by relying on topology information gathered by a surface station. In the second phase, paths are locally repaired in case of node failures.

In Chapter 6, UW-MAC, a distributed Medium Access Control (MAC) protocol tailored for UnderWater Acoustic Sensor Networks (UW-ASNs), is proposed. It is a transmitter-based Code Division Multiple Access (CDMA) scheme that incorporates a novel closed-loop distributed algorithm to set the optimal transmit power and code length. UW-MAC aims at achieving three objectives, i.e., guarantee high network throughput, low channel access delay, and low energy consumption. It is proven that UW-MAC manages to simultaneously achieve the three objectives in deep water communications, which are not severely affected by multipath. In shallow water communications, which may be heavily affected by multipath, it dynamically finds the optimal trade-off among these objectives, depending on the application requirements. UW-MAC is the first protocol that leverages CDMA properties to achieve multiple access to the scarce underwater bandwidth, while existing papers considered CDMA only from a physical layer perspective. Experiments show that UW-MAC outperforms existing MAC protocols tuned for the underwater environment under different architecture scenarios and simulation settings.

In Chapter 7, a cross-layer resource allocation problem is formulated in multi-hop wireless underwater networks as an optimization problem. While we first outline a general framework where different resource allocation problems will fit by specifying the form of particular functions, then we specialize the framework for the underwater environment.

Finally, Chapter 8 concludes the thesis.

CHAPTER II

RESEARCH CHALLENGES FOR UNDERWATER ACOUSTIC SENSOR NETWORKS

2.1 Preliminaries

In this chapter, we discuss several fundamental key aspects of underwater acoustic communications. We discuss the communication architecture of underwater sensor networks as well as the factors that influence underwater network design. The ultimate objective of this work is to encourage research efforts to lay down fundamental bases for the development of new advanced communication techniques for efficient underwater communication and networking for enhanced ocean monitoring and exploration applications.

The remainder of this chapter is organized as follows. In Section 2.2 and 2.3 we introduce the communication architectures and design challenges, respectively, of underwater acoustic networks. In Section 2.4, we investigate the underwater acoustic communication channel and summarize the associated physical layer challenges for underwater networking. In Sections 2.5, 2.6, 2.7, 2.8, and 2.9, we discuss physical, data link, network, transport, and application layer issues in underwater sensor networks, respectively. Finally, in Section 2.10 we describe some experimental implementations of underwater sensor networks.

2.2 Communication Architectures

In this section, we describe the communication architectures of underwater acoustic sensor networks. In particular, we introduce reference architectures for two-dimensional and three-dimensional underwater networks, and present several types of AUVs that can enhance the capabilities of underwater sensor networks.

The network topology is in general a crucial factor in determining the *energy consumption*, the *capacity*, and the *reliability* of a network. Hence, the network topology should be carefully engineered and post-deployment *topology optimization* should be performed, when possible.

Underwater monitoring missions can be extremely expensive because of the high cost of underwater devices. Hence, it is important that the deployed network be highly reliable, so as to avoid failure of monitoring missions due to failure of single or multiple devices. For example, it is crucial to avoid designing the network topology with single points of failure, which could compromise the overall functioning of the network.

The network capacity is also influenced by the network topology. Since the capacity of the underwater channel is severely limited, as will be discussed in Section 2.4, it is very important to organize the network topology in such a way that no *communication bottleneck* is introduced.

The communication architectures introduced here are used as a basis for discussion of the challenges associated with underwater acoustic sensor networks. The underwater sensor network topology is an open research issue in itself that needs further analytical and simulative investigation from the research community. In the remainder of this section, we discuss the following architectures:

- **Static two-dimensional UW-ASNs for ocean bottom monitoring**. These are constituted by sensor nodes that are anchored to the bottom of the ocean, as discussed in Section 2.2.1. Typical applications may be environmental monitoring, or monitoring of underwater plates in tectonics [30].

- **Static three-dimensional UW-ASNs for ocean-column monitoring**. These include networks of sensors whose depth can be controlled by means of techniques discussed in Section 2.2.2, and may be used for surveillance applications or monitoring of ocean phenomena (ocean bio-geo-chemical processes, water streams, pollution).

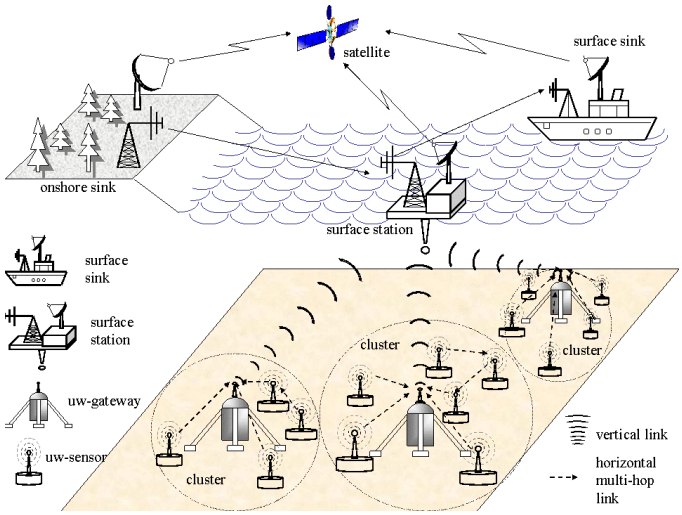

Figure 1: Architecture for 2D underwater sensor networks

- **Three-dimensional networks of Autonomous Underwater Vehicles (AUVs)**. These networks include fixed portions composed of anchored sensors and mobile portions constituted by autonomous vehicles, as detailed in Section 2.2.3.

2.2.1 Two-dimensional Underwater Sensor Networks

A reference architecture for two-dimensional underwater networks is shown in Fig. 1. A group of sensor nodes are anchored to the bottom of the ocean with deep ocean anchors. Underwater sensor nodes are interconnected to one or more *underwater gateways* (uw-gateways) by means of wireless acoustic links. Uw-gateways, as shown in Fig. 1, are network devices in charge of relaying data from the ocean bottom network to a surface station. To achieve this objective, uw-gateways are equipped with two acoustic transceivers, namely a *vertical* and a *horizontal* transceiver. The horizontal transceiver is used by the uw-gateway to communicate with the sensor nodes to: i) send commands and configuration data to the sensors (uw-gateway to sensors); and ii) collect monitored data (sensors to uw-gateway). The vertical link is used by the uw-gateways to relay data to a *surface station*. In deep water applications, vertical transceivers must be long range transceivers as the ocean can be as deep as $10\,\mathrm{km}$. The surface station is equipped with an acoustic transceiver

that is able to handle multiple parallel communications with the deployed uw-gateways. It is also endowed with a long range RF and/or satellite transmitter to communicate with the *onshore sink* (os-sink) and/or to a *surface sink* (s-sink).

Sensors can be connected to uw-gateways via direct links or through multi-hop paths. In the former case, each sensor directly sends the gathered data to the selected uw-gateway. However, in UW-ASNs, the power necessary to transmit may decay with powers greater than two of the distance [81], and the uw-gateway may be far from the sensor node. Consequently, although direct link connection is the simplest way to network sensors, it may not be the most energy efficient solution. Furthermore, direct links are very likely to reduce the network throughput because of increased acoustic interference caused by the high transmission power. In case of multi-hop paths, as in terrestrial sensor networks [8], the data produced by a source sensor is relayed by intermediate sensors until it reaches the uw-gateway. This results in energy savings and increased network capacity, but increases the complexity of the routing functionality as well. In fact, every network device usually takes part in a collaborative process whose objective is to diffuse topology information such that efficient and loop free routing decisions can be made at each intermediate node. This process involves signaling and computation. Since energy and capacity are precious resources in underwater environments, as discussed above, in UW-ASNs the objective is to deliver event features by exploiting multi-hop paths and minimizing the signaling overhead necessary to construct underwater paths at the same time.

2.2.2 Three-dimensional Underwater Sensor Networks

Three dimensional underwater networks are used to detect and observe phenomena that can not be adequately observed by means of ocean bottom sensor nodes, i.e., to perform cooperative sampling of the 3D ocean environment. In three-dimensional underwater networks, sensor nodes float at different depths to observe a given phenomenon. One possible solution would be to attach each uw-sensor node to a surface buoy, by means of wires

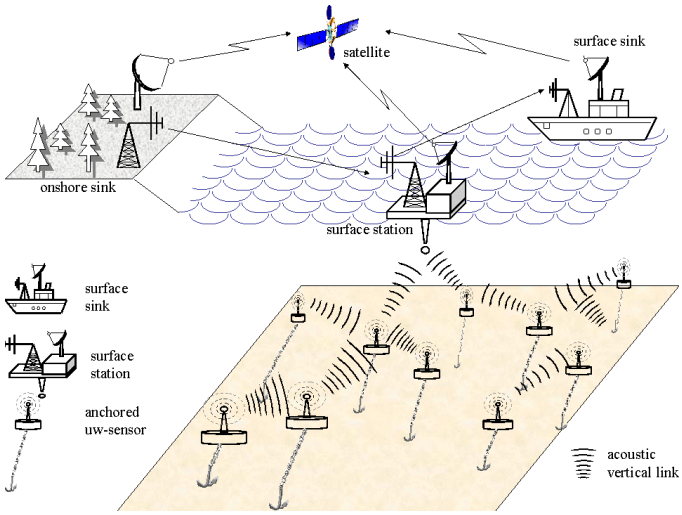

Figure 2: Architecture for 3D underwater sensor networks

whose length can be regulated so as to adjust the depth of each sensor node [16]. However, although this solution allows easy and quick deployment of the sensor network, multiple floating buoys may obstruct ships navigating on the surface, or they can be easily detected and deactivated by enemies in military settings. Furthermore, floating buoys are vulnerable to weather and tampering or pilfering.

For these reasons, a different approach can be to anchor sensor devices to the bottom of the ocean. In this architecture, depicted in Fig. 2, each sensor is anchored to the ocean bottom and equipped with a floating buoy that can be inflated by a pump. The buoy pushes the sensor towards the ocean surface. The depth of the sensor can then be regulated by adjusting the length of the wire that connects the sensor to the anchor, by means of an electronically controlled engine that resides on the sensor. A challenge to be addressed in such an architecture is the effect of ocean currents on the described mechanism to regulate the depth of the sensors.

Many challenges arise with such an architecture, that need to be solved to enable 3D monitoring, including:

- **Sensing coverage**. Sensors should collaboratively regulate their depth in order to

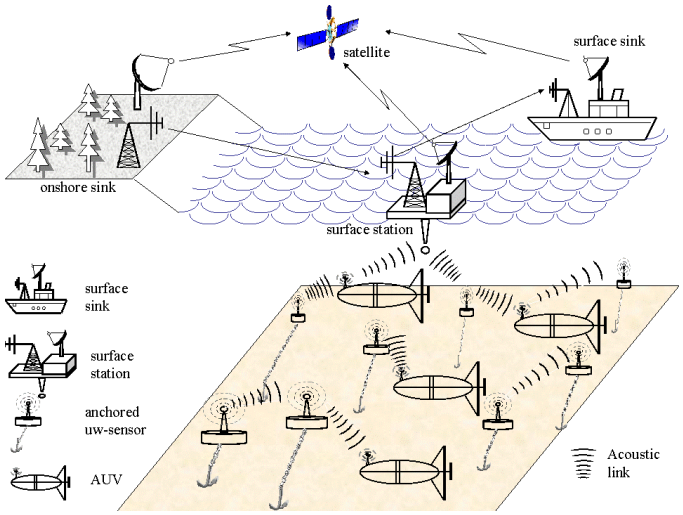

Figure 3: Architecture for 3D underwater sensor networks with AUVs

achieve 3D coverage of the ocean column, according to their sensing ranges. Hence, it must be possible to obtain sampling of the desired phenomenon at all depths.

- **Communication coverage**. Since in 3D underwater networks there may be no notion of uw-gateway, sensors should be able to relay information to the surface station via multi-hop paths. Thus, network devices should coordinate their depths in such a way that the network topology be always connected, i.e., at least one path from every sensor to the surface station always exists.

Sensing and communication coverage in a 3D environment are rigorously investigated in [74]. The diameter, minimum and maximum degree of the reachability graph that describes the network are derived as a function of the communication range, while different degrees of coverage for the 3D environment are characterized as a function of the sensing range. These techniques could be exploited to investigate the coverage issues in UW-ASNs.

2.2.3 Sensor Networks with Autonomous Underwater Vehicles

AUVs can function without tethers, cables, or remote control, and therefore they have a multitude of applications in oceanography, environmental monitoring, and underwater

resource study. Previous experimental work has shown the feasibility of relatively inexpensive AUV submarines equipped with multiple underwater sensors that can reach any depth in the ocean. Hence, they can be used to enhance the capabilities of underwater sensor networks in many ways. Figure 3 shows a reference architecture for 3D underwater sensor networks with AUVs. The integration and enhancement of fixed sensor networks with AUVs is an almost unexplored research area that requires new network coordination algorithms such as:

- **Adaptive sampling.** This includes control strategies to command the mobile vehicles to places where their data will be most useful. This approach is also known as *adaptive sampling* and has been proposed in pioneering monitoring missions. For example, the density of sensor nodes can be adaptively increased in a given area when a higher sampling rate is needed for a given monitored phenomenon.

- **Self-Configuration.** This includes control procedures to automatically detect connectivity holes caused by node failures or channel impairment and request the intervention of an AUV. Furthermore, AUVs can either be used for installation and maintenance of the sensor network infrastructure or to deploy new sensors. They can also be used as temporary relay nodes to restore connectivity.

One of the design objectives of AUVs is to make them rely on local intelligence, and be less dependent on communications from online shores [38]. In general, control strategies are needed for autonomous coordination, obstacle avoidance, and steering strategies. Solar energy systems allow increasing the lifetime of AUVs, i.e., it is not necessary to recover and recharge the vehicle on a daily basis. Hence, solar powered AUVs can acquire continuous information for periods of time of the order of months [41].

Several types of AUVs exist as experimental platforms for underwater experiments. Some of them resemble small-scale submarines (such as the Odyssey-class AUVs developed at MIT). Others are simpler devices that do not encompass such sophisticated capabilities. For example, *drifters* and *gliders* are oceanographic instruments often used in underwater explorations. Drifter underwater vehicles drift with local current and have the ability to move vertically through the water column, and are used for taking measurements at preset depths [37]. Underwater gliders [23] are battery powered autonomous underwater vehicles that use hydraulic pumps to vary their volume by a few hundred cubic centimeters to generate the buoyancy changes that power their forward gliding. When they emerge on the surface, Global Positioning System (GPS) is used to locate the vehicle. This information can be relayed to the onshore station while operators can interact by sending control information to the gliders. Depth capabilities range from $200\,\mathrm{m}$ to $1500\,\mathrm{m}$ while operating lifetimes range from a few weeks to several months. These long durations are possible because gliders move very slowly, typically $25\,\mathrm{cm/s}$ ($0.5\,\mathrm{knots}$). In [62], a control strategy for groups of gliders to cooperatively move and reconfigure in response to a sensed distributed environment is presented. The proposed framework allows preserving the symmetry of the group of gliders. The group is constrained to maintain a uniform distribution as needed, but is free to spin and possibly wiggle with current. In [27], results are reported on the application of the theory in [62] on a fleet of autonomous underwater gliders during the experiment on Monterey Bay in 2003.

2.3 Design Challenges

In this section, we describe the design challenges of underwater acoustic sensor networks. In particular, we itemize the main differences between terrestrial and underwater sensor networks, we detail key design issues and deployment challenges for underwater sensors, and we give motivations for cross-layer design approach to improve the network efficiency in the critical underwater environment.

2.3.1 Differences with Terrestrial Sensor Networks

The main differences between terrestrial and underwater sensor networks can be outlined as follows:

- **Cost.** While terrestrial sensor nodes are expected to become increasingly inexpensive, underwater sensors are expensive devices. This is especially due to the more complex underwater transceivers and to the hardware protection needed in the extreme underwater environment. Also, because of the low economy of scale caused by a small relative number of suppliers, underwater sensors are characterized by high cost.

- **Deployment.** While terrestrial sensor networks are densely deployed, in underwater, the deployment is generally more sparse.

- **Power.** The power needed for acoustic underwater communications is higher than in terrestrial radio communications because of the different physical layer technology (acoustic vs. RF waves), the higher distances, and more complex signal processing techniques implemented at the receivers to compensate for the impairments of the channel.

- **Memory.** While terrestrial sensor nodes have very limited storage capacity, uw-sensors may need to be able to do some data caching as the underwater channel may be intermittent.

- **Spatial Correlation.** While the readings from terrestrial sensors are often correlated, this is more unlikely to happen in underwater networks due to the higher distance among sensors.

2.3.2 Underwater Sensors

The typical internal architecture of an underwater sensor is shown in Fig. 4. It consists of a main controller/CPU, which is interfaced with an oceanographic instrument or sensor

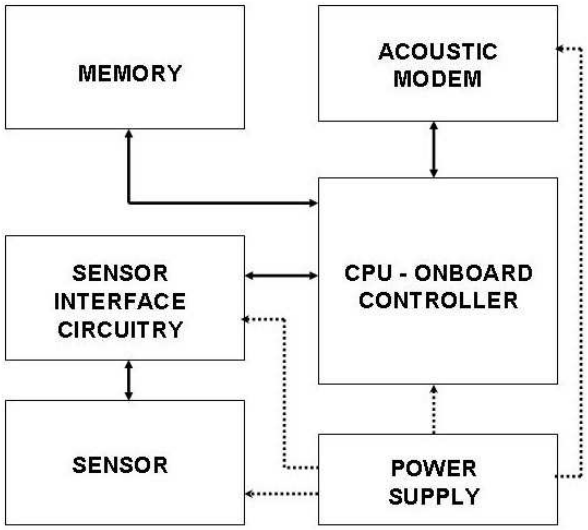

Figure 4: Internal organization of an underwater sensor node

through a sensor interface circuitry. The controller receives data from the sensor and it can store it in the onboard memory, process it, and send it to other network devices by controlling the acoustic modem. The electronics are usually mounted on a frame that is protected by a PVC housing. Sometimes all sensor components are protected by bottom-mounted instrument frames that are designed to permit azimuthally omnidirectional acoustic communications, and protect sensors and modems from potential impact of trawling gear, especially in areas subjected to fishing activities. In [20], the protecting frame is designed so as to deflect trawling gear on impact, by housing all components beneath a low-profile pyramidal frame.

Underwater sensing devices include sensors to measure the quality of water and to study its characteristics such as temperature, density, salinity (interferometric and refractometric sensors), acidity, chemicals, conductivity, pH (magnetoelastic sensors), oxygen (Clark-type electrode), hydrogen, dissolved methane gas (METS), and turbidity. Disposable sensors exist that detect ricin, the highly poisonous protein found in castor beans and thought to be a potential terrorism agent. DNA microarrays can be used to monitor both

abundance and activity level variations among natural microbial populations. Other existing underwater sensors include hydrothermal sulfide, silicate, voltammetric sensors for spectrophotometry, gold-amalgam electrode sensors for sediment measurements of metal ions (ion-selective analysis), amperometric microsensors for H_2S measurements for studies of anoxygenic photosynthesis, sulfide oxidation, and sulfate reduction of sediments. In addition, force/torque sensors for underwater applications requiring simultaneous measurements of several forces and moments have also been developed, as well as quantum sensors to measure light radiation and sensors for measurements of harmful algal blooms.

The challenges related to the deployment of low cost, low scale underwater sensors, are listed below:

- It is necessary to develop less expensive, robust "nano-sensors", e.g., sensors based on Nano-Technology, which involves development of materials and systems at the atomic, molecular, or macromolecular levels in the dimension range of approximately $1 - 500\,\mathrm{nm}$.

- It is necessary to devise periodical cleaning mechanisms against corrosion and fouling, which may impact the lifetime of underwater devices. For example, some sensors for pCO_2, pH and nitrate measurement, and fluorometers and spectral radiometers, may be limited by bio-fouling, especially on a long time scale.

- There is a need for robust, stable sensors on a high range of temperatures since sensor drift of underwater devices may be a concern. To this end, protocols for *in situ* calibrations of sensors to improve accuracy and precision of sampled data must be developed.

- There is a need for new integrated sensors for *synoptic* sampling of physical, chemical, and biological parameters to improve the understanding of processes in marine systems.

2.3.3 A Cross-layer Protocol Stack

A protocol stack for uw-sensors should combine *power awareness* and *management*, and promote *cooperation* among the sensor nodes. It should consist of *physical layer*, *data link layer*, *network layer*, *transport layer*, and *application layer* functionalities. The protocol stack should also include a *power management plane*, a *coordination plane*, and a *localization plane*. The power management plane is responsible for network functionalities aimed at minimizing the energy consumption (e.g., sleep modes, power control). The coordination plane is responsible for all functionalities that require coordination among sensors, (e.g., coordination of the sleep modes, data aggregation, 3D topology optimization). The localization plane is responsible for providing absolute or relative localization information to the sensor node, when needed by the protocol stack or by the application.

While all the research on underwater networking so far has followed the traditional layered approach for network design, it is an increasingly accepted opinion in the wireless networking community that the improved network efficiency, especially in critical environments, can be obtained with a cross-layer design approach. These techniques will entail a joint design of different network functionalities, from modem design to MAC and routing, from channel coding and modulation to source compression and transport layer, with the objective to overcome the shortcomings of a layered approach that lacks of information sharing across protocol layers, forcing the network to operate in a suboptimal mode. Hence, while in the following sections for the sake of clarity we present the challenges associated with underwater sensor networks following the traditional layered approach, we believe that the underwater environment particularly requires for cross-layer design solutions that allow a more efficient use of the scarce available resources. However, although we advocate integrating functionalities to improve network performance and to avoid duplication of functions by means of cross-layer design, it is important to consider the ease of design by following a *modular design approach*. This also allows improving and upgrading particular functionalities without the need to re-design the entire communication system.

Although systematic research on cross-layer design for underwater communications is missing, a study on the interaction between physical and MAC layers is presented in [43], where a method is proposed based on the sonar equation [90] to estimate the battery lifetime and power cost for shallow water[1] underwater acoustic sensor networks for civilian applications. The battery lifetime is modeled as dependent on four key parameters, namely internode distance, transmission frequency, frequency of data updates and number of nodes per cluster. Interestingly, since in shallow water the acoustic propagation loss increases with increasing frequency and distance (as shown in Fig. 5), it is proposed to assign lower frequencies to sensor nodes that are closer to the sink, since they also have to relay data on behalf of more distant nodes. This way, the energy consumption is somehow equalized and the network lifetime is prolonged.

2.3.4 Real-time Networking vs. Delay Tolerant Networking

As in terrestrial sensor networks, depending on the application there may be very different requirements for data delivery. For example, surveillance application may need very fast reaction to events and thus networking protocols that provide guaranteed delay-bounded delivery are required. Hence, it is necessary to develop protocols that deal with the characteristics of the underwater environment to quickly restore connectivity when lost and that react to unpaired or congested links by taking appropriate action (e.g., dynamical rerouting) to meet the given delay bound. Conversely, other applications may produce large bundles of data to be delivered to the onshore sink without particular delay constraints. With this respect, the Delay-Tolerant Networking Research Group (DTNRG) [26] developed mechanisms to resolve the intermittent connectivity, long or variable delay, asymmetric data rates, and high error rates by using a *store and forward* mechanism based on a middleware between the application layer and the lower layers. Similar methodologies may be particularly useful for applications such as those that record seismic activity, which have very

[1] In oceanic literature, *shallow water* refers to water with depth lower than $100\,\mathrm{m}$, while *deep water* is used for deeper oceans.

Table 1: Available bandwidth for different ranges in UW-A channels

	Range $[\mathrm{km}]$	**Bandwidth** $[\mathrm{kHz}]$
Very Long	1000	< 1
Long	$10 - 100$	$2 - 5$
Medium	$1 - 10$	≈ 10
Short	$0.1 - 1$	$20 - 50$
Very Short	< 0.1	> 100

low duty cycle and produce, when activated, large bundles of data that need to be relayed to a monitoring station where it can be analyzed to predict future activity. On the other hand, sensor networks intended for disaster prevention such as those that provide earthquake or tsunami warnings, require immediate delivery of information and hence real-time protocols. Therefore, the design of networking solutions for underwater acoustic sensor networks should always be aware of the difference between real-time and delay tolerant (and delay-sensitive and delay-insensitive) applications, and jointly tune existing solutions to the application needs and to the characteristics of the underwater environment.

2.4 Basics of Underwater Acoustic Propagation

Underwater acoustic communications are mainly influenced by *path loss*, *noise*, *multi-path*, *Doppler spread*, and *high and variable propagation delay*. All these factors determine the *temporal and spatial variability* of the acoustic channel, and make the available bandwidth of the *UnderWater Acoustic channel* (UW-A) limited and dramatically dependent on both range and frequency. Long-range systems that operate over several tens of kilometers may have a bandwidth of only a few kHz, while a short-range system operating over several tens of meters may have more than a hundred kHz of bandwidth. In both cases these factors lead to low bit rate [15], in the order of tens of kbit/s for existing devices.

Underwater acoustic communication links can be classified according to their range as *very long*, *long*, *medium*, *short*, and *very short* links [82]. Table 1 shows typical bandwidths of the underwater channel for different ranges. Acoustic links are also roughly classified

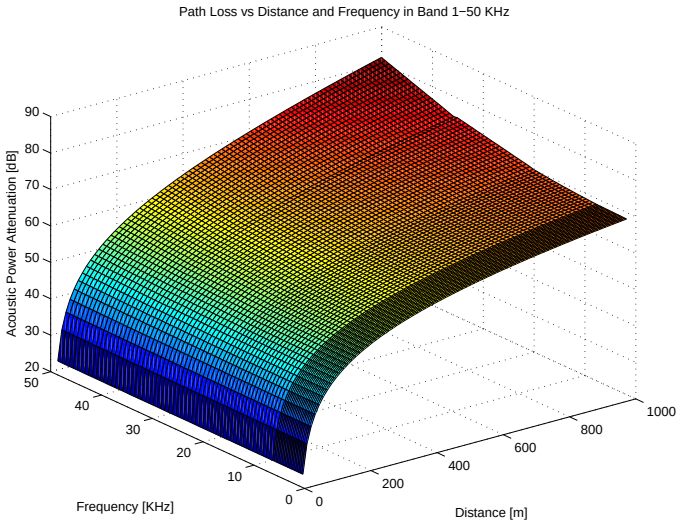

Figure 5: Path loss of short range shallow UW-A channels vs. distance and frequency in band $1 - 50\,\mathrm{kHz}$

as *vertical* and *horizontal*, according to the direction of the sound ray with respect to the ocean bottom. As will be shown later their propagation characteristics differ considerably, especially with respect to time dispersion, multi-path spreads, and delay variance. In the following, as usually done in oceanic literature, *shallow water* refers to water with depth lower than $100\,\mathrm{m}$, while *deep water* is used for deeper oceans.

Hereafter we analyze the factors that influence acoustic communications in order to state the challenges posed by the underwater channels for underwater sensor networking. These include:

- **Path loss**
  - *Attenuation.* Is mainly provoked by absorption caused by the conversion of acoustic energy into heat. The attenuation increases with distance and frequency. Figure 5 shows the acoustic attenuation with varying frequency and distance for a short range shallow water UW-A channel, according to the propagation model in [90]. The attenuation is also caused by scattering and reverberation (on rough ocean surface and bottom), refraction, and dispersion (due to

the displacement of the reflection point caused by wind on the surface). Water depth plays a key role in determining the attenuation.

  - *Geometric Spreading*. This refers to the spreading of sound energy as a result of the expansion of the wavefronts. It increases with the propagation distance and is independent of frequency. There are two common kinds of geometric spreading: *spherical* (omni-directional point source), which characterizes deep water communications, and *cylindrical* (horizontal radiation only), which characterizes shallow water communications.

- **Noise**

  - *Man made noise.* This is mainly caused by machinery noise (pumps, reduction gears, power plants), and shipping activity (hull fouling, animal life on hull, cavitation), especially in areas encumbered with heavy vessel traffic.

  - *Ambient Noise.* Is related to hydrodynamics (movement of water including tides, current, storms, wind, and rain), and to seismic and biological phenomena. In [34], boat noise and snapping shrimps have been found to be the primary sources of noise in shallow water by means of measurement experiments on the ocean bottom.

- **Multi-path**

  - Multi-path propagation may be responsible for severe degradation of the acoustic communication signal, since it generates Inter Symbol Interference (ISI).

  - The multi-path geometry depends on the link configuration. Vertical channels are characterized by little time dispersion, whereas horizontal channels may have extremely long multi-path spreads.

  - The extent of the spreading is a strong function of depth and the distance between transmitter and receiver.

- **High delay and delay variance**
  - The propagation speed in the UW-A channel is five orders of magnitude lower than in the radio channel. This large propagation delay ($0.67\,\mathrm{s/km}$) can reduce the throughput of the system considerably.
  - The high delay variance is even more harmful for efficient protocol design, as it prevents from accurately estimating the Round Trip Time (RTT), which is the key parameter for many common communication protocols.
- **Doppler spread**
  - The Doppler frequency spread can be significant in UW-A channels [82], causing a degradation in the performance of digital communications: transmissions at a high data rate cause many adjacent symbols to interfere at the receiver, requiring sophisticated signal processing to deal with the generated ISI.
  - The Doppler spreading generates a simple frequency translation, which is relatively easy for a receiver to compensate for; and a continuous spreading of frequencies, which constitutes a non-shifted signal, which is more difficult to compensate for.
  - If a channel has a Doppler spread with bandwidth B and a signal has symbol duration T, then there are approximately BT uncorrelated samples of its complex envelope. When BT is much less than unity, the channel is said to be *underspread* and the effects of the Doppler fading can be ignored, while, if greater than unity, it is said to be *overspread* [48].

2.5 Physical Layer

Until the beginning of the last decade, due to the challenging characteristics of the underwater channel, underwater modem development was based on *non-coherent* Frequency

Shift Keying (FSK) modulation, since it relies on energy detection and thus does not require phase tracking, which is a very difficult task mainly because of the Doppler-spread in the UW-A channel, described in Section 2.4. In FSK modulation schemes developed for underwater, the multi-path effects are suppressed by inserting time guards between successive pulses to ensure that the reverberation, caused by the rough ocean surface and bottom, vanishes before each subsequent pulse is received. Dynamic frequency guards can also be used between frequency tones to adapt the communication to the Doppler spreading of the channel. Although non-coherent modulation schemes are characterized by a high *power efficiency*, their low *bandwidth efficiency* makes them unsuitable for high data rate multiuser networks. Hence, *coherent modulation* techniques have been developed for long-range, high-throughput systems. In the last years, *fully* coherent modulation techniques, such as Phase Shift Keying (PSK) and Quadrature Amplitude Modulation (QAM), have become practical because of the availability of powerful digital processing. Channel equalization techniques are exploited to leverage the effect of the Inter Symbol Interference (ISI), instead of trying to avoid or suppress it. Decision Feedback Equalizers (DFE) track the complex, relatively slowly varying channel response and thus provide high throughput when the channel is slowly varying. Conversely, when the channel varies faster, it is necessary to combine the DFE with a Phase Locked Loop (PLL) [84], which estimates and compensates for the phase offset in a rapid, stable manner. The use of decision feedback equalization and phase-locked loops is driven by the complexity and time variability of ocean channel impulse responses. Table 2 presents the evolution from non-coherent modems to the recent coherent modems.

Differential Phase Shift Keying (DPSK) serves as an intermediate solution between incoherent and fully coherent systems in terms of bandwidth efficiency. DPSK encodes information relative to the previous symbol rather than to an arbitrary fixed reference in the signal phase and may be referred to as a *partially coherent modulation*. While this strategy substantially alleviates carrier phase-tracking requirements, the penalty is an increased

Table 2: Evolution of modulation technique

Type	**Year**	**Rate**$[\,\mathrm{kbps}]$	**Band** $[\mathrm{kHz}]$	**Range**$[\,\mathrm{km}]$
FSK	1984	1.2	5	3_s
PSK	1989	500	125	0.06_d
FSK	1991	1.25	10	2_d
PSK	1993	$0.3 - 0.5$	$0.3 - 1$	$200_d - 90_s$
PSK	1994	0.02	20	0.9_s
FSK	1997	$0.6 - 2.4$	5	$10_d - 5_s$
DPSK	1997	20	10	1_d
PSK	1998	$1.67 - 6.7$	$2 - 10$	$4_d - 2_s$
16-QAM	2001	40	10	0.3_s

* The subscripts $_d$ and $_s$ stand for *deep* and *shallow* water

error probability over PSK at an equivalent data rate.

With respect to Table 2, it is worth noticing that early phase-coherent systems achieved higher bandwidth efficiencies (bit rate/occupied bandwidth) than their incoherent counterparts, but they did not outperform incoherent modulation schemes yet. In fact, coherent systems had lower performance than incoherent systems for long-haul transmissions on horizontal channels until ISI compensation via decision-feedback equalizers for optimal channel estimation was implemented [85]. However, these filtering algorithms are complex and not suitable for real-time communications, as they do not meet real-time constraints. Hence, sub-optimal filters have to be considered, but the imperfect knowledge of the channel impulse response that they provide leads to channel estimation errors, and ultimately to decreased performance.

Another promising solution for underwater communications is the Orthogonal Frequency Division Multiplexing (OFDM) spread spectrum technique, which is particularly efficient when noise is spread over a large portion of the available bandwidth. OFDM is frequently referred to as multi-carrier modulation because it transmits signals over multiple *sub-carriers* simultaneously. In particular, sub-carriers which experience higher Signal-to-Noise Ratio (SNR), are allotted with a higher number of bits, whereas less bits are allotted

to sub-carriers experiencing attenuation, according to the concept of *bit loading*, which requires channel estimation. Since the symbol duration for each individual carrier increases, OFDM systems perform robustly in severe multi-path environments, and achieve a high spectral efficiency.

Many of the techniques discussed above require underwater channel estimation, which can be achieved by means of probe packets [44]. An accurate estimate of the channel can be obtained with a high probing rate and/or with a large probe packet size, which however result in high overhead, and in the consequent drain of channel capacity and energy.

2.5.1 Open Research Issues

To enable physical layer solutions specifically tailored for underwater acoustic sensor networks, the following open research issues need to be addressed:

- It is necessary to develop inexpensive transmitter/receiver modems for underwater communications.
- Research is needed on design of low-complexity sub-optimal filters characterized by rapid convergence to enable real-time underwater communications with decreased energy expenditure.
- There is a need to overcome stability problem in the coupling between the Phase Locked Loop (PLL) and the Decision Feedback Equalizer (DCE).

2.6 Data Link Layer

In this section, we discuss techniques for multiple access in UW-ASNs and present open research issues to address the requirements of the data link layer in an underwater environment. Channel access control in UW-ASNs poses additional challenges because of the peculiarities of the underwater channel, in particular limited bandwidth, and high and variable delay.

Frequency Division Multiple Access (FDMA) is not suitable for UW-ASNs due to the narrow bandwidth in UW-A channels and the vulnerability of limited band systems to fading and multi-path.

Time Division Multiple Access (TDMA) shows a limited bandwidth efficiency because of the long time guards required in the UW-A channel. In fact, long time guards must be designed to account for the large propagation delay and delay variance of the underwater channel, discussed in Section 2.4, to minimize packet collisions from adjacent time slots. Moreover, the variable delay makes it very challenging to realize a precise synchronization, with a common timing reference, which is required for TDMA.

Carrier Sense Multiple Access (CSMA) prevents collisions with the ongoing transmission at the transmitter side. To prevent collisions at the receiver side, however, it is necessary to add a guard time between transmissions dimensioned according to the maximum propagation delay in the network. This makes the protocol dramatically inefficient for UW-ASNs.

The use of contention-based techniques that rely on handshaking mechanisms such as RTS/CTS in shared medium access (e.g., MACA [45], IEEE 802.11) is impractical in underwater, for the following reasons: i) large delays in the propagation of RTS/CTS control packets lead to low throughput; ii) due to the high propagation delay of UW-A channels, when carrier sense is used, as in 802.11, it is more likely that the channel be sensed idle while a transmission is ongoing since the signal may not have reached the receiver yet; iii) the high variability of delay in handshaking packets makes it impractical to predict the start and finish time of the transmissions of other stations. Thus, collisions are highly likely to occur.

Many novel access schemes have been designed for terrestrial sensor networks, whose objective, similarly to underwater sensor networks, is to prevent collisions in the access channel thus maximizing the network efficiency. These similarities would suggest to tune and apply those efficient schemes in the underwater environment; on the other hand, the

main focus in medium access control in terrestrial wireless sensor networks is on energy-latency tradeoffs. Some proposed schemes aim at decreasing the energy consumption by using sleep schedules with virtual clustering. However, these techniques may not be suitable for an environment where dense sensor deployment cannot be assumed. Moreover, the additional challenges in underwater channels such as variable and high propagation delays, and very limited available bandwidth, further complicate the medium access problem in underwater environments.

Code Division Multiple Access (CDMA) is quite robust to frequency selective fading caused by underwater multi-paths, since it distinguishes simultaneous signals transmitted by multiple devices by means of pseudo-noise codes that are used for spreading the user signal over the entire available band. This allows exploiting the time diversity in the UW-A channel by leveraging *Rake filters* [80] at the receiver. These filters are designed to match the pulse spreading, the pulse shape, and the channel impulse response, so as to compensate for the effect of multi-path. CDMA allows reducing the number of packet retransmissions, which results in decreased battery consumption and increased network throughput. For example, in [31], two code-division spread-spectrum access techniques are compared in shallow water, namely Direct Sequence Spread Spectrum (DSSS) and Frequency Hopping Spread Spectrum (FHSS). Although FHSS is more prone to the Doppler shift effect, since the transmission takes place in narrow bands, this scheme is more robust to Multiple Access Interference (MAI) than DSSS. Furthermore, although FHSS is shown to lead to a higher bit error rate than DHSS, it results in simple receivers and provides robustness to the near-far problem, thus potentially simplifying the power control functionality. One of the most attractive access techniques in the recent underwater literature combines multi carrier transmission with the DSSS CDMA [44], as it may offer higher spectral efficiency than its single carrier counterpart and increase the flexibility to support integrated high data rate applications with different quality of service requirements. The main idea is to spread each data symbol in the frequency domain by transmitting all the chips of a spread symbol

at the same time into a large number of narrow subchannels. This way, high data rate can be supported by increasing the duration of each symbol, which drastically reduces ISI.

In conclusion, although the high delay spread that characterizes the horizontal link in underwater channels makes it difficult to maintain synchronization among the stations, especially when orthogonal code techniques are used [44], CDMA is a promising multiple access technique for underwater acoustic networks, particularly in shallow water where multi-paths and Doppler-spreading play a key role in the communication performance.

In [76], a protocol is proposed for networks with AUVs. The proposed scheme is based on organizing the network in multiple clusters, each composed of adjacent vehicles. Inside each cluster, TDMA is used with long band guards, to overcome the effect of propagation delay in underwater. In this case, TDMA is not highly inefficient since vehicles in the same cluster are close to one another. Hence, the effect of propagation delay is limited. Interference among different clusters is avoided by assigning different spreading codes to different clusters. The proposed protocol sketches also some mechanisms to reorganize clusters after node mobility.

In order to meet a required bit error rate at the data link layer of the deployed underwater sensor networks, it is mandatory to provide error control functionalities for the transmitted data, since path loss and multi-path fading affecting UW-A channels lead to high bit error rates (on the order of $10^{-2} - 10^{-5}$ [86][81]). While Automatic Repeat Request (ARQ) techniques appear not to be suitable for the underwater environment because they incur a high latency, additional energy cost, and signaling overhead due to retransmissions, Forward Error Correction (FEC) techniques can be effectively employed in such an environment. The objective of these techniques is to protect data by introducing redundant bits in the transmission so that the receiver can correct detected bit errors. In this way, retransmissions are not necessary although both the transmitter and the receiver incur additional processing power drain for encoding and decoding, respectively. There is a trade-off between the robustness of the adopted FEC technique, which depends on the amount of redundant bits

injected in the channel, and the channel efficiency. A possible solution to maximize the underwater channel efficiency in such a way as to effectively exploit its valuable available bandwidth would be to dynamically choose the optimal amount of redundant bits according to measurements of the underwater channel.

2.6.1 Open Research Issues

To enable data link layer solutions specifically tailored for underwater acoustic sensor networks, the following open research issues need to be addressed:

- In case CDMA is adopted, which we strongly advocate, it is necessary to design access codes with high auto-correlation and low cross-correlation properties to achieve minimum interference among users. This needs to be achieved even when the transmitting and receiving nodes are not synchronized.
- Research on optimal data packet length is needed to maximize the network efficiency.
- It is necessary to design low-complexity encoders and decoders to limit the processing power required to implement FEC functionalities. Researchers should evaluate the feasibility and the energy-efficiency of non-convolutional error control coding schemes.
- Distributed protocols should be devised to reduce the activity of a device when its battery is depleting without compromising network operation.

2.7 Network Layer

The *network layer* is in charge of determining the path between a source (the sensor that samples a physical phenomenon) and a destination node (usually the surface station). In general, while many impairments of the underwater acoustic channel are adequately addressed at the physical and data link layers, some other characteristics, such as the extremely long propagation delays, are better addressed at the network layer.

In the last few years there has been an intensive study in routing protocols for ad hoc wireless networks [3] and sensor networks [5]. However, because of the different nature of the underwater environment and applications, there are several drawbacks with respect to the suitability of the existing solutions for underwater acoustic networks. The existing routing protocols are usually divided into three categories, namely *proactive, reactive* and *geographical* routing protocols:

- **Proactive protocols** (e.g., DSDV [64], OLSR [40]). These protocols attempt to minimize the message latency induced by route discovery, by maintaining up-to-date routing information at all times from each node to every other node. This is obtained by broadcasting control packets that contain routing table information (e.g., distance vectors). These protocols provoke a large signaling overhead to establish routes for the first time and each time the network topology is modified because of mobility or node failures, since updated topology information has to be propagated to all the nodes in the network. This way, each node is able to establish a path to any other node in the network, which may not be needed in UW-ASNs. For this reason, proactive protocols are not suitable for underwater networks.

- **Reactive protocols** (e.g., AODV [63], DSR [42]). A node initiates a route discovery process only when a route to a destination is required. Once a route has been established, it is maintained by a route maintenance procedure until it is no longer desired. These protocols are more suitable for dynamic environments but incur a higher latency and still require source-initiated flooding of control packets to establish paths. Thus, both proactive and reactive protocols incur excessive signaling overhead because of their extensive reliance on flooding. Reactive protocols are deemed to be unsuitable for UW-ASNs as they also cause a high latency in the establishment of paths, which may be even amplified underwater by the slow propagation of acoustic signals. Furthermore, links are likely to be asymmetrical, due to bottom characteristics and variability in sound speed channel. Hence, protocols that rely on symmetrical

links, such as most of the reactive protocols, are unsuited for the underwater environment. Moreover, the topology of UW-ASNs is unlikely to vary dynamically on a short time scale.

- **Geographical Routing Protocols** (e.g., GFG [11], PTKF [57]). These protocols establish source-destination paths by leveraging localization information, i.e., each node selects its next hop based on the position of its neighbors and of the destination node. Although these techniques are very promising, it is still not clear how accurate localization information can be obtained in the underwater environment with limited energy expenditure. In fact, fine-grained localization usually requires strict synchronization among nodes, that is difficult to achieve underwater due to the variable propagation delay. In addition Global Positioning System (GPS) receivers, which may be used in terrestrial systems to accurately estimate the geographical location of sensor nodes, do not work properly underwater. In fact, GPS uses waves in the $1.5\,\mathrm{GHz}$ band and those waves do not propagate in water.

Some recent papers propose network layer protocols specifically tailored for underwater acoustic networks. In [92], a routing protocol is proposed that autonomously establishes the underwater network topology, controls network resources and establishes network flows which relies on a centralized network manager running on the surface station. The manager implements routing agents that periodically probe the nodes to estimate the channel characteristics. This information is exploited by the manager to establish efficient data delivery paths in a centralized fashion, which allows avoiding congestion and providing some form of Quality of Service (QoS) guarantee. The performance evaluation of the proposed mechanisms has not been thoroughly studied yet.

In [81] it is shown with simple acoustic propagation models [13] that multi-hop routing saves energy in underwater networks with respect to single hop communications, especially with distances of the order of some kilometers. Based on this, a simple ad hoc underwater network is designed and simulated where routes are established by a central manager based

on neighborhood information gathered by all nodes by means of poll packets.

In general, while most developed protocols for terrestrial ad hoc networks, mostly due to scalability and mobility concerns, are based on *packet switching*, i.e., the routing function is performed separately for each single packet and paths are dynamically established, *virtual circuit* routing techniques can be considered in UW-ASNs. In these techniques, paths are established *a priori* between each source and sink, and each packet follows the same path. This may require some form of centralized coordination and implies a less flexible architecture, but allows exploiting powerful optimization tools on a centralized manager (e.g., the surface station) to achieve optimal performance at the network layer (minimum delay paths, energy efficient paths, etc.), with minimum communication signaling overhead.

Furthermore, routing schemes that account for the 3D underwater environment need to be devised. Especially, in the 3D case the effect of currents should be taken into account, since the intensity and the direction of currents are dependent on the depth of the sensor node. Thus, underwater currents can modify the relative position of sensor devices and also cause connectivity holes, especially when ocean-column monitoring is performed in deep waters.

2.7.1 Open Research Issues

There exist many open research issues for the development of efficient routing solutions for underwater acoustic sensor networks, as outlined below:

- There is a need to develop algorithms to provide strict or loose latency bounds for time critical applications. To this respect, it should be considered that while the delay for an acoustic signal to propagate from one node to another mainly depends on the distance of the two nodes, the delay variance also depends on the nature of the link, i.e., the delay variance in horizontal acoustic links is generally larger than in vertical links because of multipaths [82].

- For delay tolerant applications, there is a need to develop mechanisms to handle loss

of connectivity without provoking immediate retransmissions. Strict integration with transport and data link layer mechanisms may be advantageous to this end.

- It is necessary to devise routing algorithms that are robust with respect to the intermittent connectivity of acoustic channels. The quality of acoustic links is highly unpredictable, since it mainly depends on fading and multi-path, which are hard phenomena to model.

- Accurate modeling is needed to better understand the dynamics of data transmission at the network layer. Moreover, credible simulation models and tools need to be developed.

- Algorithms and protocols need to be developed that detect and deal with disconnections caused by failures, unforeseen mobility of nodes, or battery depletion. These solutions should be local so as to avoid communication with the surface station and global reconfiguration of the network, and should minimize the signaling overhead.

- Local route optimization algorithms are needed to react to consistent variations in the metrics describing the energy efficiency of the underwater channel. These variations can be caused by increased bit error rates due to acoustic noise and relative displacement of communicating nodes.

- Mechanisms are needed to integrate AUVs in underwater networks and to enable communication between sensors and AUVs. In particular, all the information available to sophisticated AUVs (trajectory, localization) could be exploited to minimize the signaling needed for reconfigurations.

- In case of geographical routing protocols, it is necessary to devise efficient underwater positioning systems.

2.8 Transport Layer

A transport layer protocol is needed in UW-ASNs to achieve *reliable transport* of event features, and to perform *flow control* and *congestion control*. Most existing TCP implementations are unsuited for the underwater environment since the flow control functionality is based on a window-based mechanism that relies on an accurate estimate of the Round Trip Time (RTT). The long RTT, which characterizes the underwater environment, would affect the throughput of most TCP implementations. Furthermore, the variability of the underwater RTT would make it hard to effectively set the timeout of the window-based mechanism, which most current TCP implementations rely on.

Existing rate-based transport protocols seem to be unsuited for this challenging environment as well, since they rely on feedback control messages sent back by the destination to dynamically adapt the transmission rate. The long and variable RTT can thus cause instability in the feedback control. For these reasons, it is necessary to devise new strategies to achieve flow control and reliability in UW-ASNs.

A transport layer protocol designed for the underwater environment, Segmented Data Reliable Transport (SDRT), has been recently proposed in [93]. SDRT addresses the challenges of underwater sensor networks for reliable data transport, i.e., large propagation delays, low bandwidth, energy efficiency, high error probabilities, and highly dynamic network topologies. The basic idea of SDRT is to use Tornado codes to recover errored packets to reduce retransmissions. The data packets are transmitted block-by-block and each block is forwarded hop-by-hop. SDRT keeps sending packets inside a block before it gets back a positive feedback and thus wastes energy. To reduce such energy consumption, a window control mechanism is adopted. SDRT transmits the packets within the window quickly, and the remaining packets at a lower rate. A mathematical model is developed to estimate the window size and the FEC block size. The performance of SDRT is also illustrated by simulations.

Encoding and decoding using Tornado codes are computation-intensive operations even

though Tornado codes use only XOR operations. This leads to increased energy consumption. In SDRT, there is also no mechanism to guarantee the end-to-end reliability as an hop-by-hop transfer mode is used. Each node along the path must first decode the FEC block and then encode it again to transmit it to the next hop. Again, the total computation overhead will be too high for the network. Similarly, for hop-by-hop operations, each sensor must keep calculating the mean values of window and the FEC block sizes, which can cause a high computational overhead and accordingly higher energy consumption at each sensor. The overhead due to redundant packets will also be high because of high error probabilities. This overhead is dependent on the accuracy in estimating the window size. If the window size is too large, more packets are sent than necessary. In addition, SDRT does not address one of the fundamental challenges for UW-ASN, i.e., shadow zones, and relies on an in-sequence packet forwarding scheme. While this may be enough for some applications, for time-critical data sensors may need to forward packets continuously even in case of holes in the sequence with an out-of-sequence packet delivery mechanism. SDRT is a first attempt to propose a transport protocol for UW-ASN and addresses some of the aforementioned design principles. However, it is still an evolving work and needs further improvements, as it creates redundant transmissions and is computation-intensive.

A complete transport layer solution for the underwater environment should be based on the following design principles:

- *Shadow zones.* Although correct handling of shadow zones requires assistance from the routing layer, a transport protocol should consider these cases.

- *Minimum energy consumption.* A transport protocol should be explicitly designed to minimize the energy consumption.

- *Rate-based transmission of packets.* A transport protocol should be based on rate-based transmission of data units as it allows nodes flexible control over the rates.

- *Out-of-sequence packet forwarding.* Packets should be continuously forwarded to

accelerate the packet delivery process.

- *Timely reaction to local congestion.* A transport protocol should adapt to local conditions immediately, to decrease the response time in case of congestion. Thus, rather than sinks, intermediate nodes should be capable of determining and reacting to local congestion.

- *Cross-layer-interaction-based protocol operation.* Losses of connectivity or partial packet losses (i.e., bit or packet errors) should trigger the protocol to take appropriate actions. Therefore, unlike in the layered communications paradigm, transport protocol operations and critical decisions should be supported by the available information from lower layers.

- *Reliability.* A hop-by-hop reliability mechanism surfaces as a prevalent solution as it provides energy efficient communication. However, there should also be mechanism to guarantee the end-to-end reliability.

- *SACK-based loss recovery.* Many feedbacks with ACK mechanisms would throttle down the utilization of the bandwidth-limited channel unnecessarily. Thus, the notion of selective acknowledgment (SACK), which helps preserve energy, should be considered for loss scenarios where it is not possible to perform error recovery at lower layers only.

Open research issues for transport layer solutions are given below:

- New flow control strategies need to be devised to tackle the high delay and delay variance of the control messages sent back by the receivers.

- New effective mechanisms tailored to the underwater acoustic channel need to be developed to efficiently infer the cause of packet losses.

- New reliability-metric definitions need to be proposed, based on the event model and on the underwater acoustic channel model.

- The effects of multiple concurrent events on the reliability and network performance requirements must be studied.
- It is necessary to statistically model loss of connectivity events to devise mechanisms to enable delay-insensitive applications.
- It is necessary to devise solutions to handle the effects of losses of connectivity caused by shadow zones.

2.9 Application Layer

Although many application areas for underwater sensor networks can be outlined, to the best of our knowledge the definition of an application layer protocol for UW-ASNs remains largely unexplored.

The purpose of an application layer is multi-fold: i) provide a network management protocol that makes hardware and software details of the lower layers transparent to management applications; ii) provide a language for querying the sensor network as a whole; iii) assign tasks and advertise events and data.

No efforts in these areas have been made to date that address the specific needs of the underwater acoustic environment. A deeper understanding of the application areas and of the communication problems in underwater sensor networks is crucial to outline some design principles on how to extend or reshape existing application layer protocols [8] for terrestrial sensor networks.

Some of the latest developments in middleware may be studied and adapted to realize a versatile application layer for underwater sensor networks. For example, the San Diego Supercomputing Center Storage Resource Broker (SRB) [9] is a client-server middleware that provides a uniform interface for connecting to heterogeneous data resources over a network and accessing replicated data sets. SRB provides a way to access data sets and resources based on their attributes and/or logical names rather than their names or physical locations.

2.10 Experimental Implementations of Underwater Sensor Networks

A few experimental implementations of underwater acoustic sensor networks have been reported in the last few years. In this section we describe two of them, one mainly concerned with military application and the other with oceanographic observations.

The Front-Resolving Observational Network with Telemetry (FRONT) project at the University of Connecticut relies on acoustic telemetry and ranging advances pursued by the US Navy referred to as "telesonar" technology [20]. The Seaweb network for FRONT Oceanographic Sensors involves telesonar modems deployed in conjunction with three types of nodes, namely *sensors*, *gateways*, and *repeaters*. Sensors are oceanographic instruments connected serially to an acoustic modem. Gateways are surface buoys that relay data from the subsurface network to the shore. Repeaters are acoustic modems that relay data packets. In the various Seaweb/FRONT experiments, 20 sensors and repeaters have been deployed in shallow water (20 to 60 meter deep). By means of long range ocean bottom active sensors, Acoustic Correlation Current Profilers (ACCP), sampling of the 3D water column is achieved with a 2D network architecture. The network enables sensor-to-shore data delivery and shore-to-sensor remote control.

Researchers from different fields gathered at the Monterey Bay Aquarium Research Institute (MBARI) in August 2003 for a month-long experiment to quantify gains in predictive skills for principal circulation trajectories, i.e., to study upwelling of cold, nutrient-rich water in the Monterey Bay. Autonomous vehicle paths (AUVs, gliders, etc.), as well as other ships, vessels and platforms, enabled unexampled observational capabilities. Extensive data are reported that show the variation of the characteristics of the circulation of water during the various days of the experiment.

The work in [20] describes on-the-field experience with networked acoustic modems. The setup of several real-time monitoring experiments of ocean currents performed in front of Block Island, RI, is outlined. However, the paper does not provide details on the implemented networking protocols.

CHAPTER III

DEPLOYMENT ANALYSIS FOR UNDERWATER ACOUSTIC SENSOR NETWORKS

3.1 Preliminaries

In this chapter, we consider two communication architectures for UW-ASNs, i.e., the *two-dimensional architecture*, where sensors are anchored to the bottom of the ocean, and the *three-dimensional architecture*, where sensors float at different ocean depths covering the entire monitored volume region. While the former is designed for networks whose objective is to monitor the ocean bottom, the latter is more suitable to detect and observe phenomena that cannot be adequately observed by means of ocean bottom sensor nodes. We propose different deployment strategies, and provide a mathematical analysis to study deployment issues concerning both architectures, with the objectives below:

- Determine the minimum number of sensors needed to be deployed to achieve the target sensing and communication coverage dictated by the application;
- Provide guidelines on how to choose the optimal deployment surface area, given a target region;
- Study the robustness of the sensor network to node failures, and provide an estimate of the number of redundant sensors to be deployed to compensate for possible failures.

The remainder of this chapter is organized as follows. In Section 3.2, we review related literature. In Section 3.3, we briefly describe the two-dimensional and three-dimensional architectures for UW-ASNs, and discuss the relevant deployment challenges. In Section

3.4, we derive geometric properties of the triangular-grid deployment, evaluate the trajectory of a sinking device under the presence of ocean currents, compute the deployment surface area to deploy sensors when a 2D bottom target area needs to be covered, and provide an estimate of the number of redundant sensors to compensate for possible failures. In Section 3.5, we propose and compare through simulation experiments three deployment strategies for 3D UW-ASNs.

3.2 Related Work

The problem of sensing and communication coverage for terrestrial sensor networks has been addresses in several papers. However, to the best of our knowledge, this work is the first to study deployment issues for underwater sensor networks. Many previous deployment solutions and theoretical bounds assuming spatio-temporal correlation, mobile sensors, redeployment of nodes, and particular deployment grid structures may not be feasible for the underwater environment.

In particular, in [78], methods for determining network connectivity and coverage given a node-reliability model are discussed, and an estimate of the minimum required node-reliability for meeting a system-reliability objective is provided. An interesting result is that connectivity does not necessarily imply coverage. As the node-reliability decreases, in fact, the sufficient condition for connectivity becomes weaker than the necessary condition for coverage. Although [78] provides useful theoretical bounds and insight into the deployment of wireless terrestrial sensor networks, the analysis is limited to grid structures. In [39], two coordination sleep algorithms are compared, a random and a coordinated sleep scheme. It is shown that when the density of the network increases, the duty cycle of the network can be decreased for a fixed coverage. Although [39] provides sound coverage algorithms for terrestrial sensor networks, its results cannot be directly applied to the underwater environment where the sensor density is much lower than in the terrestrial case, and spatio-temporal correlation cannot often be assumed [7]. In [98], sensor coverage is

achieved by moving sensor nodes after an initial random deployment. However, [98] requires either mobile sensor nodes or redeployment of nodes, which may not be feasible for UW-ASNs. In [74], sensing and communication coverage in a three-dimensional environment are rigorously investigated. The diameter, minimum and maximum degree of the reachability graph that describes the network are derived as a function of the communication range, while different degrees of coverage (1-coverage and, more in general, k-coverage) for the 3D environment are characterized as a function of the sensing range. Interestingly, it is shown that the sensing range r required for 1-coverage is greater than the transmission range t that guarantees network connectivity. Since in typical applications $t \geq r$, the network is guaranteed to be connected when 1-coverage is achieved. Although these results were derived for terrestrial networks, they can also be applied in the underwater environment. Thus, in this chapter, we will focus on the sensing coverage when discussing deployment issues in 3D UW-ASNS, as in three-dimensional networks it implicitly implies the communication coverage.

3.3 Communication Architectures

We consider two communication architectures for underwater sensor networks, i.e., a *two-dimensional* and a *three-dimensional architecture* [7], and identify the relevant deployment challenges. As in terrestrial sensor networks, in UW-ASNs it is necessary to provide *communication coverage*, i.e., all sensors should be able to establish multi-hop paths to the sink, and *sensing coverage*, i.e., the monitored area should be covered by the sensors. More formally, the *sensing range* r of a sensor is the radius of the sphere that models the region monitored by the sensor (sensing sphere). A portion $\mathcal{A}_\eta$ of the monitored region $\mathcal{A}$ is said to be *k-covered* if every point in $\mathcal{A}_\eta$ falls within the sensing sphere of at least k sensors. The *k-coverage ratio* η_k of a monitored region $\mathcal{A}$ is the fraction of the volume/area that is k-covered by a 3D/2D UW-ASN, respectively. In the following, we will consider the case of $k = 1$ both for 2D and 3D networks to obtain simple *1-coverage* η_1 of the region, since

underwater sensors may be expensive devices and spatio-temporal correlation may not be assumed [7].

3.3.1 Two-dimensional UW-ASNs

A reference architecture for two-dimensional underwater sensor networks is shown in Fig. 1, where deployed sensor nodes are anchored to the bottom of the ocean. Underwater sensors may be organized in a cluster-based architecture, and be interconnected to one or more *underwater gateways* (uw-gateways) by means of wireless acoustic links. Uw-gateways are network devices in charge of relaying data from the ocean bottom network to a surface station. They are equipped with a long-range *vertical* transceiver, which is used to relay data to a *surface station*, and with a *horizontal* transceiver, which is used to communicate with the sensor nodes to send commands and configuration data, and to collect monitored data. The surface station is equipped with an acoustic transceiver, which may be able to handle multiple parallel communications with the uw-gateways, and with a long-range radio transmitter and/or satellite transmitter, which is needed to communicate with an *onshore sink* and/or to a *surface sink*.

The main challenges that arise with such two-dimensional architecture are: i) determine the minimum number of sensors and uw-gateways that need to be deployed to achieve the target sensing and communication coverage, which are dictated by the application requirements; ii) provide guidelines on how to choose the optimal deployment surface area, given a target bottom area; iii) study the topology robustness of the sensor network to node failures, and provide an estimate of the number of redundant sensor nodes to be deployed to compensate for failures. In Section 3.4, we discuss in detail these issues and provide solutions.

3.3.2 Three-dimensional UW-ASNs

Three-dimensional underwater networks are used to detect and observe phenomena that cannot be adequately observed by means of ocean bottom uw-sensor nodes, i.e., to perform

cooperative sampling of the 3D ocean environment. In this architecture, sensors float at different depths to observe a given phenomenon. One possible solution would be to attach each sensor node to a surface buoy, by means of wires whose length can be regulated to adjust the depth of each sensor node. However, although this solution enables easy and quick deployment of the sensor network, multiple floating buoys may obstruct ships navigating on the surface, or they can be easily detected and deactivated by enemies in military settings. Furthermore, floating buoys are vulnerable to weather and tampering or pilfering.

A different approach is to anchor winch-based sensor devices to the bottom of the ocean, as depicted in Fig. 2. Each sensor is anchored to the ocean bottom and is equipped with a floating buoy that can be inflated by a pump. The buoy pulls the sensor towards the ocean surface. The depth of the sensor can then be regulated by adjusting the length of the wire that connects the sensor to the anchor, by means of an electronically controlled engine that resides on the sensor [7].

Many challenges arise with such architecture, which need to be solved to enable underwater monitoring, including: i) sensors should collaboratively regulate their depth to achieve 3D *sensing coverage* of the ocean column, according to their sensing ranges; ii) sensors should be able to relay information to the surface station via multi-hop paths, as in 3D underwater networks there may be no notion of uw-gateway. Thus, network devices should coordinate their depths in such a way as to guarantee that the network topology be always connected, i.e., at least one path from every sensor to the surface station always exists, and achieve *communication coverage*. We discuss sensing and communication coverage in 3D UW-ASNs in Section 3.5, and propose three deployment solutions.

3.4 Deployment in a 2D Environment

In this section, we provide a mathematical analysis of the graph properties of sensor devices that are deployed on the surface of the ocean, sink, and reach the ocean bottom. To achieve

this, we study the trajectory of sinking devices (sensors and uw-gateways) when they are deployed on the ocean surface with known initial conditions (position and velocity). This allows us to capture both the case when sensor nodes are *randomly deployed* on the ocean surface, e.g., scattered from an airplane, or the case when sensors are *accurately positioned*, e.g., released from a vessel.

To address the deployment challenges presented in the previous section, in Section 3.4.1 we propose the *triangular-grid* deployment, and derive useful geometric properties. In Section 3.4.2, we study the dynamics of a sinking object and evaluate its trajectory under the presence of ocean currents. In Section 3.4.3, we characterize the different sinking behavior of sensors and uw-gateways, with the objective of describing their average horizontal displacement and study the main communication properties of sensor clusters. In Section 3.4.4, we derive the side margins that should be used to deploy sensors on the ocean surface when a 2D target area needs to be covered on the ocean bottom under the presence of currents. Finally, in Section 3.4.5, we derive an estimate of the number of redundant sensors to be deployed to compensate for possible failures and provide the network with robustness.

3.4.1 Triangular-grid Coverage Properties

In this section, we propose the *triangular-grid* deployment, and derive useful geometric properties. Let us consider the common case of sensors with same sensing range r. The optimal deployment strategy to cover a two-dimensional rectangular area using the minimum number of sensors is to center each sensor at the vertex of a grid of equilateral triangles, as shown in Fig. 6. With this configuration, by adjusting the distance d among sensors, i.e., the side of the equilateral triangles, it is possible to achieve *full coverage*, i.e., $\eta = 1$. In addition, this enables to optimally control the coverage ratio η, defined as the ratio between the covered area and the target area. In particular, as it will be mathematically proven in the following, when $d = \sqrt{3}r$ the coverage ratio η is equal to 1, i.e., the uncovered area ABC

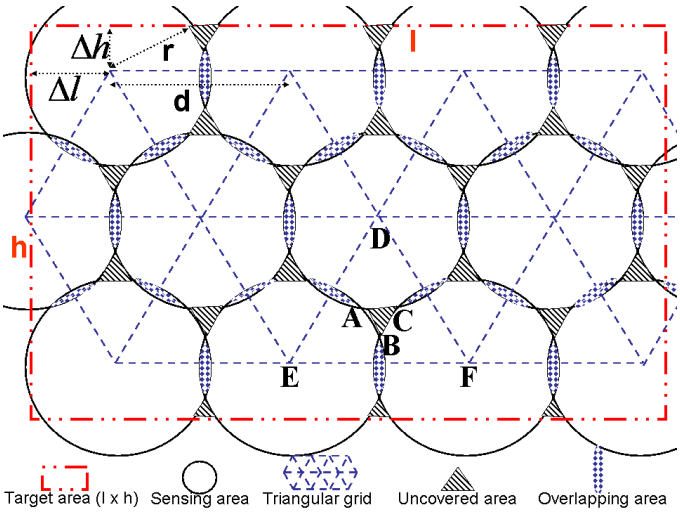

Figure 6: *Triangular-grid deployment.* Grid structure and side margins

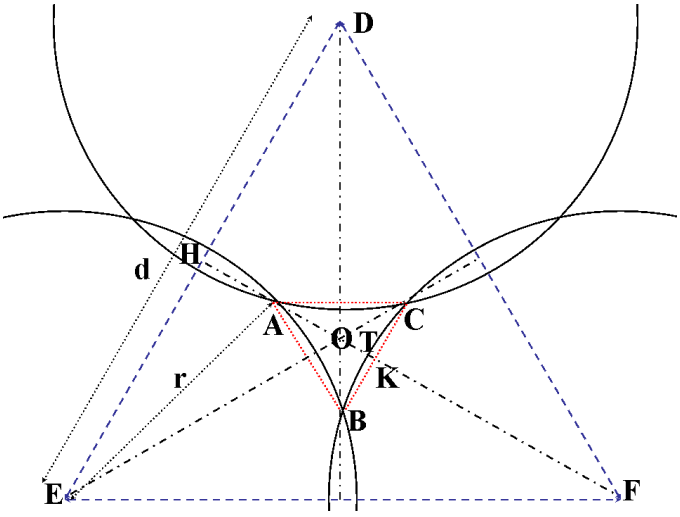

Figure 7: *Triangular-grid deployment.* Uncovered area

depicted in Figs. 6 and 7 is zero, and the overlapping areas are minimized. This allows to achieve the full coverage of a target area, but requires the highest number of sensors. Conversely, as the distance among sensors increases, i.e., the number of deployed sensors decreases, the coverage ratio decreases. Therefore, there is a trade-off between the number of deployed sensors and the achievable sensing coverage. We are interested in finding the minimum number of sensors that need to be deployed to guarantee a target sensing coverage η^*, which is dictated by the application requirements. To this end, we present the following theorem.

Theorem 1 *In an equilateral grid the sensing coverage $\eta(d,r)$, i.e., the ratio of the covered area and the target area, is*

$$\eta(d,r) = \eta\left(\frac{d}{r}\right) = \begin{cases} \frac{\mathcal{A}_{DEF}-\mathcal{A}_{ABC}}{\mathcal{A}_{DEF}} = 1 - \frac{\mathcal{A}_{ABC}}{\frac{\sqrt{3}}{4}d^2} & \frac{d}{r} \in [0,2] \\ \frac{3\cdot\frac{\pi r^2}{6}}{\frac{\sqrt{3}}{4}d^2} = \frac{2\pi}{\sqrt{3}} \cdot (\frac{d}{r})^{-2} & \frac{d}{r} \in (2,\infty), \end{cases} \tag{1}$$

where:

$$\begin{aligned} &\mathcal{A}_{ABC} = \tfrac{\sqrt{3}}{4}\left(\tfrac{d}{2} - \sqrt{3r^2 - \tfrac{3}{4}d^2}\right)^2 - 3r^2 \arcsin\tfrac{\overline{BC}}{2r} \\ &+\tfrac{3}{4}\overline{BC}\sqrt{4r^2 - \overline{BC}^2}, \qquad \overline{BC} = \tfrac{d}{2} - \sqrt{3r^2 - \tfrac{3}{4}d^2}. \end{aligned} \tag{2}$$

Proof With reference to Fig. 7, which represents a zoomed portion of Fig. 6, $\overline{AE} = r$ and $\overline{EH} = d/2$, where r is the sensing range and d is the distance between sensors. Since the triangle DEF is equilateral by construction, $\overline{HO} = (\sqrt{3}/6)d$. Consequently, since $\overline{AH} = \sqrt{r^2 - d^2/4}$, it holds $\overline{AO} = \overline{HO} - \overline{AH} = (\sqrt{3}/6)d - \sqrt{r^2 - d^2/4}$. As triangle DEF is equilateral, triangle ABC is equilateral too. Since $\overline{AO} = (\sqrt{3}/3)\overline{BC}$, then $\overline{BC} = d/2 - \sqrt{3r^2 - (3/4)d^2}$. Therefore, the area of triangle ABC is $\mathcal{A}^{\triangle}_{ABC} = (\sqrt{3}/4)\overline{BC}^2$. To be able to express the sensing coverage $\eta(d,r)$ as a function of d and r, we need to compute the area $\mathcal{A}_{ABC}$ of the *uncovered region* ABC among the circles with centers in D, E, and F, and radius r. This can be computed as $\mathcal{A}_{ABC} = \mathcal{A}^{\triangle}_{ABC} - 3 \cdot \mathcal{A}_{BTCK}$, where $\mathcal{A}_{BTCK}$ coincides with the difference of the areas of the circular sector $BTCF$ and the triangle BCF, i.e., $\mathcal{A}_{BTCK} = \mathcal{A}_{BTCF} - \mathcal{A}^{\triangle}_{BCF} = r^2 \arcsin(\overline{BC}/2r) - (\overline{BC}/4)\sqrt{4r^2 - \overline{BC}^2}$. Consequently,

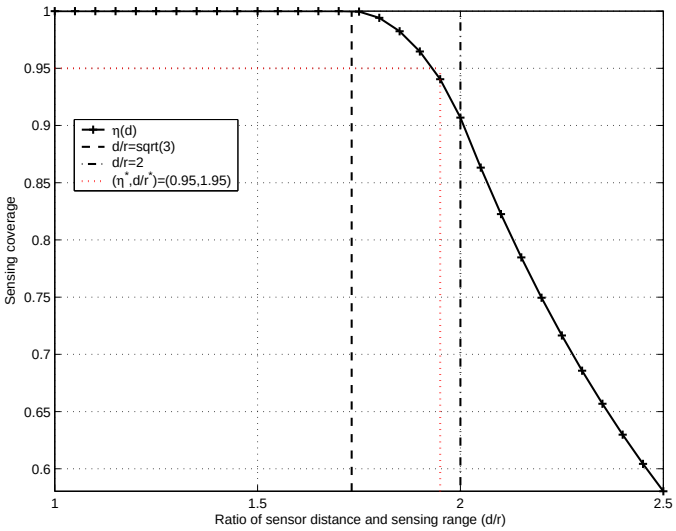

Figure 8: *Triangular-grid deployment.* Sensing coverage

$\mathcal{A}_{ABC} = (\sqrt{3}/4)\left(d/2 - \sqrt{3r^2 - (3/4)d^2}\right)^2 - 3r^2 \arcsin(\overline{BC}/2r) + (3/4)\overline{BC}\sqrt{4r^2 - \overline{BC}^2}$, where $\overline{BC} = d/2 - \sqrt{3r^2 - (3/4)d^2}$, which gives (1) in the non-trivial case $d/r \in [0, 2]$. As far as the case $d/r \in (2, \infty)$ is concerned, no overlapping areas are formed, and the coverage η can be computed straightforward.

Corollary 1 *In an equilateral grid the sensing coverage depends only on the ratio of the inter-sensor distance d and the sensing range r, and not on their absolute values, i.e., $\eta(d, r) = \eta(d/r)$.*

Let us note in (1) that, when $d/r \leq \sqrt{3}$, it holds $\mathcal{A}^{\triangle}_{ABC} = \mathcal{A}_{ABC} = 0$, which means that in this case the highest possible coverage is achieved ($\eta = 1$). Moreover, $\mathcal{A}_{ABC}(d)$ is a monotonically increasing function when d/r ranges in $[\sqrt{3}, 2]$, which makes the coverage $\eta(d, r)$ a monotonically decreasing function when $d/r > \sqrt{3}$. Figure 8 reports the sensing coverage as a decreasing function of the ratio of d and r. For a target sensing coverage $\eta^* = 0.95$, it is shown that the optimal ratio is $d^*/r = 1.95$.

In order to compute the minimum number of sensors that need to be deployed to cover a target area with sides l and h using the proposed equilateral grid, we should first find the

optimal *margins* Δl and Δh from the center of the upper-left sensing circle, as shown in Fig. 6. In particular, given the application-dependent target coverage η^*, from Fig. 8 we compute the optimal ratio d^*/r. In order for the uncovered areas on the border of the target area to have the same coverage ratio η^*, the margins should be selected as $\Delta h = \overline{HO} + \overline{OT} = (\sqrt{3}/2)d^* - r$, where $\overline{OT} = \overline{OF} - \overline{TF} = (\sqrt{3}/3)d - r$, and $\Delta l = 2\overline{OH}\cos(\pi/6) = d^*/2$. If we denote as N^* the minimum number of sensors, we have $N^* = N_l^* \cdot N_h^*$, where N_l^* and N_h^* represent the minimum number of sensors deployed along sides l and h, respectively. Consequently, the following relations need to be satisfied,

$$2\Delta l + (N_l^* - 1)d^* \geq l \;\Rightarrow\; N_l^* = \left\lceil \tfrac{l-d^*}{d^*} + 1 \right\rceil$$
$$2\Delta h + (N_h^* - 1)d^* \sin(\pi/6) \geq h \;\Rightarrow\; N_h^* = \left\lceil \tfrac{2\sqrt{3}h - 6d^* + 4\sqrt{3}r}{3d^*} + 1 \right\rceil.$$

Finally, the minimum number of sensors N^* required to cover a target area with sides l and h, under the constraints of providing a ratio d^*/r to satisfy the target coverage ratio η^* is

$$N^*(l, h, d^*, r) = \left\lceil \frac{l - d^*}{d^*} + 1 \right\rceil \cdot \left\lceil \frac{2\sqrt{3}h - 6d^* + 4\sqrt{3}r}{3d^*} + 1 \right\rceil. \tag{3}$$

In Figs. 9-11, (3) is plotted for three different target areas, i.e., $A_1 = 100\text{x}100\,\text{m}^2$, $A_2 = 300\text{x}200\,\text{m}^2$, and $A_3 = 1000\text{x}1000\,\text{m}^2$, and for several sensing ranges r in the interval $[10, 35]\,\text{m}$.

3.4.2 Trajectory of a Sinking Object

In this section, we study the dynamics of a sinking object and evaluate its trajectory under the presence of ocean currents. In particular, we first consider the ideal case in which the velocity of the ocean current does not change with depth; then, we extend the model to capture the more realistic case in which the velocity of the current depends on depth.

According to Newton's first law of motion, the acceleration $\vec{\mathbf{a}}$ describing the sinking in the water of an object with a density ρ and volume V is determined by the following vectorial motion law,

$$\vec{\mathbf{F}}_{\mathbf{W}} + \vec{\mathbf{F}}_{\mathbf{B}} + \vec{\mathbf{F}}_{\mathbf{R}} + \vec{\mathbf{F}}_{\mathbf{C}} = \rho V \cdot \vec{\mathbf{a}}, \tag{4}$$

where:

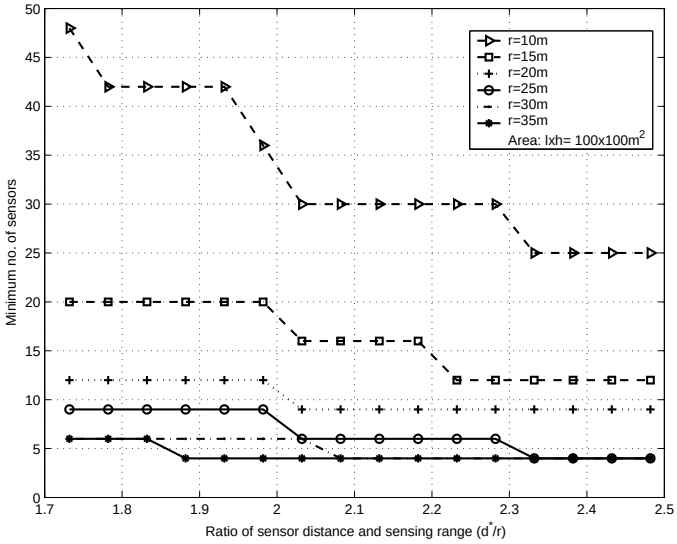

Figure 9: *Minimum number of sensors in triangular-grid deployment vs. sensor distance over sensing range.* $A_1 = 100\text{x}100\,\text{m}^2$

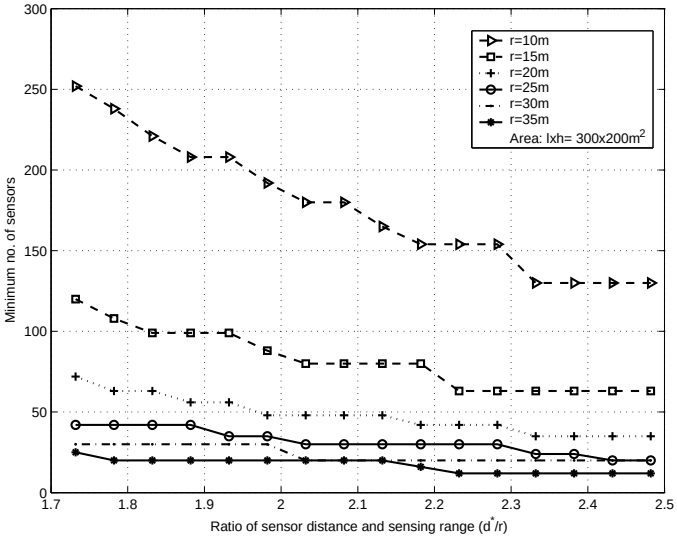

Figure 10: *Minimum number of sensors in triangular-grid deployment vs. sensor distance over sensing range.* $A_2 = 300\text{x}200\,\text{m}^2$

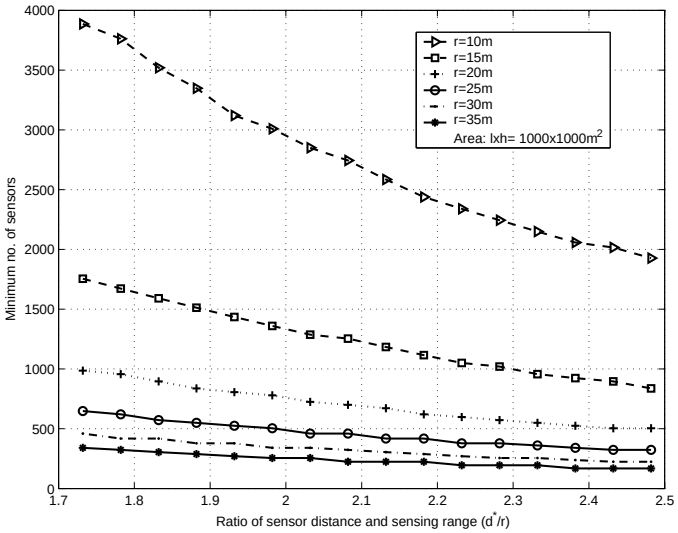

Figure 11: *Minimum number of sensors in triangular-grid deployment vs. sensor distance over sensing range.* $A_3 = 1000\text{x}1000\,\mathrm{m}^2$

- $\vec{\mathbf{F}}_{\mathbf{W}} = \rho V \cdot \vec{\mathbf{g}}$ is the *weight force*, which depends on the density $\rho\,[\mathrm{Kg/m^3}]$ and volume $V\,[\mathrm{m^3}]$ of the sinking object, and on the terrestrial gravitational acceleration $g = 9.81\,\mathrm{m/s^2}$;

- $\vec{\mathbf{F}}_{\mathbf{B}} = -\rho_w V \cdot \vec{\mathbf{g}}$ is the *buoyant force* due to the Archimede's principle, which is equal to the weight of the displaced fluid, where $\rho_w = 1050\,\mathrm{Kg/m^3}$ represents the average density of salty water;

- $\vec{\mathbf{F}}_{\mathbf{R}} = -K\rho_w \mu A_R \cdot \vec{\mathbf{v}}$ is the *fluid resistance force*, which is proportional through the constant $K = 0.2\,\mathrm{Nm^2s/Kg}$ [77] to the velocity $\vec{\mathbf{v}}\,[\mathrm{m/s}]$ of the object, to its cross-section $A_R\,[\mathrm{m^2}]$, and to a parameter μ accounting for the resistance caused by the object shape;

- $\vec{\mathbf{F}}_{\mathbf{C}} = C\sigma A_C \cdot (\vec{\mathbf{v}}_{\mathbf{c}} - \vec{\mathbf{v}})$ is the *force of the current*, which is proportional through the constant $C = 721.7\,\mathrm{Ns/m^3}$ [77] to the difference between the velocity of the ocean current $\vec{\mathbf{v}}_{\mathbf{c}}\,[\mathrm{m/s}]$ and the object velocity $\vec{\mathbf{v}}\,[\mathrm{m/s}]$, to the cross-section $A_C\,[\mathrm{m^2}]$ of the object facing the current, and to an object-dependent shape factor σ.

We project (4) onto the x-, y-, and z- axes, which are directed as shown in Fig. 12, and we denote the dynamic position of the sinking object as $\mathbf{P} = (x, y, z)$, its velocity as $\vec{\mathbf{v}} = (\dot{x}, \dot{y}, \dot{z})$, and its acceleration as $\vec{\mathbf{a}} = (\ddot{x}, \ddot{y}, \ddot{z})$. We then consider the velocity of the

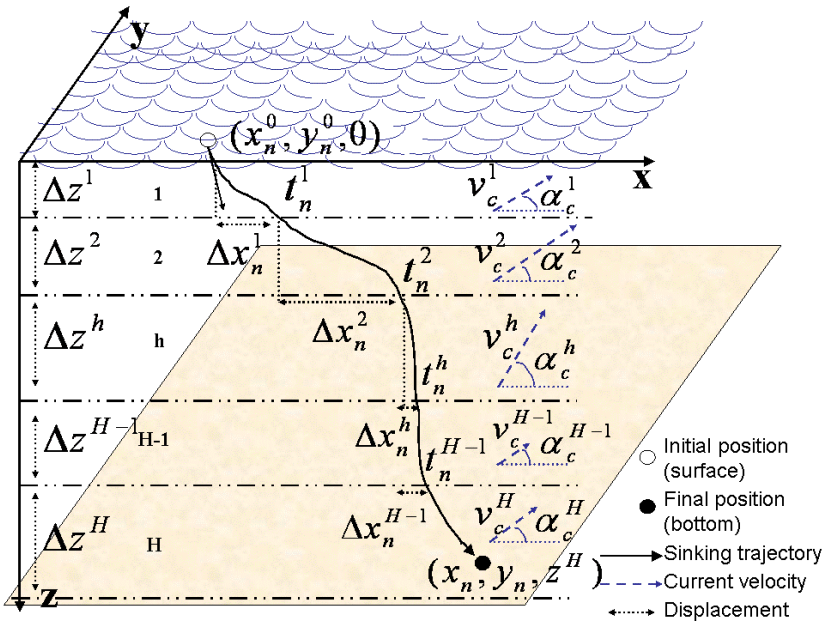

Figure 12: Trajectory of a sinking object

current $\vec{\mathbf{v}}_\mathbf{c} = (v_c^x, v_c^y, v_c^z)$, which, for the sake of clarity, is first assumed to be independent on the ocean depth (we will then relax this assumption). Under the assumption that no significant vertical movement of ocean water is observed, i.e., the considered area is neither an *upwelling* nor a *downwelling area*, the current along the z-axes can be neglected ($v_c^z \approx 0$), and (4) leads to three scalar laws,

$$x:\ F_C^x = \rho V \ddot{x}; \quad y:\ F_C^y = \rho V \ddot{y}; \quad z:\ F_W^z + F_B^z + F_R^z = \rho V \ddot{z}. \tag{5}$$

Specifically, we obtain the following dynamic system equations,

$$\begin{cases} \ddot{x} + \frac{C\sigma A^{xy}}{\rho V}\dot{x} = \frac{C\sigma A^{xy}}{\rho V} v_c^x \\ \ddot{y} + \frac{C\sigma A^{xy}}{\rho V}\dot{y} = \frac{C\sigma A^{xy}}{\rho V} v_c^y \\ \ddot{z} + \frac{K\mu\rho_w A^z}{\rho V}\dot{z} = g\frac{\rho-\rho_w}{\rho}, \end{cases} \tag{6}$$

where A^{xy} and A^z represent the horizontal and vertical cross-sections, respectively. By solving this dynamic system, with the initial conditions of the object on the surface at time t^0, i.e., its position $\mathbf{P}(t^0) = (x(t^0), y(t^0), 0)$ and velocity $\vec{\mathbf{v}}(t^0) = (\dot{x}(t^0), \dot{y}(t^0), \dot{z}(t^0))$, we

obtain the solution,

$$\begin{cases} x(t) = x(t^0) + v_c^x \cdot (t - t^0) + \frac{\dot{x}(t^0) - v_c^x}{C\sigma A^{xy}/\rho V} \cdot [1 - e^{-\frac{C\sigma A^{xy}}{\rho V} \cdot (t - t^0)}] \\ y(t) = y(t^0) + v_c^y \cdot (t - t^0) + \frac{\dot{y}(t^0) - v_c^y}{C\sigma A^{xy}/\rho V} \cdot [1 - e^{-\frac{C\sigma A^{xy}}{\rho V} \cdot (t - t^0)}] \\ z(t) = v_\infty^z \cdot (t - t^0) + [\dot{z}(t^0) - v_\infty^z] \cdot [1 - e^{-\frac{K\rho_w \mu A^z}{\rho V} \cdot (t - t^0)}], \end{cases} \tag{7}$$

where we denoted as $v_\infty^z = \frac{gV(\rho - \rho_w)}{K\rho_w \mu A^z}$ $[\mathrm{m/s}]$ the *terminal velocity* along z, which is computed by imposing in (5) the following force equilibrium, $F_W^z + F_B^z + F_R^z = 0$, i.e., $\ddot{z} = 0$ in (6).

Let us now generalize this result by considering the more realistic case in which the velocity of the ocean current depends on depth, i.e., $\vec{\mathbf{v}}_\mathbf{c} = (v_c^x(z), v_c^y(z), 0)$. There are two types of marine currents each caused by a range of distinct drivers, *non tidal* ocean currents, such as the Gulf Stream, and *tidal* streams. The complex hydrodynamic system of currents is powered by many forces, the crux being the playoff between the joint forces of solar heating of tropical surface waters and the polar contributions of cold fresh water ice-melt flooding into the ocean and the general cooling of the salty ocean water. While studying the global current systems makes up the larger part of the science of *oceanography*, in this chapter we focus on the effect of *local streams* in the monitored volume region. In particular, we consider an ocean volume with constant depth z^H (*flat bottom*), and H different ocean current layers $h = 1, ..., H$, of width Δz^h. We model the current on each plane xy in a layer h to be a piecewise constant function with module v_c^h and angular deviation from the x-axes α_c^h, as depicted in Fig. 12. This allows us to model the *thermohaline circulation* (also known as the ocean's conveyor belt), i.e., deep ocean current, sometimes called *submarine rivers*, that flows with constant velocity and direction within certain depths, driven by density and temperature gradients.

Given these assumptions, our objective is to calculate the horizontal displacement of a sinking object on the x- and y-axes in each of the layers it sinks through. To accomplish this, we recursively apply the solution (7) to the dynamic system (6) to each layer, using as initial conditions of the object the final position and velocity computed in the previous layer. If we denote the initial position of object n as $(x_n^0, y_n^0, 0)$ and its velocity as $(\dot{x}_n^0, \dot{y}_n^0, \dot{z}_n^0)$,

given all its physical characteristics such as volume V_n, density ρ_n, cross-sections A_n^{xy} and A_n^z, and horizontal and vertical shape factors, μ_n and σ_n, respectively, we can track the position of n while it sinks. Specifically, we have

$$\begin{cases} x_n(t) = x_n^0 + \sum_{i=1}^{h-1} \Delta x_n^i + v_c^h \cos\alpha_c^h \cdot (t - t_n^{h-1}) + \\ \quad + \frac{\dot{x}_n(t_n^{h-1}) - v_c^h \cos\alpha_c^h}{C\sigma_n A_n^{xy}/\rho_n V_n} \cdot [1 - e^{-\frac{C\sigma_n A_n^{xy}}{\rho_n V_n} \cdot (t - t_n^{h-1})}] \\ y_n(t) = y_n^0 + \sum_{i=1}^{h-1} \Delta y_n^i + v_c^h \sin\alpha_c^h \cdot (t - t_n^{h-1}) + \\ \quad + \frac{\dot{y}_n(t_n^{h-1}) - v_c^h \sin\alpha_c^h}{C\sigma_n A_n^{xy}/\rho_n V_n} \cdot [1 - e^{-\frac{C\sigma_n A_n^{xy}}{\rho_n V_n} \cdot (t - t_n^{h-1})}] \\ t_n^{h-1} \le t \le t_n^h \\ z_n(t) = \min\{v_{\infty n}^z \cdot (t - t_n^0) + \\ \quad + [\dot{z}_n^0 - v_{\infty n}^z] \cdot [1 - e^{-\frac{K\rho_w \mu_n A_n^z}{\rho_n V_n} \cdot (t - t_n^0)}]; z^H\}, \end{cases} \tag{8}$$

where t_n^0 and t_n^h are the instants object n is released on the ocean surface and exits layer h, respectively. More precisely, t_n^h is the instant for which it holds $z_n(t_n^h) = z^h = \sum_{i=1}^{h} \Delta z^i$, i.e., the depth of the object coincides with the sum of the width Δz^i of each layer i the object sank through, as shown in Fig. 12.

In (8), the total displacement on the x- and y-axes when the sinking object is inside layer h is *recursively* computed as the sum of the displacements in each of the $h-1$ previously crossed layers $i = 1, ..., h-1$, plus the displacement in layer h itself. These displacements are determined as partial solution of the dynamic system (6) in each layer, and have the following structure,

$$\begin{cases} \Delta x_n^i = v_c^i \cos\alpha_c^i \cdot (t_n^i - t_n^{i-1}) + \\ \quad + \frac{\dot{x}_n(t_n^{h-1}) - v_c^h \cos\alpha_c^h}{C\sigma_n A_n^{xy}/\rho_n V_n} \cdot [1 - e^{-\frac{C\sigma_n A_n^{xy}}{\rho_n V_n} \cdot (t_n^i - t_n^{i-1})}] \\ \Delta y_n^i = v_c^i \sin\alpha_c^i \cdot (t_n^i - t_n^{i-1}) + \\ \quad + \frac{\dot{y}_n(t_n^{h-1}) - v_c^h \sin\alpha_c^h}{C\sigma_n A_n^{xy}/\rho_n V_n} \cdot [1 - e^{-\frac{C\sigma_n A_n^{xy}}{\rho_n V_n} \cdot (t_n^i - t_n^{i-1})}]. \end{cases} \tag{9}$$

Finally, to be able to determine the position of object n from (8), we need to substitute in (8) and (9) the x- and y-component of the velocity the object has when it enters layer $h = 1, ..., H$, i.e., $(\dot{x}_n(t_n^{h-1}), \dot{y}_n(t_n^{h-1}))$, which can be computed as exit velocity from layer

$h-1$ by solving (6). We report these velocities in the following,

$$\begin{cases} \dot{x}_n(t_n^{h-1}) = v_c^{h-1}\cos\alpha_c^{h-1} + \\ +[\dot{x}_n(t_n^{h-2}) - v_c^{h-1}\cos\alpha_c^{h-1}]\cdot e^{-\frac{C\sigma_n A_n^{xy}}{\rho_n V_n}\cdot(t_n^{h-1}-t_n^{h-2})} \\ \dot{y}_n(t_n^{h-1}) = v_c^{h-1}\sin\alpha_c^{h-1} + \\ +[\dot{y}_n(t_n^{h-2}) - v_c^{h-1}\sin\alpha_c^{h-1}]\cdot e^{-\frac{C\sigma_n A_n^{xy}}{\rho_n V_n}\cdot(t_n^{h-1}-t_n^{h-2})}, \end{cases} \tag{10}$$

which can be recursively computed given that $\dot{x}_n(t_n^0)$ and $\dot{y}_n(t_n^0)$ are the known initial velocities on the surface.

Equations (8), (9), and (10) allow us to track the dynamic position of object n while it sinks, given complete knowledge about the structure of the currents in the volume of interest. In practice, however, we may only leverage some statistical information on the currents, which can be used to estimate the final position of a deployed object. While this offers a mathematical tool to study the dynamic of a sinking object, our ultimate objective is to be able to infer the statistical sensing and communication properties of a two-dimensional sensor network that reaches the ocean bottom, as will be discussed in the following section.

3.4.3 Communication Properties of 2D UW-ASNs

In this section, we characterize the different sinking behavior of sensors and uw-gateways, with the objective of describing: i) the average horizontal displacement of sensors and uw-gateways when different depths and current velocities are considered; ii) the main properties of the clusters that have an uw-gateway as cluster head, e.g., study the maximum and average sensor-gateway distance when the number of deployed gateways varies; iii) the average and standard deviation of number of sensors in each cluster.

Let us consider a set of sensors $\mathcal{S}$ with cardinality $S = |\mathcal{S}|$ characterized by the same density $\rho_{\mathcal{S}}$, volume V_S, cross-sections $A_{\mathcal{S}}^{xy}$ and $A_{\mathcal{S}}^{z}$, and shape factors $\mu_{\mathcal{S}}$ and $\sigma_{\mathcal{S}}$, and a set of uw-gateways $\mathcal{G}$ with $G = |\mathcal{G}|$, in general with different values of $\rho_{\mathcal{G}}$, $V_{\mathcal{G}}$, $A_{\mathcal{G}}^{xy}$, $A_{\mathcal{G}}^{z}$, $\mu_{\mathcal{G}}$, and $\sigma_{\mathcal{G}}$. Given the matrices of the known initial positions of the deployed sensors

and uw-gateways, $\underline{\mathbf{P_S^0}} = [\mathbf{P_1^0}|\cdots|\mathbf{P_s^0}|\cdots|\mathbf{P_S^0}]^T$ and $\underline{\mathbf{P_G^0}} = [\mathbf{P_1^0}|\cdots|\mathbf{P_g^0}|\cdots|\mathbf{P_G^0}]^T$, respectively, where $\mathbf{P_s^0} = [x_s^0\ y_s^0\ 0]^T\ \forall s \in \mathcal{S}$ and $\mathbf{P_g^0} = [x_g^0\ y_g^0\ 0]^T\ \forall g \in \mathcal{G}$ are position column vectors, and the matrices of their known initial velocities, $\underline{\mathbf{v_S^0}} = [\mathbf{v_1^0}|\cdots|\mathbf{v_s^0}|\cdots|\mathbf{v_S^0}]^T$ and $\underline{\mathbf{v_G^0}} = [\mathbf{v_1^0}|\cdots|\mathbf{v_g^0}|\cdots|\mathbf{v_G^0}]^T$, where $\mathbf{v_s^0} = [\dot{x}_s^0\ \dot{y}_s^0\ \dot{z}_s^0]^T\ \forall s \in \mathcal{S}$ and $\mathbf{v_g^0} = [\dot{x}_g^0\ \dot{y}_g^0\ \dot{z}_g^0]^T\ \forall g \in \mathcal{G}$ are velocity column vectors, the final positions on the ocean bottom of the sensors and uw-gateways, $\underline{\mathbf{P_S^f}}$ and $\underline{\mathbf{P_G^f}}$, respectively, can be derived using (8), (9), and (10) when all deployed devices have reached the bottom, i.e., when $t = t^f \geq \max\{\max_{s\in\mathcal{S}} t_s^H; \max_{g\in\mathcal{G}} t_g^H\}$. Specifically,

$$\underline{\mathbf{P_S^f}} = \underline{\mathbf{P_S^0}} + \underline{\mathbf{\Delta P}_\mathcal{S}}(\underline{\mathbf{v_S^0}}), \quad \underline{\mathbf{P_G^f}} = \underline{\mathbf{P_G^0}} + \underline{\mathbf{\Delta P}_\mathcal{G}}(\underline{\mathbf{v_G^0}}) \tag{11}$$

where $\mathbf{\Delta P}_\mathcal{S}(\mathbf{v_S^0})$ and $\mathbf{\Delta P}_\mathcal{G}(\mathbf{v_G^0})$ are matrices accounting for the total displacements accumulated while the sensors and uw-gateways, respectively, were sinking through the ocean current layers, i.e.,

$$\underline{\mathbf{\Delta P}_\mathcal{S}} = \begin{bmatrix} . & \sum_{h=1}^H \Delta x_s^h & . \\ . & \sum_{h=1}^H \Delta y_s^h & . \\ . & z^H & . \end{bmatrix}^T, \underline{\mathbf{\Delta P}_\mathcal{G}} = \begin{bmatrix} . & \sum_{h=1}^H \Delta x_g^h & . \\ . & \sum_{h=1}^H \Delta y_g^h & . \\ . & z^H & . \end{bmatrix}^T. \tag{12}$$

In (12), each element can be computed as in (9). Note that the dependence on the initial velocity in (12) has been omitted for the sake of notation simplicity.

In Fig. 13, we show the expected horizontal displacement $\Delta d = \sqrt{\Delta x^2 + \Delta y^2}$ of sensors and uw-gateways when different depths and current velocities are considered. In particular, we consider $\rho_s = 2000\,\mathrm{kg/m^3}$, $\rho_g = 2500\,\mathrm{kg/m^3}$, $V_s = 0.5 \cdot 10^{-3}\,\mathrm{m^3}$, and $V_g = 10^{-3}\,\mathrm{m^3}$ to account for the common physical characteristics of underwater sensor nodes and uw-gateways, which reflect into different sinking properties, as formalized in (11). Note that gateways accumulate smaller displacements than sensors since their sinking times are shorter. In Fig. 14, we depict the maximum and average sensor-gateway distance when the number of deployed gateways increases. In particular, we consider three deployment volumes ($V_1 = 100\text{x}100\text{x}50\,\mathrm{m^3}$, $V_2 = 300\text{x}200\text{x}100\,\mathrm{m^3}$, and $V_3 = 1000\text{x}1000\text{x}500\,\mathrm{m^3}$) and a one-layer current scenario ($H = 1$) with $v_c^{max} = 1\,\mathrm{m/s}$.

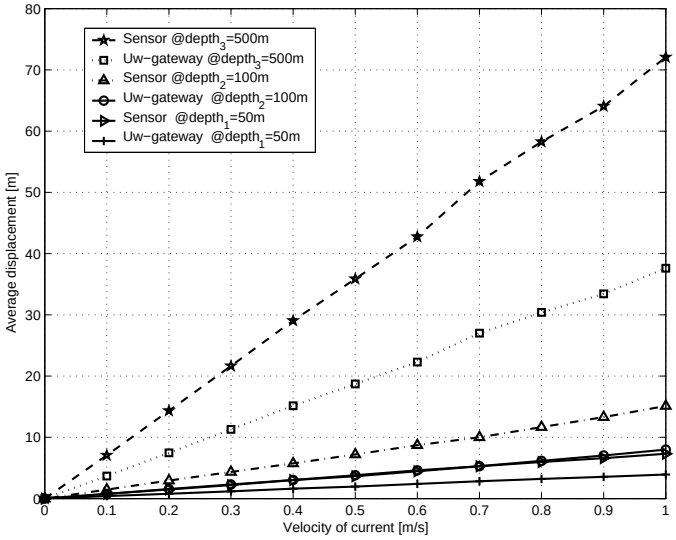

Figure 13: Average horizontal displacement of sensors and uw-gateways vs. current velocity (for three different depths)

According to the specific sensor transmission range t, Fig. 14 allows setting the minimum number of uw-gateways that need to be deployed. In Fig. 15, we present the normalized average and standard deviation of number of sensors per uw-gateway when two deployment strategies are considered, the *random* and the *grid deployment*. Interestingly, while the average number of sensors does not depend on the deployment strategy, the sensor dispersion is much lower in a grid structure, independently on the number of gateways deployed. This is a general result that does not depend on the considered scenario.

3.4.4 Deployment Surface Area: Side Margins

In this section, we compute the deployment surface area where sensors should be deployed, when a 2D target area needs to be covered on the bottom of the ocean. As described in Sections 3.4.2 and 3.4.3, ocean currents may significantly modify the sinking trajectories of sensors and uw-gateways. Therefore, the surface deployment should take into account the effect of the currents, to position as many deployed sensors inside the target area as possible. To achieve this, in the following we consider a *worst-case scenario* where the effect of currents, in terms of sensor displacements, is captured. The objective is to dimension the

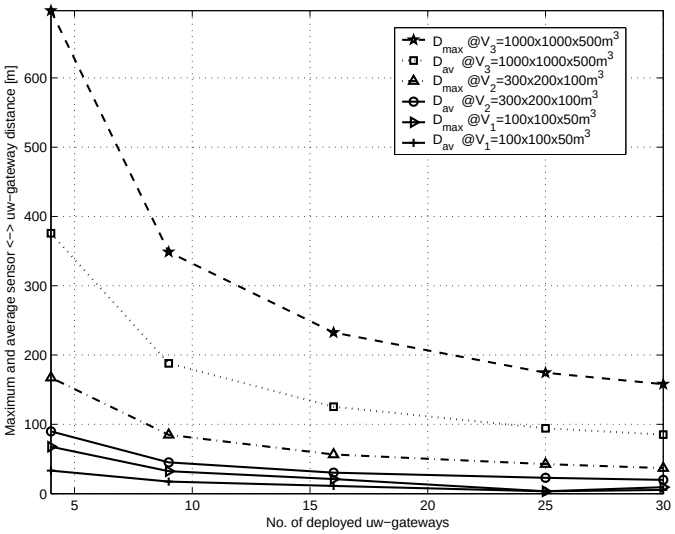

Figure 14: Maximum and average sensor-gateway distance vs. number of deployed gateways (in three different volumes, and with $v_c^{max} = 1\,\mathrm{m/s}$)

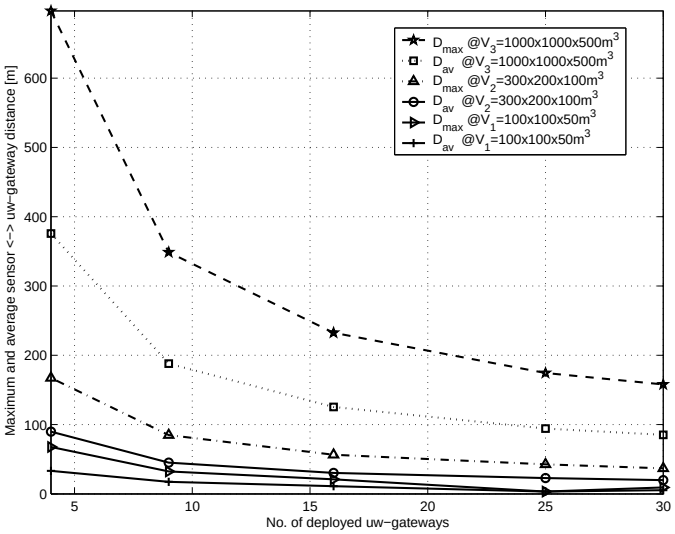

Figure 15: Normalized average and standard deviation of number of sensors per uw-gateway vs. number of deployed gateways (for grid and random deployment strategies, in three different volumes, and with $v_c^{max} = 1\,\mathrm{m/s}$)

deployment surface area, i.e., to asses proper *surface side margins*.

With reference to Fig. 16, we consider a bottom target area with sides l and h, and analyze the two cases of *unknown current direction* (a), where we denote as $\Delta d_{max} = \sqrt{\Delta x_{max}^2 + \Delta y_{max}^2}$ the maximum horizontal displacement a sinking sensor can experience, i.e., how far in the horizontal plane xy a sensor can drift (see Fig. 12), and *known current direction* (b), where we denote as Δd_{max} the same metric used in the previous case and as $\Delta\alpha_{max}$ the maximum angular deviation of the current from its known direction β, which is the angle the direction of the current forms with side h of the target area, as depicted in Fig. 16(b). Note that, without loss in generality, it always holds that $\beta \in [0, \pi/2)$. More specifically, the dotted *circular sector* in Fig. 16(b), characterized by radius Δd_{max} and angle $2\Delta\alpha_{max}$, represents the region of the ocean bottom that may be reached by a sensor that is deployed on the ocean surface exactly on the vertex of the circular sector itself. This region represents the statistical uncertainty in the final anchor position of a sensor caused by drifting due to ocean currents during the sinking.

As far as the side margins in the unknown current direction case are concerned, from geometric properties of Fig. 16(a) it holds,

$$\begin{cases} l^* = l + 2\Delta d_{max} \\ h^* = h + 2\Delta d_{max}, \end{cases} \tag{13}$$

while for the known current direction case (Fig. 16(b)) it holds,

$$\begin{cases} l^* = l + \Delta d_{max} \cdot \{\max\left[0; \sin(\beta - \Delta\alpha_{max})\right] + \sin(\beta + \Delta\alpha_{max})\} \\ h^* = h + \Delta d_{max} \cdot \{\max\left[\cos(\beta - \Delta\alpha_{max}); \cos(\beta + \Delta\alpha_{max})\right]\}. \end{cases} \tag{14}$$

In (13) and (14), the worst-case maximum displacement and maximum angular deviation a sensor can experience are,

$$\Delta d_{max} = \frac{z^H}{H \cdot v_\infty^z} \cdot \sum_{h=1}^{H} v_c^{h,max} \tag{15}$$

$$\Delta\alpha_{max} = \arctan \frac{\sum_{h=1}^{H} v_c^{h,max} \cdot \sin \alpha_c^{h,max}}{\sum_{h=1}^{H} v_c^{h,max} \cdot \cos \alpha_c^{h,max}}, \tag{16}$$

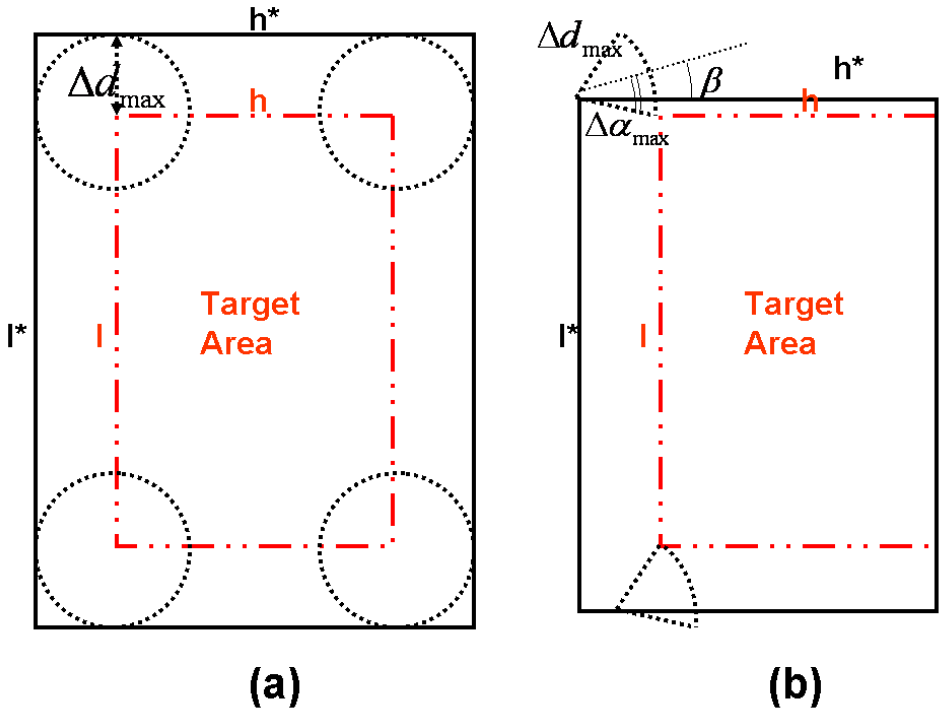

Figure 16: Deployment surface area for unknown (a) and known (b) current direction β, given a bottom target area lxh

where z^H is the ocean depth, H is the number of ocean current layers, v_∞^z is the terminal velocity (see Section 3.4.2), and $v_c^{h,max}$ and $\alpha_c^{h,max}$ are the maximum current velocity and angular deviation in layer h, respectively. The mathematical derivation of (14), (15), and (16) is omitted for lack of space. Interestingly, given the same target area, the side surface margins in the unknown current direction case (13) are larger than those computed if some information about the current direction can be leveraged (14). This is also shown in Fig. 16, where the surface areas (outside solid rectangles) in the two cases are noticeably different, while the target area (inside dotted rectangle) is the same.

3.4.5 Reliability Margin

In this section, we provide an estimate of the number of redundant sensors required to endow the network with robustness to node failures, which in the underwater may be caused by fouling and corrosion. In particular, we study the required topology redundancy to

Table 3: Redundant sensors ΔN^* to compensate for failures

Obs. Time T [days]	**30**	**60**	**90**	**120**	**150**	**180**
$\Gamma_1^* = 0.90$	2	4	5	7	8	9
$\Gamma_2^* = 0.95$	3	5	6	7	9	10
$\Gamma_3^* = 0.99$	4	6	8	9	11	12

statistically compensate for node failures within a predetermined observation period, i.e., the length of the monitoring mission. If we assume node failures to be independent and occurring according to a Poisson distribution, the minimum number of redundant sensors ΔN^* to be deployed to compensate for Poissonian failures is,

$$\sum_{n=0}^{\Delta N^*} \frac{(\lambda T)^n \cdot e^{-\lambda T}}{n!} \geq \Gamma^*, \tag{17}$$

where $\lambda\,[\mathrm{day}^{-1}]$ represents the sensor failure rate, $T\,[\mathrm{day}]$ the observation time, n the number of sensors that experience a failure within the observation time, and Γ^* the target success probability, i.e., the probability that no more than ΔN^* failures be experienced during the observation time. Table 3 reports the number of redundant sensors that need to be deployed to compensate for Poisson sensor failures occurring during several observation times under three different success probabilities, when $\lambda = 1/(365/12)\,\mathrm{day}^{-1}$, i.e., in average a sensor experiences one failure every month.

3.5 Deployment in a 3D Environment

In this section, we propose three deployment strategies for three-dimensional UW-ASNs to obtain a target *1-coverage* $\eta_1^* = \eta^*$ of the 3D region, i.e., the *3D-random*, the *bottom-random*, and the *bottom-grid* strategies. As previously discussed, it is shown in [74] that the sensing range r required for 1-coverage is greater than the transmission range t that guarantees network connectivity. Since in typical applications $t \geq r$, the network is guaranteed to be connected when 1-coverage is guaranteed. Thus, in the following we focus on the sensing coverage. In all these deployment strategies, winch-based sensor devices are

anchored to the bottom of the ocean in such a way that they cannot drift with currents. Sensor devices are equipped with a floating buoy that can be inflated by a pump by means of an electronically controlled engine that resides on the sensor. This way, they can adjust their depth and float at different depths in order to observe a given phenomenon, as described in Section 3.3.2. In all the proposed deployment strategies, described hereafter, sensors are assumed to know their final positions by exploiting localization techniques.

3D-random. This is the simplest deployment strategy, and does not require any form of coordination from the surface station. Sensors are randomly deployed on the bottom of the 3D volume, where they are anchored. Then, each sensor randomly chooses its depth, and, by adjusting the length of the wire that connects it to the anchor, it floats to the selected depth. Finally, each sensor informs the surface station about its final position.

Bottom-random. As in the previous strategy, sensors are randomly deployed on the bottom, where they are anchored. Differently from the 3D-random scheme, the surface station is informed about their position on the bottom. Then, the surface station calculates the depth for each sensor in order to achieve the target 1-coverage ratio η^*. Finally, each sensor is assigned its target depth and floats to the desired position.

Bottom-grid. This deployment strategy needs to be assisted by one or multiple AUVs, which deploy the underwater sensors to predefined target locations to obtain a grid deployment on the bottom of the ocean. Each sensor is also assigned a desired depth by the AUV and accordingly floats to achieve the target coverage ratio η^*.

Algorithm 1 reports the pseudo code of the procedure run on the surface station to find the optimal depths of the sensor nodes, for the bottom-random and bottom-grid strategies. The positions of the sensor nodes are represented by a matrix $\underline{\mathbf{P}} = [\mathbf{P_1} \,|\, \mathbf{P_i} \,|\, \mathbf{P_{N-1}}]^T$, where $\mathbf{P_i}$ represents the 3D coordinates of the i^{th} sensor. The N^{th} node (also N for simplicity) represents the sink, which is located on the surface of the ocean. For example, $\mathbf{P_i}(3)$ represents the z coordinate of the i^{th} sensor. We refer to a discrete set of values, equally spaced with step $step_z$ between 0 (surface) and z_{max} (ocean bottom), for the depth of the

sensor nodes. The function $\hat{\eta}(\underline{\mathbf{P}},\ \mathcal{A},\ r)$ estimates the coverage ratio η given the positions of the sensors $\underline{\mathbf{P}}$, the target volume $\mathcal{A}$, and their sensing range r.

Algorithm 1 3D Coverage Optimization

```
while (h ≤ max_steps and η < η*) do
  for (i = 1; i < N; i++) do
    for (j = 0; j ≤ z_max/step_z; j++) do
      z_old = P_i(3)
      P_i(3) = j * step_z
      η_new = η̂(P, A, r)
      if (η_new > η) then
        η = η_new
      else
        P_i(3) = z_old
      end if
    end for
  end for
  h++
end while
```

In the following we calculate the minimum number of sensors needed to achieve a desired target 1-coverage ratio η^* for the proposed deployment strategies. As shown in Figs. 17-19, given a fixed number of sensors we achieve a better coverage ratio with increasing complexity of the deployment strategy. In fact, the coverage ratio obtained with the bottom-grid strategy is greater than the coverage ratio obtained with the bottom-random strategy, which is in turn greater than the coverage ratio of the 3D-random strategy. Moreover, given a target coverage ratio, the minimum number of sensors needed to achieve the desired coverage ratio decreases with the complexity of the deployment strategy. Figure 20 shows a comparison between the minimum normalized sensing range that guarantees coverage ratios of 1 and 0.9 with the bottom-random strategy and the theoretical bound on the minimum normalized sensing range derived in [74], where the authors investigate sensing and communication coverage in a 3D environment. According to Theorem 4 in [74], the 3D volume is guaranteed to be *asymptotically almost surely* 1-covered iff $\frac{4}{3}\pi\frac{n}{V}r^3 = \ln n + \ln\ln n + \omega(n)$, with $1 << \omega(n) << \ln\ln n$, where V is the volume

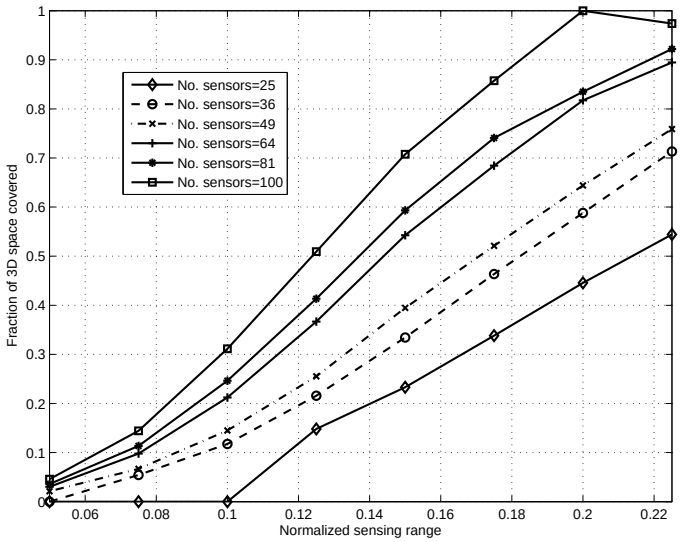

Figure 17: *Three-dimensional scenario.* 3D coverage with a 3D random deployment

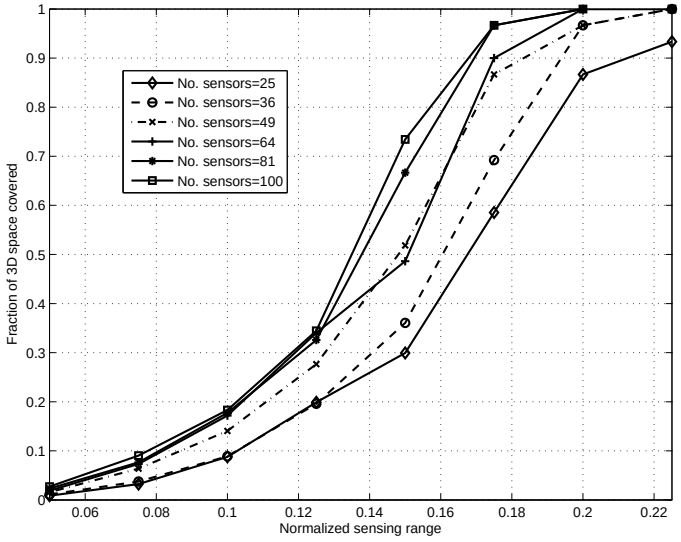

Figure 18: *Three-dimensional scenario.* Optimized 3D coverage with a 2D bottom-random deployment

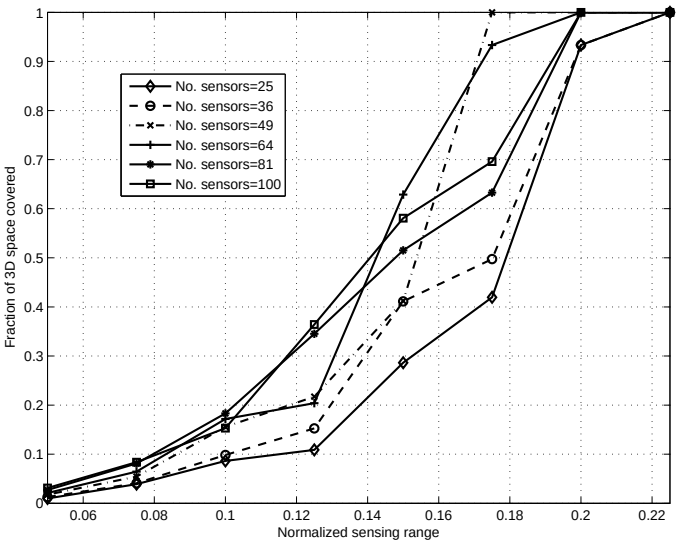

Figure 19: *Three-dimensional scenario.* Optimized 3D coverage with a 2D bottom-grid deployment

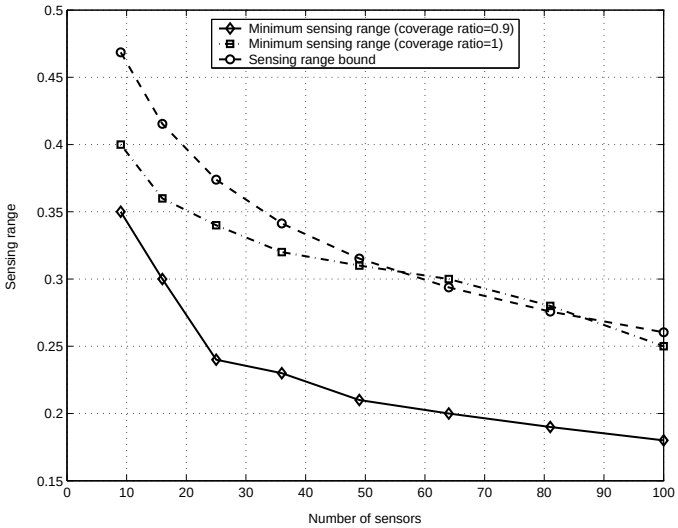

Figure 20: Theoretical and experimental sensing range

of the region to be covered, n the number of deployed sensors, and r their sensing range. Hence, to draw Fig. 20 we set $\omega(n) = \frac{1+\ln\ln n}{2}$. This shows that the bottom-random deployment strategy very closely approximates the theoretically predicted bound, i.e., the minimum sensing range that guarantees 1-coverage with probability 1 is almost the same as that predicted by the model in [74].

CHAPTER IV

DISTRIBUTED ROUTING ALGORITHMS FOR UNDERWATER ACOUSTIC SENSOR NETWORKS

4.1 Preliminaries

Many researchers are currently engaged in developing networking solutions for terrestrial wireless ad hoc and sensor networks. Although there exist many recently developed network protocols for wireless sensor networks, the unique characteristics of the underwater acoustic communication channel, such as limited bandwidth capacity and high propagation delays [70], require new efficient and reliable data communication protocols. Major challenges in the design of UW-ASNs are: i) the propagation delay is five orders of magnitude higher than in radio frequency (RF) terrestrial channels, and variable; ii) the underwater acoustic channel is severely impaired, especially because of multipath and fading; iii) the available bandwidth is limited; iv) high bit error rates and temporary losses of connectivity (shadow zones) can be experienced; v) underwater sensors are prone to failures because of fouling and corrosion; vi) battery power is limited and usually batteries cannot be easily recharged, also because solar energy cannot be exploited.

Most impairments of the underwater acoustic channel are adequately addressed at the physical layer, by designing receivers able to deal with high bit error rates, fading, and the inter-symbol interference (ISI) caused by multipath. Conversely, characteristics such as the extremely long and variable propagation delays are better addressed at higher layers. For example, the delay variance in horizontal acoustic links is generally larger than in vertical links due to multipath [82]. In fact, the quality of acoustic links is highly unpredictable, since it mainly depends on fading and multipath, which are not easily modeled phenomena.

Moreover, as in terrestrial sensor networks, energy conservation is one of the major concerns, since batteries cannot be easily recharged or replaced. Finally, the bandwidth of the underwater links is severely limited, and, differently from the terrestrial case, dependent on the link distance [87]. Hence, routing protocols designed for underwater acoustic networks must be extremely bandwidth and energy efficient.

In this chapter, we propose two geographical routing algorithms for the 3D underwater environment that are designed to distributively meet the requirements of delay-insensitive and delay-sensitive underwater sensor network applications. The proposed distributed routing solutions are tailored for the characteristics of the underwater environment, e.g., they take explicitly into account the very high propagation delay, which may vary in horizontal and vertical links, the different components of the transmission loss, the impairment of the physical channel, the extremely limited bandwidth, the high bit error rate, and the limited battery energy. These characteristics lead to very low efficiencies of the underwater acoustic channel when a common random access technique is adopted to transmit a data packet.

Conversely, our routing solutions allow achieving two apparently conflicting objectives, i.e., increasing the efficiency of the acoustic channel by transmitting a *train* of short packets *back-to-back*; and limiting the packet error rate by keeping the length of the transmitted packets short. The packet-train concept is exploited in the routing algorithms proposed in this chapter. The algorithms are distributed routing solutions for delay-insensitive and delay-sensitive applications, and allow each node to *jointly* select its best next hop, the optimal transmitted power, and the forward error correction (FEC) rate for each packet, with the objective of minimizing the energy consumption, while taking the condition of the underwater channel and the application requirements into account.

The first routing algorithm deals with delay-insensitive applications, and sets the optimal combination of transmitting power and FEC strength in such a way as to exploit those links that can guarantee a low packet error rate to maximize the probability that a

packet is correctly decoded at the receiver, thus minimizing the number of required packet retransmissions and the overall energy required for successful transmissions.

The second routing algorithm is designed for delay-sensitive applications. The objective is to minimize the energy consumption, while statistically limiting the end-to-end packet delay and packet error rate. To accomplish this, the algorithm estimates at each hop the time to reach the sink and leverages statistical properties of underwater links. As in the previous delay-insensitive routing solution, each node jointly selects its best next hop, the transmitted power, and the forward error correction rate for each packet. However, differently from the first routing algorithm, in order to meet the delay-sensitive application requirements, next hops are selected by also considering maximum per-packet allowed delay. In addition, unacknowledged packets are not retransmitted to limit the delay.

In both routing algorithms, the emphasis on energy consumption is justified by the need for extended lifetime deployments of underwater sensor networks. While survivability is another fundamental aspect of sensor networks, this has been dealt with in [65], where a two-phase resilient routing algorithm for long-term applications in UW-ASNs was proposed.

In addition, we propose an optimization problem to set the packet size for underwater communications when a particular forward error correction scheme is adopted, given the 3D volume of water that the application needs to monitor, the density of the sensor network, and the application requirements.

The remainder of this chapter is organized as follows. In Section 4.2, we discuss the suitability of the existing ad hoc and sensor routing solutions for the underwater environment, and motivate the use of geographical routing in this environment. In Section 4.3, we introduce the network and propagation models. In Section 4.4, we analyze the packet-train concept to improve the underwater acoustic channel efficiency, and cast the optimal packet size problem for underwater communications when a particular FEC scheme is adopted. In Section 4.5, we introduce a distributed routing algorithm for delay-insensitive applications,

while in Section 4.6 we adapt it to statistically meet the end-to-end delay-sensitive application requirements. Finally, in Section 4.7 we show the performance results of the proposed solutions.

4.2 Related Work

Some recent papers propose network layer protocols specifically tailored for underwater acoustic networks. In [92], a routing protocol is proposed that autonomously establishes the underwater network topology, controls network resources, and establishes network flows, which relies on a centralized network manager running on a surface station. The manager establishes efficient data delivery paths in a centralized fashion, which allows avoiding congestion and providing some form of quality of service guarantee. Although the idea is promising, the performance of the proposed mechanisms has not been thoroughly studied. In [65], the problem of data gathering for three-dimensional underwater sensor networks tailored for long-term monitoring missions is investigated at the network layer. A two-phase resilient routing solution is developed, with the objective of guaranteeing survivability of the network to node and link failures. In the first phase, energy-efficient node-disjoint primary and backup paths are optimally configured, by relying on topology information gathered by a surface station, while in the second phase paths are locally repaired in case of node failures. In [94], a vector-based forwarding routing is developed, which does not require state information on the sensors and only involves a small fraction of the nodes in routing. The proposed algorithm, however, does not consider applications with different requirements. In [81], the authors provide a simple design example of a shallow water network, where routes are established by a central manager based on neighborhood information gathered from all nodes by means of poll packets. However, the paper does not describe routing issues in detail, e.g., it does not discuss the criteria used to select data paths. Moreover, sensors are only deployed linearly along a stretch, while the characteristics of the 3D underwater environment are not investigated. In [91], a long-term monitoring

platform for underwater sensor networks consisting of static and mobile nodes is proposed, and hardware and software architectures are described. The nodes communicate point-to-point using a high-speed optical communication system, and broadcast using an acoustic protocol. The mobile nodes can locate and hover above the static nodes for data muling, and can perform useful network maintenance functions such as deployment, relocation, and recovery. However, due to the limitations of optical transmissions, communication is enabled only when the sensors and the mobile mules are in close proximity.

4.3 Network Models

The 3D underwater network can be represented as a graph $\mathcal{G}(\mathcal{V}, \mathcal{E})$, where $\mathcal{V} = \{v_1, .., v_N\}$ is a finite set of nodes in a finite-dimension 3D volume, with $N = |\mathcal{V}|$, and $\mathcal{E}$ is the set of links among nodes, i.e., e_{ij} equals 1 if nodes v_i and v_j are within each other's transmission range. Node v_N (also N for simplicity) represents the sink, i.e., the surface station. Each link e_{ij} is associated with its mean propagation delay $\overline{T_{ij}^q}$ and with the standard deviation of the propagation delay, σ_{ij}^q. In [90], the underwater acoustic propagation speed $q(z, S, t)\,[\mathrm{m/s}]$ is accurately modeled as

$$\begin{aligned} q(z,S,t) = 1449.05 + 45.7 \cdot t - 5.21 \cdot t^2 + 0.23 \cdot t^3 + \\ +(1.333 - 0.126 \cdot t + 0.009 \cdot t^2) \cdot (S - 35) + 16.3 \cdot z + 0.18 \cdot z^2, \end{aligned} \tag{18}$$

where $t = T/10$ (T is the temperature in $^\circ\mathrm{C}$), S is the salinity in ppt, and z is the depth in km. The above expression provides a useful tool to determine the propagation speed, and thus the propagation delay, in different operating conditions, and yields values in $[1460, 1520]\,\mathrm{m/s}$. Note that all these values, i.e., e_{ij}, $\overline{T_{ij}^q}$ and σ_{ij}^q, are dependent on the 3D positions of nodes v_i and v_j (also i and j for simplicity in the following). Finally, $\mathcal{S}$ is the set of sources, which includes those sensors that sense information from the underwater environment and send it to the surface station N.

The underwater transmission loss describes how the acoustic intensity decreases as an acoustic pressure wave propagates outwards from a sound source. The transmission loss

$TL(d, f)\,[\mathrm{dB}]$ that a narrow-band acoustic signal centered at frequency $f\,[\mathrm{kHz}]$ experiences along a distance $d\,[\mathrm{m}]$ can be described by the Urick propagation model [90],

$$TL(d, f) = \chi \cdot 10Log(d) + \alpha(f) \cdot d + A. \tag{19}$$

In (19), the first term account for *geometric spreading*, which refers to the spreading of sound energy as a result of the expansion of the wavefronts. It increases with the propagation distance and is independent of frequency. There are two kinds of geometric spreading: *spherical* (omni-directional point source, spreading coefficient $\chi = 2$), which characterizes deep water communications, and *cylindrical* (horizontal radiation only, spreading coefficient $\chi = 1$), which characterizes shallow water communications. In-between cases show a spreading coefficient χ in the interval $(1, 2)$, depending on water depth and link length. The second term accounts for *medium absorption*, where $\alpha(f)\,[\mathrm{dB/m}]$ represents an absorption coefficient that describes the dependency of the transmission loss on the frequency band (see Fig. 21). Finally, the last term, expressed by the quantity $A\,[\mathrm{dB}]$, is the so-called *transmission anomaly*, and roughly accounts for the degradation of the acoustic intensity caused by multiple path propagation, refraction, diffraction, and scattering of sound caused by particulates, bubbles, and plankton within the water column. Its value is higher for shallow-water horizontal links (up to $10\,\mathrm{dB}$), which are more affected by multipath [90]. More details can be found in [28] and [43].

4.4 Packet Train and Optimal Packet Size

In this section, we study the effect of the characteristics of the underwater environment on the acoustic channel utilization efficiency and provide guidelines for the design of routing solutions. Specifically, when a common random access technique is adopted to transmit a data packet in the shared acoustic medium, a trade-off between channel efficiency and packet size occurs. Conversely, our routing solutions allow achieving two apparently conflicting objectives, i.e., increasing the efficiency of the acoustic channel by transmitting a *train* of short packets *back-to-back*; and limiting the packet error rate by keeping the

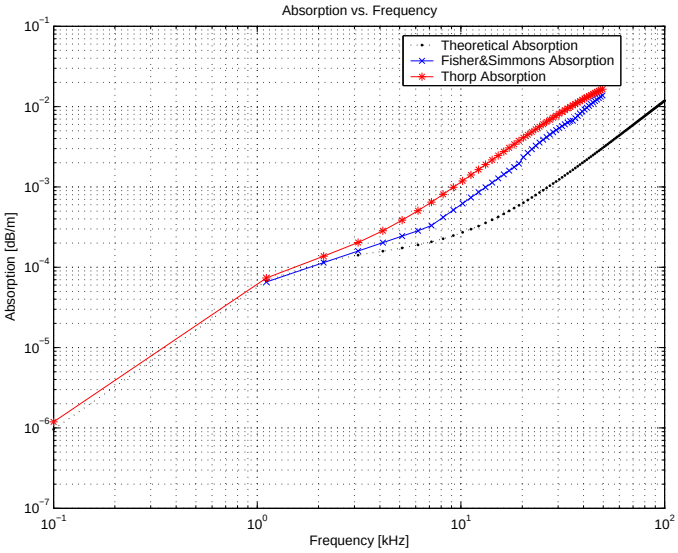

Figure 21: Theoretical, Fisher&Simon's, and Thorp's medium absorption coefficient $\alpha(f)$ vs. frequency $f \in [10^{-1}, 10^{2}]\,\mathrm{kHz}$

length of the transmitted packets short. The packet-train concept is exploited in the routing algorithms proposed in this paper.

In particular, we analyze the *packet-train* scheme to enhance the channel efficiency and derive the optimal packet size. While the optimal packet size at the data link layer in an underwater channel has been analytically derived in [83], our analysis accounts for cross-layer interactions with medium access control (MAC) and forward error correction (FEC) schemes. The packet optimization analysis in [83], in fact, does not consider the additional overhead caused by the adopted FEC scheme, nor does it evaluate the number of required packet retransmissions, which depends on the experienced packet error rate (PER), i.e., on the state of the underwater channel.

4.4.1 Single-packet Transmission Scheme

We consider a shared channel where a device transmits a data packet when it senses the channel idle, and the corresponding device advertises a correct reception with a short acknowledge (ACK) packet, as shown in Fig. 22. We assume that the payload of the data packet to be transmitted has size L_P^D bits, while the header has size L_P^H bits. Moreover,

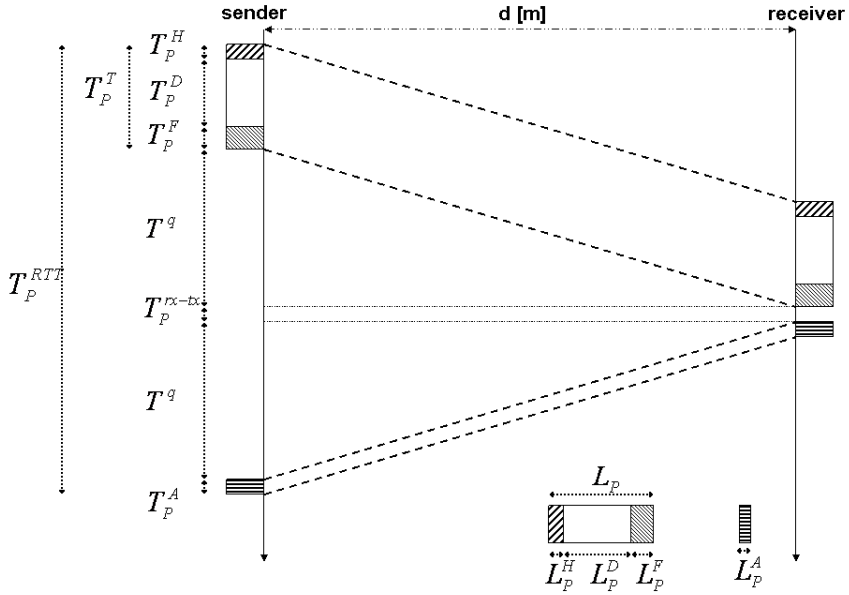

Figure 22: Single-packet transmission scheme

the packet may be protected with a FEC mechanism, which introduces a redundancy of L_P^F bits. The ACK packet is assumed to be L_P^A bits long. Given a transmission rate r, the *packet round-trip time* T_P^{RTT} is

$$T_P^{RTT} = T_P^H + T_P^D + T_P^F + 2 \cdot T^q + T_P^{rx-tx} + T_P^A, \tag{20}$$

where T_P^H, T_P^D, T_P^F, and T_P^A are the transmission times of the header, payload, FEC overhead, and ACK packet, respectively, while T^q is the propagation delay, and T_P^{rx-tx} is the time needed to process the packet and switch the circuitry from receiving to transmitting mode. We define the *channel utilization efficiency* η as

$$\eta = \frac{1}{r} \cdot \frac{L_P^D}{\hat{N}^{TX} \cdot T_P^{RTT}}, \tag{21}$$

where $\hat{N}^{TX}$ represents the average number of transmissions needed for the packet to be successfully decoded at the receiver, i.e.,

$$\hat{N}^{TX} = \frac{1}{1 - \psi^{\mathcal{F}}(L_P, L_P^F, BER)}, \tag{22}$$

where $\psi^{\mathcal{F}}()$ represents the *packet error rate* (PER) given the packet size L_P and the *bit error rate* (BER) on the link, when a FEC scheme $\mathcal{F}$ with redundancy L_P^F is adopted. Equation (22) assumes independent errors among adjacent packets, which holds when the channel coherence time is shorter than the average retransmission delay, i.e., the average time that a sender needs to retransmit an unacknowledged packet. We refer to the expression $r \cdot \eta = L_P^D/(\hat{N}^{TX} \cdot T_P^{RTT})$ in (21) as *effective link capacity* between the sender and the receiver; it represents the average bit rate achievable by a contention-free medium access control protocol when a single-packet transmission scheme is adopted.

By substituting (20) into (21), we obtain

$$\eta = \frac{L_P^D}{\hat{N}^{TX} \cdot [L_P^D + L_P^H + L_P^F + L_P^A + r \cdot (2\frac{d}{q} + T_P^{rx-tx})]}, \tag{23}$$

where the propagation delay T^q is expressed as the ratio between the distance d between the sender and the receiver, and the speed q of the signal in the medium, expressed in (18).

Figures 23 and 24 show the channel efficiency (23) for an underwater environment, where we set the speed of sound in water to $q = 1500\,\mathrm{m/s}$ (see Section 4.3), and the transmission rate to $r = 50\,\mathrm{Kbps}$ [82]. In particular, Fig. 23 refers to transmissions without forward error correction (i.e., $L_P^F = 0$), while Fig. 24 refers to a $(255, 239)$ Reed-Solomon (R-S) FEC [68]. Although a thorough study of the performance of different FEC schemes in the underwater environment is out of the scope of this work, we chose Reed-Solomon FEC since large block codes are easy to generate and provide excellent burst-error detection and correcting ability. Note that R-S codes are widely used in conjunction with Viterbi-decoded convolutional codes to correct the errors made by the Viterbi decoder. In fact, because of the nonlinear nature of Viterbi decoding, these errors occur in bursts even when channel errors are random, as with Gaussian noise. The bit error rate on the channel is assumed to be linearly increasing with decreasing signal-to-noise ratio (SNR), for the sake of simplicity. In particular, the BER is assumed to range in the interval $[10^{-2}, 10^{-6}]$, as indicated in [81]. In addition, errors are assumed to be uniformly distributed in time. The two figures consider a range of distances between $100\,\mathrm{m}$ and $500\,\mathrm{m}$. As can be seen in

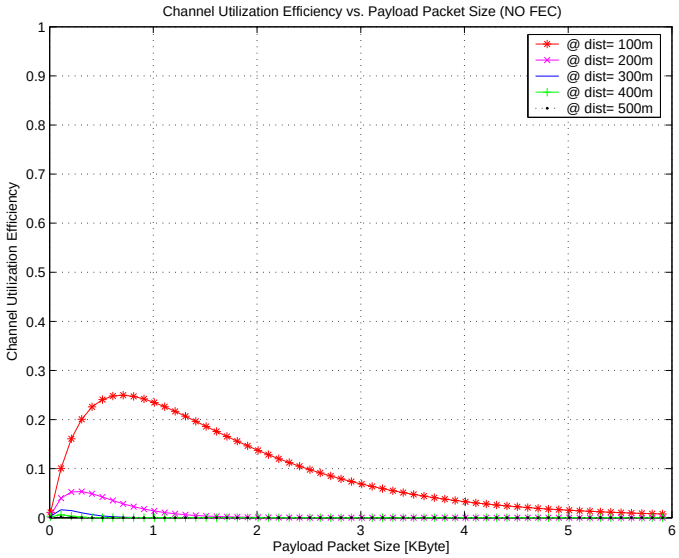

Figure 23: *Underwater and terrestrial channel utilization efficiency for different distances* $(100\,\mathrm{m} - 500\,\mathrm{m})$. Underwater channel efficiency vs. packet payload size without FEC

Fig. 23, the maximum channel efficiency is 0.25 over a distance of $100\,\mathrm{m}$ with packet payload size equal to about $0.8\,\mathrm{KByte}$, while it drops below 0.05 for distances greater than $200\,\mathrm{m}$. When we apply a $(255, 239)$ R-S FEC technique in the same environment, a maximum channel utilization efficiency of 0.77 can be achieved over $100\,\mathrm{m}$ with packet payloads of $5\,\mathrm{KByte}$. The efficiency degrades abruptly with increasing distance, and the optimal packet size, i.e., the packet size that yields maximum channel efficiency on a given distance, decreases as well. Larger packets tend to improve the channel efficiency; at the same time, given a bit error rate, the packet error rate increases with increasing packet size, thus increasing the average number of transmissions for a single packet. Hence, the optimal packet size is determined as the equilibrium between these two contrasting phenomena.

Figure 25 shows the same phenomena for a terrestrial radio channel, where we set the propagation speed q to $3 \cdot 10^8\,\mathrm{m/s}$ and the transmission rate r to $1\,\mathrm{Mbps}$. The bit error rate on the channel is assumed to be linearly increasing with decreasing SNR (between 10^{-3} and 10^{-7}). With respect to the underwater environment, the channel efficiency values are higher and degrade more smoothly with increasing distance. In general, the optimal packet

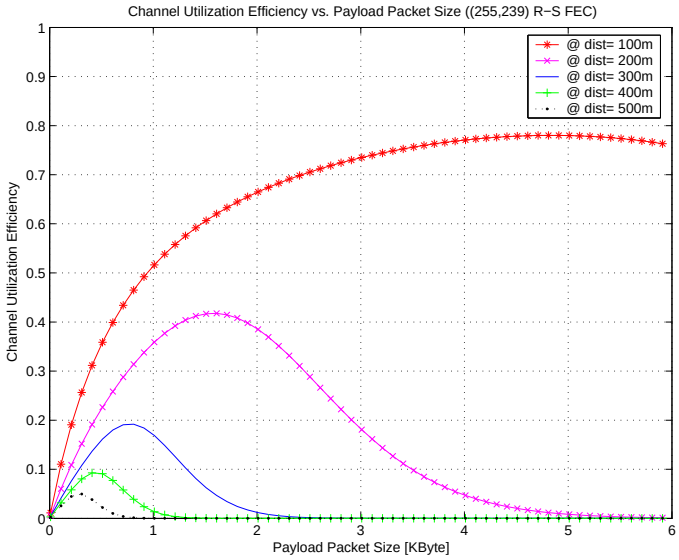

Figure 24: *Underwater and terrestrial channel utilization efficiency for different distances* $(100\,\mathrm{m} - 500\,\mathrm{m})$. Underwater channel efficiency vs. packet payload size with $(255, 239)$ Reed-Solomon FEC

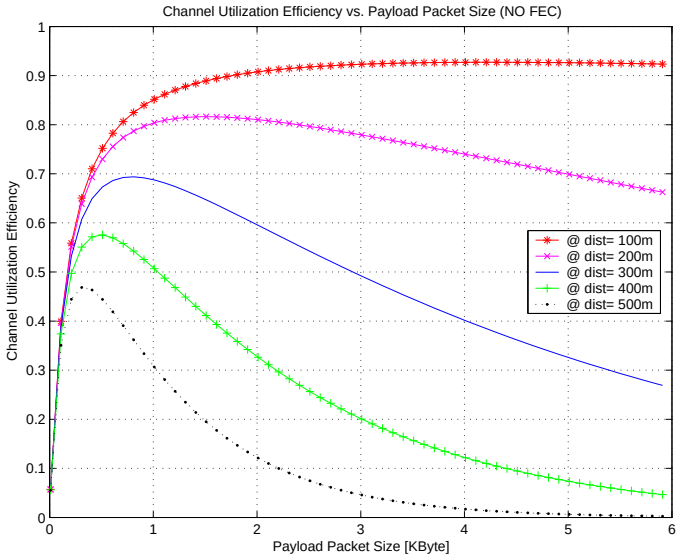

Figure 25: *Underwater and terrestrial channel utilization efficiency for different distances* $(100\,\mathrm{m} - 500\,\mathrm{m})$. Terrestrial channel efficiency vs. packet payload size without FEC

sizes in this environment are smaller with respect to the underwater case. If we then protect a packet with FEC techniques, we obtain very high efficiencies (in the order of $0.9 - 0.95$) for a wide range of distances and packet sizes.

4.4.2 Packet Train and Optimal Packet Size

In the previous section, we considered a shared channel where a device adopts a *single-packet* transmission scheme, i.e., transmits a data packet when it senses the channel idle, and the corresponding device advertises a correct reception with a short acknowledgement (ACK) packet. The payload of the data packet to be transmitted is assumed to have size L_P^D bits, while the header L_P^H bits. Moreover, the packet may be protected with a FEC mechanism, which introduces a redundancy of L_P^F bits. We observe the following facts when a single-packet transmission scheme is used in the underwater environment:

- The channel efficiency is very low. This, combined with very low data rates, may be detrimental for communications. Hence, it is crucial to maximize the efficiency in exploiting the available resources.

- Underwater communications greatly benefit from the use of forward error correction (FEC) and hybrid automatic request (ARQ) mechanisms. In fact, combined FEC and ARQ strategies can consistently decrease the average number of transmissions. The increasing packet error rate on longer-range underwater links can be compensated for by either decreasing the packet length, or by applying stronger FEC/ARQ schemes.

- The channel efficiency drops abruptly with increasing distance, and with varying packet size. In particular, i) the average number of packet retransmissions increases as the packet size increases, ii) the efficiency decreases as the number of retransmissions increases, and iii) the efficiency increases as the packet payload size increases. Consequently, the optimal packet size should be determined by considering the trade-off between channel efficiency and retransmissions.

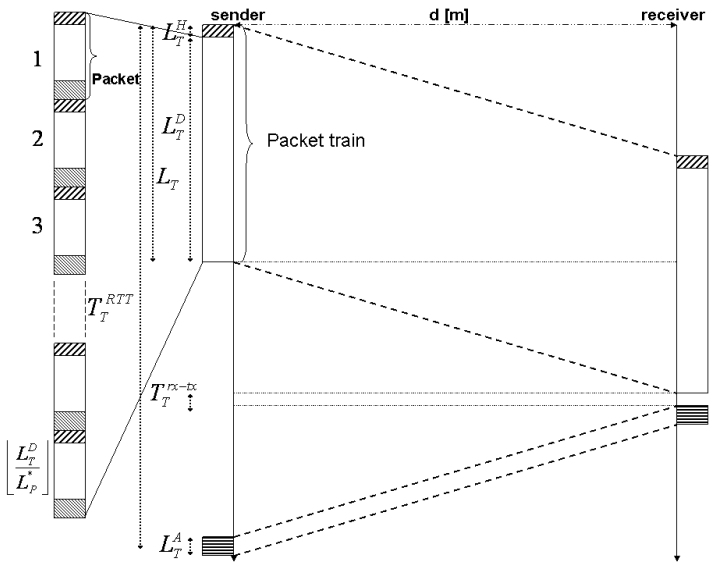

Figure 26: *Packet-train performance.* Packet-train transmission scheme

To overcome the problems raised by the single-packet transmission scheme, which ultimately lead to low channel efficiencies, we exploit the concept of *packet train*. As shown in Fig. 26, a packet train is a *juxtaposition* of packets, which are transmitted *back-to-back* by a node without releasing the channel, in a *single atomic transmission*. For delay-insensitive applications, the corresponding node sends for each train an ACK packet, which can either *cumulatively acknowledge* the whole train, i.e., all the consecutively transmitted packets, or it can *selectively* request the retransmission of specific packets (which are then included in the next train). In general, a selective repeat approach is to be preferred.

The strategy proposed here allows increasing the efficiency of the acoustic channel by increasing the length of the transmitted train, without compromising on the packet error rate, i.e., keeping the transmitted packets short. In other words, we *decouple* the effect of the packet size from the choice of the length of the train, i.e., the number of consecutive packets transmitted back-to-back by a node: while the former determines the packet error rate, the latter can be increased as needed in order to increase the channel efficiency. In

fact, the channel efficiency associated with the packet-train scheme is

$$\eta = \eta_T(L_T) \cdot \eta_P(L_P, L_P^F). \tag{24}$$

In (24), $\eta_T(L_T)$ is the packet-train efficiency, i.e., the ratio between the train payload transmission time and the *train round-trip time* T_T^{RTT} (see Fig. 26) normalized to the bit rate r,

$$\eta_T(L_T) = \frac{L_T^D}{L_T^D + L_T^H + L_T^A + r \cdot (2\frac{d}{q} + T_T^{rx-tx})}, \tag{25}$$

where L_T, L_T^D, L_T^H, and L_T^A are the train, payload, header, and ACK length, and T_T^{rx-tx} is the time needed to process the train and switch the circuitry from receiving to transmitting mode; $\eta_P(L_P, L_P^F)$ is the packet efficiency, i.e., the ratio of the packet payload and the packet size multiplied by the average number of transmissions $\hat{N}^{TX}$ such that a packet is successfully decoded at the receiver, which is defined as

$$\eta_P(L_P, L_P^F) = \frac{L_P - L_P^H - L_P^F}{\hat{N}^{TX} \cdot L_P}. \tag{26}$$

Equation (24) accounts for the decoupling between train length, which solely affects the train efficiency η_T, and choice of the packet structure, which solely affects the packet efficiency η_P.

The optimal packet size (L_P^*) and optimal FEC redundancy $(L_P^{F^*})$ are chosen in such a way as to maximize the packet efficiency η_P, as cast in the optimal packet size problem.

$\mathbf{P_P^{size}}$: Optimal Packet Size Problem in UW-ASNs

$$\begin{aligned}
Given: &\quad \overline{P}_{max}^{TX},\ r,\ f_0,\ \overline{N_0},\ \Pr\{l\},\ \psi^{\mathcal{F}},\ \Phi^{\mathcal{M}},\ PER_{max}^{e2e} \\
Find: &\quad L_P^*,\ L_P^{F^*} \\
Maximize: &\quad \eta_P(L_P, L_P^F) = \tfrac{L_P - L_P^H - L_P^F}{\hat{N}^{TX} \cdot L_P} \\
Subject\ to: & \\
&\overline{BER} = \Phi^{\mathcal{M}}\left(\frac{\overline{P}_{max}^{TX}}{r \cdot \overline{N_0} \cdot \overline{TL}}\right);\ \overline{TL} = \int_0^\infty TL(l, f_0) \cdot \Pr\{l\} dl;
\end{aligned} \tag{27}$$

$$(Delay - insensitive\ Applications)$$

$$\hat{N}^{TX} = \frac{1}{1 - \psi^{\mathcal{F}}\left(L_P, L_P^F, \overline{BER}\right)}; \tag{28}$$

$$(Delay - sensitive\ Applications)$$

$$\hat{N}^{TX} = 1; \tag{29}$$

$$1 - \left[1 - \psi^{\mathcal{F}}\left(L_P, L_P^F, \overline{BER}\right)\right]^{N_{max}^{Hop}} \leq PER_{max}^{e2e}. \tag{30}$$

Where:

- $P_{i,max}^{TX}\,[\mathrm{W}]$ is the maximum transmitting power for node i, and $\overline{P}_{max}^{TX}\,[\mathrm{W}]$ is the average among all nodes of the maximum transmitting power.
- $TL(l, f_0)$ is the transmission loss at distance l and frequency f_0, as described in Section 4.3, while $r\,[\mathrm{bps}]$ is the bit rate.
- $\Pr\{l\}$ is the distance distribution between neighboring nodes, which depends on how nodes are statistically deployed in the volume; for a random 3D deployment, $\Pr\{l\}$ is derived in [59].
- $\hat{N}^{TX}$ is the estimated number of transmissions of a packet such that it is correctly decoded at the receiver; (28) assumes independent errors among adjacent packets, which holds in underwater acoustic channels where the coherence time is shorter than the average retransmission delay, i.e., the average time that a sender needs to retransmit an unacknowledged packet.
- $\Phi^{\mathcal{M}}\left(\frac{\overline{P}_{max}^{TX}}{r \cdot \overline{N_0} \cdot \overline{TL}}\right)$ represents the average bit error rate $(\overline{BER})$ on a link; it is a function of the ratio between the average energy of the received bit $\overline{P}_{max}^{TX}/(r \cdot \overline{TL})$ and the expected noise $\overline{N_0}$ at the receiver, and it depends on the modulation scheme $\mathcal{M}$; in general, the noise has a thermal, an ambient, and a man-made component; studies of shallow water noise measurements [34] suggest considering an average value of $70\,\mathrm{dB}_{\mu\mathrm{Pa}}$ for the ambient noise.

- $\psi^{\mathcal{F}}\big(L_P, L_P^F, BER\big)$ represents the average packet error rate $(\overline{PER})$, given the packet size L_P, the FEC redundancy L_P^F, and the average bit error rate $(\overline{BER})$, and it depends on the adopted FEC technique $\mathcal{F}$.

- PER_{max}^{e2e} is the application maximum allowed end-to-end packet error rate, while N_{max}^{Hop} is the maximum expected number of hops, function of the network diameter [74].

The optimal packet size L_P^* is found by maximizing the packet efficiency η_P in (26) for different FEC schemes $\mathcal{F}$ and code rates L_P^F, under a proper set of application-dependent constraints, i.e., $\{(27), (28)\}$ for delay-insensitive applications, and $\{(27), (29), (30)\}$ for delay-sensitive applications.

The packet size is optimized given the distance distribution between neighboring nodes $(\Pr\{l\})$, which determines the average transmission loss $\overline{TL}$, and ultimately the $\overline{BER}$, computed as a function $\Phi^{\mathcal{M}}()$ of the modulation scheme $\mathcal{M}$ and the average signal-to-noise ratio at the receiver, as formally defined in (27). Thus, $\mathbf{P_P^{size}}$ finds the optimal packet size and packet FEC redundancy, given the device characteristics $\big(\overline{P}_{max}^{TX}, r, f_0, \psi^{\mathcal{F}}, \Phi^{\mathcal{M}}\big)$, the deployment volume and node density, which impact the distribution between neighboring nodes $(\Pr\{l\})$, and the average ambient noise $(\overline{N_0})$, as

$$(L_P^*, L_P^{F*}) = argmax_{(L_P, L_P^F)}\, \eta_P(L_P, L_P^F). \tag{31}$$

Figure 27 shows the underwater packet efficiency η_P when the packet payload size L_P^D varies, for different distances ($100\,\mathrm{m}$ and $500\,\mathrm{m}$). In particular, for a volume with an average node distance of $100\,\mathrm{m}$, the highest packet efficiency $(\eta_P^* = 0.94)$ is achieved with a packet payload size of $L_P^{D^*} = 0.55\,\mathrm{KByte}$ and a $(255, 251)$ Reed-Solomon (R-S) FEC, while for a volume with an average node distance of $500\,\mathrm{m}$, the highest packet efficiency $(\eta_P^* = 0.91)$ is achieved with a packet payload size of $L_P^{D^*} = 0.9\,\mathrm{KByte}$ and a $(255, 239)$ R-S FEC. Figure 28 depicts the train efficiency η_T when the train payload length L_T^D varies, for different distances ($100\,\mathrm{m}$-$500\,\mathrm{m}$). Since the train efficiency monotonically increases

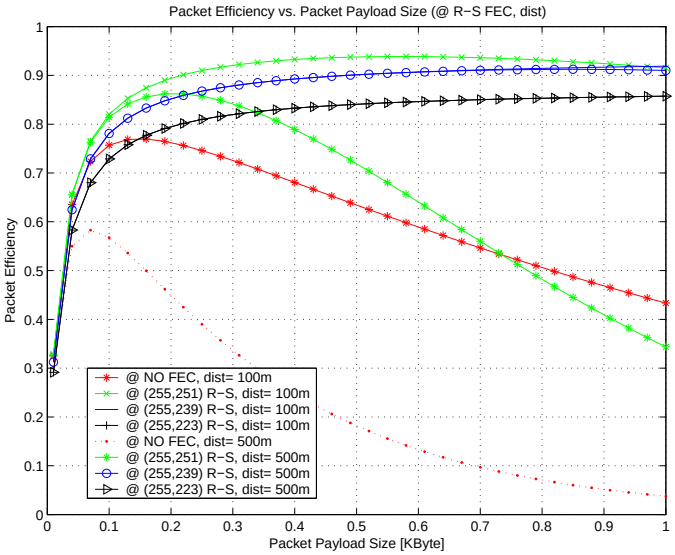

Figure 27: *Packet-train performance.* Underwater packet efficiency vs. packet payload size for different distances ($100\,\mathrm{m}$ and $500\,\mathrm{m}$)

as the train payload length increases for every distance, we can increase the train efficiency as needed with the only constraints being that: i) sensor buffer size is limited, and ii) short-term fairness among sensors competing to access the medium decreases as the train payload length increases.

To summarize, $\mathbf{P_P^{size}}$ finds *off-line* the optimal packet size and packet FEC redundancy for delay-insensitive and delay-sensitive applications, whereas the distributed algorithms proposed in the following sections adjust *on-line* the strength of the FEC technique by tuning the amount of FEC redundancy according to the dynamic channel conditions, given the *fixed* packet size L_P^*. The choice of a fixed packet size for UW-ASNs is motivated by the need for system simplicity and ease of sensor buffer management. In fact, a design proposing per-hop optimal packet size, e.g., solving $\mathbf{P_P^{size}}$ for any link distance and use the resulting *distance-dependent* optimal packet size in the routing algorithms, would encounter several implementation problems, such as the need for segmentation and reassembled functionalities that incur tremendous overhead, which are unlikely affordable by low-end sensors.

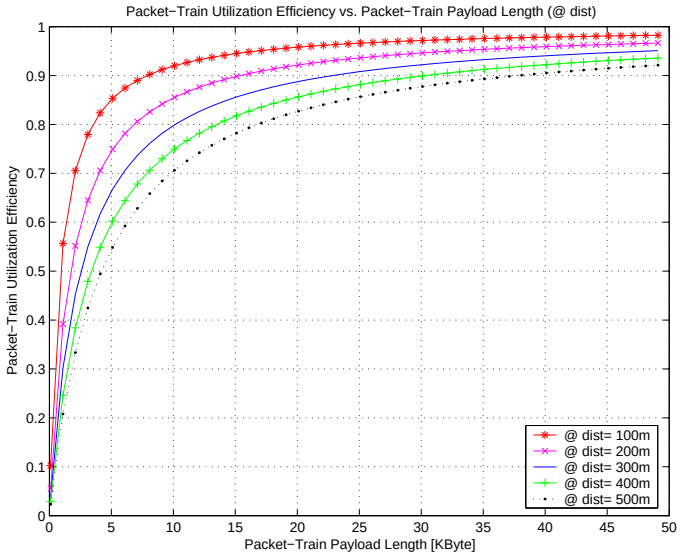

Figure 28: *Packet-train performance.* Packet-train efficiency vs. packet-train payload length for different distances ($100\,\mathrm{m}$-$500\,\mathrm{m}$)

Throughout this section, we referred to a simple CSMA-like MAC, where a device transmits a data packet when it senses the shared channel idle, and the corresponding device advertises correct reception with a short ACK packet. Although we do not advocate this access scheme for this environment, the results of our analysis are valid when a modified version of the widely used 802.11 MAC is adopted for UW-ASNs. Moreover, the results about the channel efficiency motivate the need for the development of a new multiple access technique for the underwater environment. To this end, we developed a distributed CDMA-based MAC tailored for the underwater environment, which is described in Chapter 6.

4.5 Delay-insensitive Routing Algorithm

In this section, we introduce a distributed geographical routing solution for delay-insensitive underwater applications. Most prior research in geographical routing protocols assumes that nodes can either work in a *greedy mode* or in a *recovery mode*. When in greedy mode, the node that currently holds the message tries to forward it towards the destination. The recovery mode is entered when a node fails to forward a message in the greedy mode, since

none of its neighbors is a feasible next hop. Usually this occurs when the node observes a void region between itself and the destination. Such a node is referred to as *concave* node. For example, the GPSR algorithm [46] makes greedy forwarding decisions. When a packet reaches a concave node, GPSR tries to recover by routing around the perimeter of the void region. Recovery mechanisms, which allow a packet to be forwarded to the destination when a concave node is reached, are out of the scope of this work. Hence, the protocol proposed in this section assumes that no void regions exist, although it can be enhanced by combining it with one of the existing recovery mechanisms (e.g., [11]).

The objective of our proposed routing solution is to efficiently exploit the underwater acoustic channel and to minimize the energy consumption. Therefore, the proposed algorithm relies on the packet-train transmission scheme, which is discussed in Section 4.4. In a distributed fashion, it allows each node to *jointly* select its best next hop, the transmitted power, and the FEC code rate for each packet, with the objective of minimizing the energy consumption, while taking the condition of the underwater channel into account. Furthermore, it tries to exploit those links that guarantee a low packet error rate, in order to maximize the probability that the packet is correctly decoded at the receiver. For these reasons, the energy efficiency of the link is weighted with the number of retransmissions required to achieve link reliability, with the objective of saving energy. We can now cast the delay-insensitive distributed routing problem.

$\mathbf{P}^{\mathbf{dist}}_{\mathbf{insen}}$: Delay-insensitive Distributed Routing Problem

$$
\begin{aligned}
Given: \quad & i,\, \mathcal{S}_i,\, \mathcal{P}_i^N,\, L_P^*,\, L_P^H,\, E_{elec}^b,\, r,\, \hat{N}_{0j},\, P_{i,max}^{TX} \\
Find: \quad & j^* \in \mathcal{S}_i \cap \mathcal{P}_i^N,\; P_{ij^*}^{TX\,*} \in [0, P_{i,max}^{TX}],\; {L_{Pij^*}^F}^* \\
Minimize: \quad & E_i^{(j)} = E_{ij}^b \cdot \tfrac{L_P^*}{L_P^* - L_P^H - L_{Pij}^F} \cdot \hat{N}_{ij}^{TX} \cdot \hat{N}_{ij}^{Hop} \qquad (32) \\
Subject\ to: \quad & \\
& E_{ij}^b = 2 \cdot E_{elec}^b + \frac{P_{ij}^{TX}}{r}; \qquad (33)
\end{aligned}
$$

$$L_{Pij}^{F} = \Psi^{\mathcal{F}^{-1}}\left(L_P^*, PER_{ij}, \Phi^{\mathcal{M}}\left(\frac{P_{ij}^{TX}}{\hat{N}_{0j}\cdot r\cdot TL_{ij}}\right)\right); \tag{34}$$

$$\hat{N}_{ij}^{TX} = \frac{1}{1-PER_{ij}};\ \hat{N}_{ij}^{Hop} = \max\left(\frac{d_{iN}}{< d_{ij} >_{iN}}, 1\right). \tag{35}$$

Where:

- $L_P^* = L_P^H + L_{Pij}^F + L_{P\,ij}^N\,[bit]$ is the ***fixed*** optimal packet size, solution of $\mathbf{P_P^{size}}$, where L_P^H is the ***fixed*** header size of a packet, while L_{Pij}^F is the *variable* FEC redundancy that is included in each packet transmitted from node i to node j; thus, $L_{P\,ij}^N = L_P^* - L_P^H - L_{Pij}^F$ is the *variable* payload size of each packet transmitted in a train on link (i, j).

- $E_{elec}^b = E_{elec}^{trans} = E_{elec}^{rec}\,[\mathrm{J/bit}]$ in (33) is the *distance-independent* energy to transit one bit, where E_{elec}^{trans} is the energy per bit needed by transmitter electronics (PLLs, VCOs, bias currents, etc.) and digital processing, and E_{elec}^{rec} represents the energy per bit utilized by receiver electronics. Note that E_{elec}^{trans} does not represent the overall energy to transmit a bit, but only the distance-independent portion of it.

- $E_{ij}^b = 2\cdot E_{elec}^b + P_{ij}^{TX}/r\,[\mathrm{J/bit}]$ in (33) accounts for the energy to transmit one bit from i to j, when the transmitted power and the bit rate are $P_{ij}^{TX}\,[\mathrm{W}]$ and $r\,[\mathrm{bps}]$, respectively. The second term represents the *distance-dependent* portion of the energy necessary to transmit a bit.

- TL_{ij} in (34) is the transmission loss from i to j (see Section 4.3).

- $\hat{N}_{ij}^{TX}$ in (32) is the average number of transmissions of a packet sent by node i such that the packet is correctly decoded at receiver j.

- $\hat{N}_{ij}^{Hop} = \max\left(\frac{d_{iN}}{<d_{ij}>_{iN}}, 1\right)$ in (35) is the estimated number of hops from node i to the surface station (sink) N when j is selected as next hop, where d_{ij} is the distance between i and j, and $< d_{ij} >_{iN}$ (which we refer to as *advance*) is the projection of d_{ij} onto the line connecting node i with the sink.

- $BER_{ij} = \phi^{\mathcal{M}}(E^b_{rec}/\hat{N}_{0j})$ in (34) represents the bit error rate on link (i,j); it is a function of the ratio between the energy of the received bit, $E^b_{rec} = P^{TX}_{ij}/(r \cdot TL_{ij})$, and the expected noise at node j, $\hat{N}_{0j}$, and it depends on the adopted modulation scheme $\mathcal{M}$.

- $L^F_{Pij} = \psi^{\mathcal{F}^{-1}}(L^*_P, PER_{ij}, BER_{ij})$ returns the needed FEC redundancy, given the optimal packet size L^*_P, the packet error rate and bit error rate on link (i,j), and it depends on the adopted FEC technique $\mathcal{F}$.

- $\mathcal{S}_i$ is the *neighbor set* of node i, while $\mathcal{P}^N_i$ is the *positive advance set*, composed of nodes closer to sink N than node i, i.e., $j \in \mathcal{P}^N_i$ iff $d_{jN} < d_{iN}$.

According to the proposed distributed routing algorithm for delay-insensitive applications, node i will select j^* as its best next hop iff

$$j^* = argmin_{j \in \mathcal{S}_i \cap \mathcal{P}^N_i} E^{(j)^*}_i, \tag{36}$$

where $E^{(j)^*}_i$ represents the minimum energy required to successfully transmit a payload bit from node i to the sink, taking the condition of the underwater channel into account, when i selects j as next hop. This link metric, objective function (32) in $\mathbf{P^{dist}_{insen}}$, takes into account the number of packet transmissions ($\hat{N}^{TX}_{ij}$) associated with link (i,j), given the optimal packet size (L^*_P), and the optimal combination of FEC ($L^F_{Pij}{}^*$) and transmitted power (P^{TX*}_{ij}). Moreover, it accounts for the average hop-path length ($\hat{N}^{Hop}_{ij}$) from node i to the sink when j is selected as next hop, by assuming that the following hops will guarantee the same advance towards the surface station (sink). While this approach to estimate the number of remaining hops towards the surface station is simple, several advantages can be pointed out, as described in [88], such as: i) it does not incur any signaling overhead since it is locally computed and does not require end-to-end information exchange; ii) its accuracy increases as the density increases; iii) its accuracy increases as the distance between the surface station and the current node decreases. For these reasons, we decided to use

this method rather than trying to estimate the exact number of hops towards the destination. Simulation performance in Section 4.7 shows the effectiveness of this choice.

The link metric $E_i^{(j)^*}$ in (36) stands for the optimal energy per payload bit when i transmits a packet train to j using the optimal combination of power $P_{ij}^{TX^*}$ and FEC redundancy ${L_{Pij}^F}^*$ to achieve link reliability, jointly found by solving problem $\mathbf{P_{insen}^{dist}}$. This interpretation allows node i to optimally decouple $\mathbf{P_{insen}^{dist}}$ into two *sub-problems*: first, minimize the link metric $E_i^{(j)}$ for each of its feasible next-hop neighbors; second, pick as best next hop that node j^* associated with the minimal link metric. This means that the generic node i does not have to solve a complicated optimization problem to find its best route towards a sink. Rather, it only needs to sequentially solve the two aforementioned low-complexity subproblems, each characterized by a complexity $O(|\mathcal{S}_i \cap \mathcal{P}_i^N)|$, i.e., proportional to the number of its neighboring nodes with positive advance towards the sink. Moreover, this operation does not need to be performed each time a sensor has to route a packet, but only when the channel conditions have consistently changed. To summarize, the proposed routing solution allows node i to select as next hop that node j^* among its neighbors that satisfies the following requirements: i) it is closer to the surface station than i, and ii) it minimizes the link metric $E_i^{(j)^*}$.

4.6 Delay-sensitive Routing Algorithm

Similarly to the delay-insensitive algorithm introduced in Section 4.5, this algorithm allows each node to distributively select the optimal next hop, transmitting power, and FEC packet rate, with the objective of minimizing the energy consumption. However, this algorithm includes two new constraints to statistically meet the delay-sensitive application requirements:

1. The end-to-end packet error rate should be lower than an application-dependent threshold PER_{max}^{e2e};

2. The probability that the end-to-end packet delay be over a delay bound B_{max}, should

be lower than an application-dependent parameter γ.

As a design guideline to meet these requirements, differently from the routing algorithm tailored for delay-insensitive applications, the proposed algorithm does not retransmit corrupted or lost packets at the link layer. Rather, it discards corrupted packets. Moreover, it time-stamps packets when they are generated by a source so that it can discard expired packets. To save energy, while statistically limiting the end-to-end packet delay, we rely on an *earliest deadline first* scheduling, which dynamically assigns higher priority to packets closer to their deadline. We can now cast the delay-sensitive distributed routing problem.

$\mathbf{P_{sen}^{dist}}$: Delay-sensitive Distributed Routing Problem

$$
\begin{aligned}
Given: \quad & i,\, \mathcal{S}_i,\, \mathcal{P}_i^N,\, E_{elec}^b,\, r,\, \hat{N}_{0j},\, P_{i,max}^{TX},\, \Delta B_i^{(m)},\, \hat{Q}_{ij} \\
Find: \quad & j^* \in \mathcal{S}_i \cap \mathcal{P}_i^N,\ P_{ij^*}^{TX^*} \in [0, P_{i,max}^{TX}],\ {L_{Pij^*}^F}^* \\
Minimize: \quad & E_i^{(j)} = E_{ij}^b \cdot \tfrac{L_P^*}{L_P^* - L_P^H - L_{Pij}^F} \cdot \hat{N}_{ij}^{Hop} \qquad (37) \\
Subject\ to: \quad &
\end{aligned}
$$

$$E_{ij}^b = 2 \cdot E_{elec}^b + \frac{P_{ij}^{TX}}{r}; \qquad (38)$$

$$L_{Pij}^F = \Psi^{\mathcal{F}^{-1}}\left(L_P^*, PER_{ij}, \Phi^{\mathcal{M}}\left(\frac{P_{ij}^{TX}}{\hat{N}_{0j} \cdot r \cdot TL_{ij}}\right)\right); \qquad (39)$$

$$\hat{N}_{ij}^{Hop} = \max\left(\frac{d_{iN}}{< d_{ij} >_{iN}}, 1\right); \qquad (40)$$

$$1 - \left(1 - PER_{ij}\right)^{\lceil \hat{N}_{ij}^{Hop} \rceil} \leq PER_{max}^{e2e}; \qquad (41)$$

$$\frac{\tilde{d_{ij}}}{\overline{q_{ij}}} + \delta(\gamma) \cdot \sigma_{ij}^q \leq \min_{m=1,..,M}\left(\frac{\Delta B_i^{(m)}}{\hat{N}_{ij}^{Hop}}\right) - \hat{Q}_{ij} - \frac{L_P^*}{r}. \qquad (42)$$

In the following, we explain the extra notations and variables used in the problem formulation for delay-sensitive applications:

- $M = \lfloor (L_T^* - L_T^H)/L_P^* \rfloor$ in (42) is the *fixed* number of packets transmitted in a train on each link, where L_T^* and L_P^* are the optimal train length and packet size, respectively.

- PER_{max}^{e2e} in (41) and B_{max} [s] are the application-dependent end-to-end packet error rate threshold and delay bound, respectively.

- $\Delta B_i^{(m)} = B_{max} - \left[t_{i,now}^{(m)} - t_0^{(m)}\right]$ [s] in (42) is the time-to-live of packet m arriving at node i, where $t_{i,now}^{(m)}$ is the arriving time of m at i, and $t_0^{(m)}$ is the time m was generated, which is time-stamped in the packet header by its source.

- $T_{ij} = L_P^*/r + T_{ij}^q$ [s] accounts for the packet transmission delay and the propagation delay associated with link (i, j), according to Section 4.3; according to measurements on underwater channels reporting symmetric delay distribution of multipath rays [82], we consider a Gaussian distribution for T_{ij}, i.e., $T_{ij} \backsim \mathcal{N}\left(L_P^*/r + \overline{T_{ij}^q}, {\sigma_{ij}^q}^2\right)$.

- $\overline{Q}_i$ [s] and $\overline{Q}_j$ [s] are the average queueing delays of node i (at the time the node computes its next hop) and neighboring node j, respectively.

- $\hat{Q}_{ij}$ [s] in (42) is the network queueing delay estimated by node i when j is selected as next hop, computed according to the information carried by incoming packets and broadcast by neighboring nodes, as will be detailed in the next section.

The formulation of $\mathbf{P}_{\mathbf{sen}}^{\mathbf{dist}}$ is quite similar to $\mathbf{P}_{\mathbf{insen}}^{\mathbf{dist}}$, except for two important differences:

1. The objective function (37) does not include $\hat{N}_{ij}^{TX}$ as in (32), since no selective packet retransmission is performed;

2. Two new constraints are included, (41) and (42), which address the two considered delay-sensitive application requirements, i.e., the end-to-end packet error rate should be lower than an application-dependent threshold PER_{max}^{e2e}, and the probability that the end-to-end packet delay be over a delay bound B_{max}, should be lower than an application-dependent parameter γ, respectively.

Note that (41) adjusts the packet error rate PER_{ij} that will be experienced by packet m on link (i, j) to respect the application end-to-end packet error rate requirement (PER_{max}^{e2e}), given the estimated number of hops to reach the sink if j is selected as next hop ($\hat{N}_{ij}^{Hop}$). Interestingly, since the packet is assumed to be correctly forwarded up to node i, there is no need to consider the hop count number in (41), i.e., the number of hops of packet m from the source to the current node i. In fact, since node i is assumed to receive the packet, the conditional probability of it being correct is one. Finally, constraint (42) is mathematically derived in the following section. The complexity of $\mathbf{P_{sen}^{dist}}$ is $O(|\mathcal{S}_i \cap \mathcal{P}_i^N)|$, i.e., proportional to the number of neighboring nodes with positive advance towards the sink.

4.6.1 Statistical Link Delay Model

In this section, we derive constraint (42) in $\mathbf{P_{sen}^{dist}}$ that each link needs to meet to statistically bound the end-to-end packet delay. To this end, we model the propagation delay of each link (i, j) as a random variable T_{ij}^q, with mean equal to $\overline{T_{ij}^q}$ and variance ${\sigma_{ij}^q}^2$. The mean $\overline{T_{ij}^q} = \tilde{d_{ij}}/\overline{q_{ij}}$ is computed as the ratio of the average multiple path length $\tilde{d_{ij}}$ and the average underwater propagation speed of an acoustic wave propagating from node i to node j (see Section 4.3). In vertical links, sound rays propagate directly without bouncing on the bottom or surface of the ocean. Hence, the multipath effect is negligible, and $\tilde{d_{ij}} \approx d_{ij}$. Conversely, in shallow-water horizontal links, several rays propagate by bouncing on the bottom and surface of the ocean along with the direct ray. Hence, $\tilde{d_{ij}}$ is generally larger than d_{ij}. This is due to the fact that in state-of-the-art underwater receivers, multipath can be compensated for by waiting for the energy associated with delayed rays. This way, it is possible to capture the energy spread on multiple paths, and thus guarantee a smaller BER given a fixed SNR. However, the price for this is that the end-to-end delay may be heavily affected by the propagation delay of several rays.

By leveraging statistical properties of links, we want the probability that a packet exceed its end-to-end delay bound B_{max} to be lower than an application-dependent fixed parameter

γ. To achieve this, it should hold

$$\Pr\left\{\left[t_{i,now}^{(m)} - t_0^{(m)}\right] + B_{iN}^{(j)} \geq B_{max}\right\} = \Pr\left\{B_{iN}^{(j)} \geq \Delta B_i^{(m)}\right\} \leq \gamma, \tag{43}$$

where $B_{iN}^{(j)}$ is the expected delay a packet will incur from node i to the surface station N when j is chosen as next hop, and $\Delta B_i^{(m)} = B_{max} - \left[t_{i,now}^{(m)} - t_0^{(m)}\right]$ is the time-to-live of packet m arriving at node i. Node i can estimate the remaining-path delay by projecting, for each possible next hop j, the estimated network queueing delay $\hat{Q}_{ij}$ and the transmission delay T_{ij} to the remaining estimated hops $\hat{N}_{ij}^{Hop}$, i.e.,

$$B_{iN}^{(j)} \approx (T_{ij} + \hat{Q}_{ij}) \cdot \hat{N}_{ij}^{Hop}, \tag{44}$$

where

$$\hat{Q}_{ij} = \frac{t_{i,now}^{(m)} - t_0^{(m)} - \sum_{(k,h)\in\mathcal{L}_i^{(m)}} \overline{T}_{kh} + \overline{Q}_i + \overline{Q}_j}{N_{HC}^{(m)} + 2}. \tag{45}$$

In (45), the numerator represents the sum of all the queueing delays experienced by packet m in its path $\mathcal{L}_i^{(m)}$, which includes the links from the source generating packet m to node i, and the average queueing delays $\overline{Q}_j$ and $\overline{Q}_j$, computed by node i and periodically broadcast by j, respectively. The denominator in (45) represents the number of nodes forwarding the packet, including node i, which depends on the hop count $N_{HC}^{(m)}$, i.e., the number of hops of packet m from the source to the current node.

By substituting (44) into (43), and by assuming a Gaussian distribution for T_{ij}, (43) can be rewritten as

$$\Pr\left\{T_{ij} \geq \frac{\Delta B_i^{(m)}}{\hat{N}_{ij}^{Hop}} - \hat{Q}_{ij}\right\} = \frac{1}{2}\left[1 - erf\left(\frac{\frac{\Delta B_i^{(m)}}{\hat{N}_{ij}^{Hop}} - \hat{Q}_{ij} - \overline{T_{ij}}}{\sqrt{2}\cdot\sigma_{ij}^q}\right)\right] \leq \gamma, \tag{46}$$

where the erf function is defined as

$$erf(\Gamma) = \frac{2}{\sqrt{\pi}}\int_0^{\Gamma} e^{-t^2} dt. \tag{47}$$

Since $\overline{T_{ij}} = L_T^*/r + \overline{T_{ij}^q}$, and $\overline{T_{ij}^q} = \tilde{d_{ij}}/\overline{q_{ij}}$, (46) simplifies to

$$\frac{\tilde{d_{ij}}}{\overline{q_{ij}}} + \delta(\gamma)\cdot\sigma_{ij}^q \leq \frac{\Delta B_i^{(m)}}{\hat{N}_{ij}^{Hop}} - \hat{Q}_{ij} - \frac{L_P^*}{r}, \tag{48}$$

Table 4: Simulation performance parameters

	Scen. 1	**Scen. 2**	**Scen. 3**
Appl. Type [Delay-]	insensitive	insensitive	sensitive
Traffic Type	background	event-driven	event-driven
No. Sensors - Sources	$100 - 100$	$100 - 15$	$100 - 15$
Volume $[\mathrm{m}^3]$	100x100x100	500x500x50	500x500x50
Packet Size $[\mathrm{Byte}]$	500	500	100
Rate $[\mathrm{bps}]$	10	$150, 300, 600$	$150, 300, 600$
Max. Power $[\mathrm{W}]$	0.5	5	5

where $\delta(\gamma) = \sqrt{2} \cdot erf^{-1}(1 - 2\gamma)$ only depends on γ. In particular, $\delta(\gamma)$ increases with decreasing values of γ. In addition, in order to consider, as a precautionary guideline, the tightest constraint among all those associated with the M packets to be transmitted in a train, a '$\min$' operator is added, which leads to (42). Note that, while constraint (42) does not bound the delay of a packet, it tries to increase the probability that a packet reach the sink within its delay bound. To achieve this, the proposed algorithm only relies on the past access delay information carried by the packet, and on information about its 1-hop neighborhood, and not on end-to-end signaling. This information is obtained by broadcast messages. However, to limit the overhead caused by these messages, each node advertises its access delay only when it exceeds a pre-defined threshold. Hence, this mechanism allows the routing algorithm to dynamically adapt to the ongoing traffic and the resulting congestion.

4.7 Performance Evaluation

In this section, we present the simulation performance of the proposed routing solutions for delay-insensitive and delay-sensitive UW-ASN applications, introduced in Sections 4.5 and 4.6, respectively.

We extended the wireless package of the J-Sim simulator [1], which implements the whole protocol stack of a sensor node, to simulate the characteristics of the underwater environment. In particular, we modeled the underwater transmission loss, the transmission

and propagation delays, and the physical layer characteristics of underwater receivers. As far as the MAC layer is concerned, we adapted the behavior of IEEE 802.11 to the underwater environment, although we do not advocate this access scheme for this environment. Firstly, we disabled the RTS/CTS handshaking, as it yields unacceptable delays in a low-bandwidth high-delay environment. Secondly, we tuned all the parameters of IEEE 802.11 according to the physical layer characteristics. For example, the value of the *slot time* in the 802.11 backoff mechanism has to account for the propagation delay at the physical layer [10]. Hence, while it is set to $20\,\mu\mathrm{s}$ for 802.11 DSSS (Direct Sequence Spread Spectrum), we found that a value of $0.18\,\mathrm{s}$ is needed to allow devices a few hundred meters apart to share the underwater medium. This implies that the delay introduced by the backoff contention mechanism is several orders of magnitude higher than in terrestrial channels, which in turn leads to very low channel utilizations. For this reason, we set the values of the contention windows CW_{min} and CW_{max} [10] to 4 and 32, respectively, whereas in 802.11 DSSS they are set to 32 and 1024. We performed three sets of experiments to analyze the performance of the proposed routing solutions.

The main parameters differentiating the three experimental scenarios are summarized in Table 4, while the common parameters are reported hereafter: 100 sensors are randomly deployed in a 3D volume, the initial node energy is set to $1000\,\mathrm{J}$, and the available bandwidth is $50\,\mathrm{kHz}$. In Scenario 1, presented in Section 4.7.1, all deployed sensors are low-rate sources, which allows us to simulate a low-intensity delay-insensitive background monitoring traffic from the entire 3D volume of $100\mathrm{x}100\mathrm{x}100\,\mathrm{m}^3$. Conversely, in Scenarios 2 and 3, presented in Section 4.7.2, we compare the main performance differences between the delay-insensitive and delay-sensitive routing algorithms, when 100 sensors are randomly deployed in a 3D volume of $500\mathrm{x}500\mathrm{x}50\,\mathrm{m}^3$. Note that, differently from Scenario 1, in these sets of experiments only some sensors inside an event area of radius $100\,\mathrm{m}$ (centered inside the 3D monitoring volume) are sources of data packets of size equal to $500\,\mathrm{Byte}$ and $100\,\mathrm{Byte}$ for delay-insensitive and delay-sensitive applications, respectively.

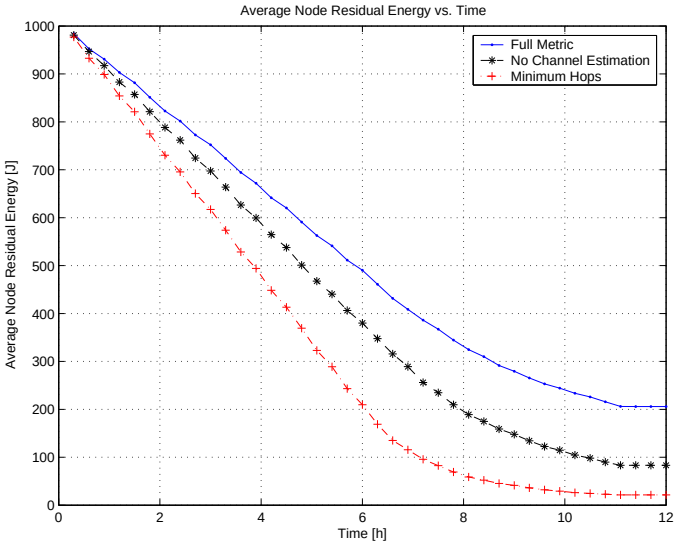

Figure 29: *Scenario 1: Delay-insensitive routing.* Average node residual energy vs. time, for different link metrics

4.7.1 Scenario 1: Delay-insensitive Background Traffic

We considered 100 sensors randomly deployed in a 3D volume of 100x100x$100\,\mathrm{m}^3$, which may represent a small harbor. We set the maximum transmission power to $0.5\,\mathrm{W}$ and the packet size to $500\,\mathrm{Byte}$. Moreover, all deployed sensors are low-rate sources, which allows us to simulate a low-intensity background monitoring traffic from the entire volume, i.e., each node transmit a data packet every $600\,\mathrm{s}$.

In Fig. 29 we show the average node residual energy over the simulation time. In particular, we compare the routing performance when three different link metrics are used. Specifically, the *Full Metric* (32), introduced in Section 4.5; the *No Channel Estimation*, which does not consider the channel condition, i.e., does not take the expected number of packet transmissions ($\hat{N}^{TX}$) into account; and the *Minimum Hops*, which simply minimizes the number of hops to reach the surface station. When the channel state condition is considered (Full Metric), consistent energy savings can be achieved, thus leading to prolonged network lifetime. In Figs. 30 and 31, we show the average number of hops and the average packet delays, respectively, when the different link metrics are used. In particular,

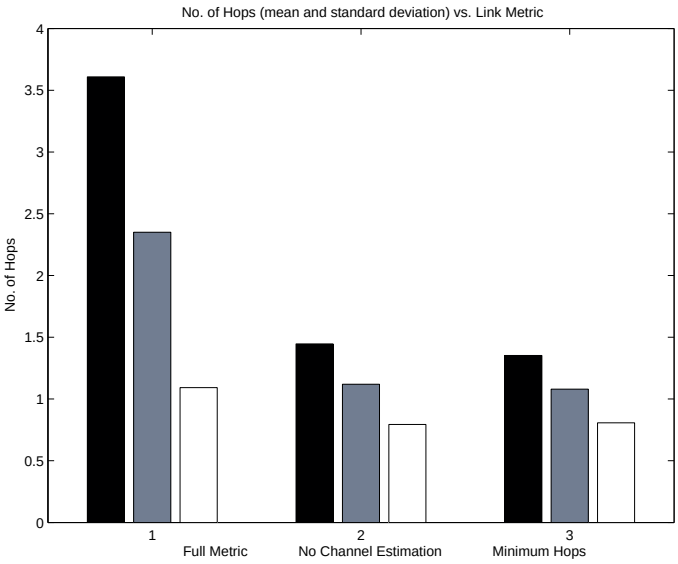

Figure 30: *Scenario 1: Delay-insensitive routing.* Average and standard deviation of number of hops vs. time, for different link metrics

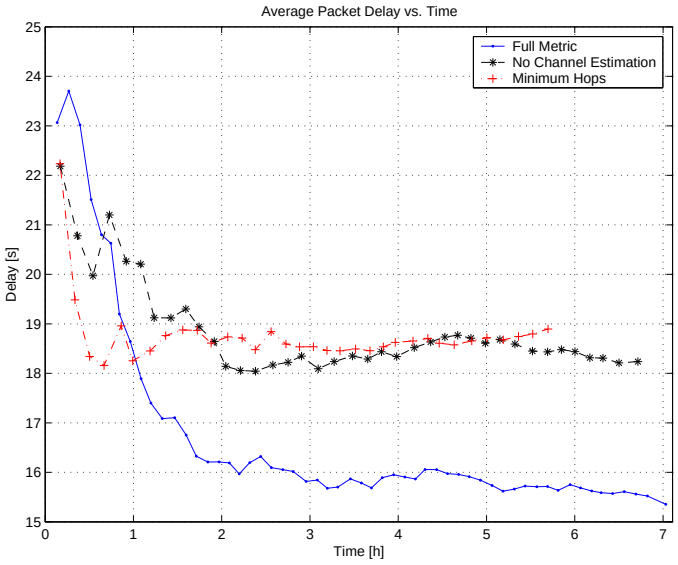

Figure 31: *Scenario 1: Delay-insensitive routing.* Average packet delay vs. time, for different link metrics

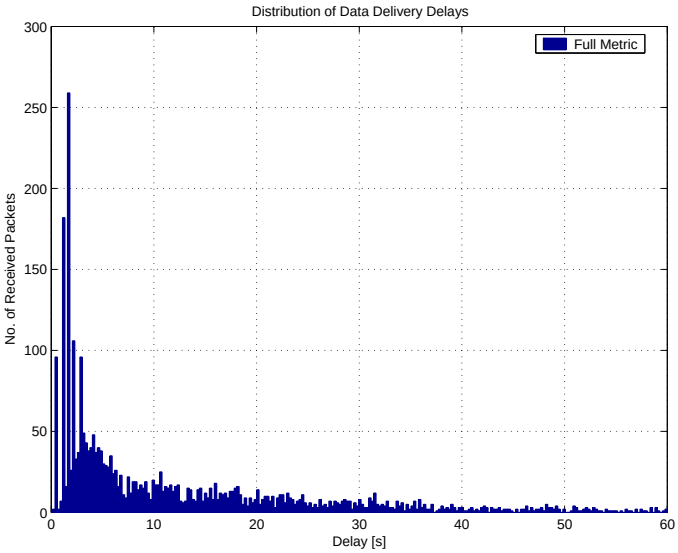

Figure 32: *Scenario 1: Delay-insensitive routing.* Distribution of data delivery delays for the Full Metric

when the full link metric is adopted, the average end-to-end packet delays are consistently smaller than with the other metrics, although data paths chosen with the Full Metric are longer, as shown in Fig. 30. Figure 32 shows the distribution of data delivery delays for the Full Metric (delay distributions associated with the other two competing metrics are omitted for lack of space). This can be explained by the lower average node queueing delays and packet transmissions, depicted in Figs. 33 and 34, respectively, observed when the Full Metric is considered. A lower number of packet transmissions (Fig. 34) is in fact to be expected, since the metric explicitly takes the state of the underwater channel into account. Hence, next hops associated to better channels are preferred. This in turn reduces the average queuing delays (Fig. 33) as packets do not necessarily need to be retransmitted.

4.7.2 Scenarios 2 and 3: Comparison Between Delay-insensitive and Delay-sensitive Event-driven Traffic

In this section, we report the main performance differences between the delay-insensitive and delay-sensitive routing algorithms, when 100 sensors are randomly deployed in a 3D

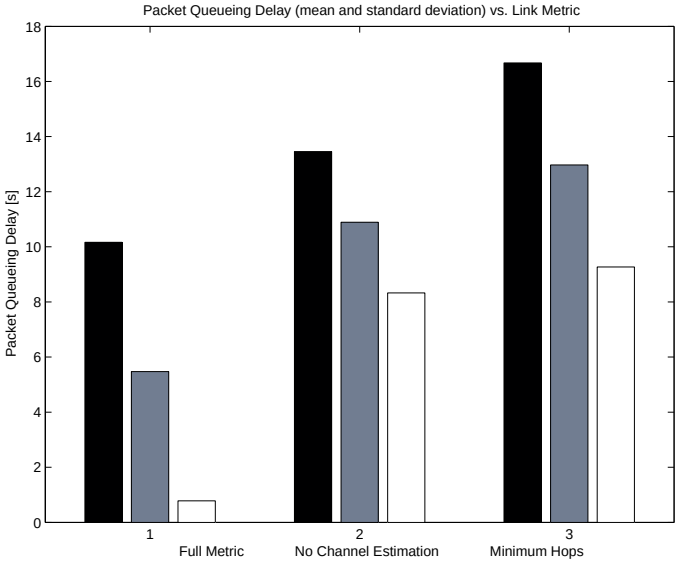

Figure 33: *Scenario 1: Delay-insensitive routing.* Average and standard deviation node queueing delays, for different link metrics

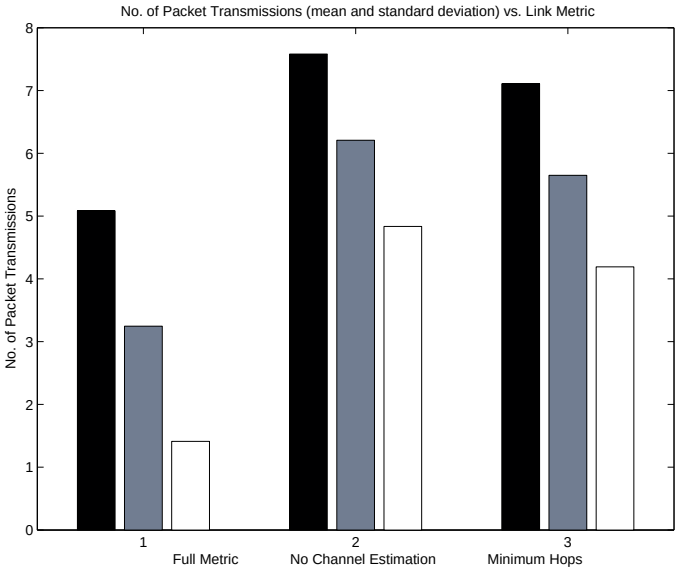

Figure 34: *Scenario 1: Delay-insensitive routing.* Average and standard deviation of number of packet transmissions, for different link metrics

volume of 500x500x$50\,\mathrm{m}^3$. Note that, differently from the previous scenario, only some sensors inside an event area of radius $100\,\mathrm{m}$ (centered inside the 3D monitoring volume) are sources of data packets of size equal to $500\,\mathrm{Byte}$ and $100\,\mathrm{Byte}$ for delay-insensitive and delay-sensitive applications, respectively. Moreover, in these simulation scenarios, we incorporated the effect of the fast fading Rayleigh channel (coherence time set to $0.5\,\mathrm{s}$), to capture the heavy multipath environment in shallow water (depth equal to $50\,\mathrm{m}$). In these sets of experiments we set the maximum transmitting power to $5\,\mathrm{W}$, as reported in Table 4, to account for the larger network diameter than in Scenario 1, i.e., $700\,\mathrm{m}$ vs. $170\,\mathrm{m}$. We performed three sets of experiments, each using different source data rates, i.e., $150,\ 300,\ 600\,\mathrm{bps}$.

Figures 35-37 and 38-40 report the end-to-end packet delay and average delay vs. time for the three considered source rates for delay-insensitive (Scenario 2) and delay-sensitive (Scenario 3) traffic. From these experiments, we noticed that when the source data rate increases, the delay-sensitive routing algorithm can statistically bound the end-to-end delay, as shown in Figs. 38-40 where the delays are always smaller than fractions of second. Conversely, the delay-insensitive routing algorithm results in very high average and peak delays, as can be seen in Figs. 35-37. The delay-sensitive routing algorithm can statistically bound the delay since next-hop nodes are chosen in such a way as to control the delay dispersion on each link, as captured by constraint (42) of $\mathbf{P}^{\mathbf{dist}}_{\mathbf{sens}}$ cast in Section 4.6. Furthermore, expired packet are discarded in order not to waste bandwidth. This is reported in Figs. 41-43, which depict generated, received, and dropped delay-sensitive traffic vs. time for different source rates. Moreover, as opposed to the delay-insensitive routing algorithm, which manages to deliver all the generated traffic at the expenses of packet delays, corrupted packets carrying delay-sensitive data are not retransmitted, which is reflected in the small sensor queue size. With this regard, Figs. 44-46 compare the evolution of the queue and average queue size for the two proposed routing algorithms. While in Scenario 2 tens of packets are in average enqueued by sensor nodes, in Scenario 3 only a few packets fill

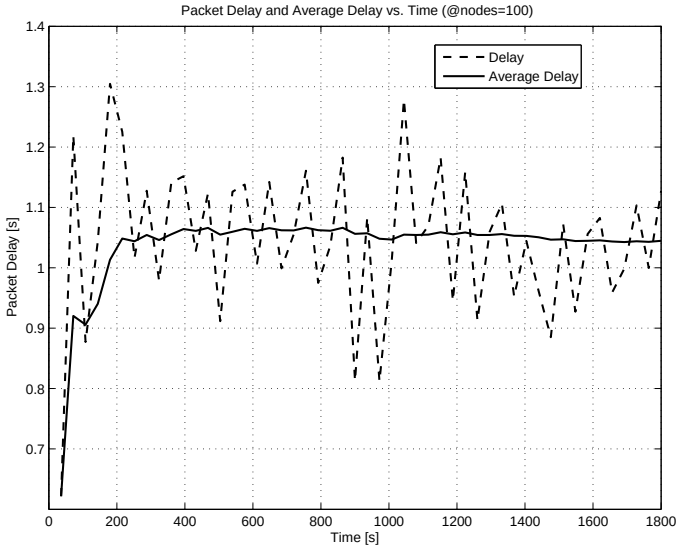

Figure 35: *Scenario 2: Delay-insensitive routing.* Packet delay and average delay vs. time for source rate equal to $150\,\mathrm{bps}$

Table 5: Scenarios 2 and 3: Surface Station and Average Energy per Bit

Source Rate $[\mathrm{bps}]$	**150**	**300**	**600**
Scenario 2. Surface Station Energy per Bit $[\mu\mathrm{J/bit}]$	8	6.5	7.5
Scenario 2. Node Average Energy per Bit $[\mu\mathrm{J/bit}]$	7	4	5.5
Scenario 3. Surface Station Energy per Bit $[\mu\mathrm{J/bit}]$	21	17	18
Scenario 3. Node Average Energy per Bit $[\mu\mathrm{J/bit}]$	9	6	5

the queues. Table 5 reports the surface station (sink) and average required energy per correctly received bit for the three different source data rates. Interestingly, in both scenarios the minimum sink and average energy per bit (in the order of tens of $\mu\mathrm{J/bit}$) is associated with the intermediate data rate, i.e., $300\,\mathrm{bps}$, when sources generate a consistent amount of traffic without causing network congestion. In addition, due to packet retransmissions, in Scenario 2 the energy per bit dissipated by relaying nodes is almost the same as that required by the surface station to receive and acknowledge incoming packets. Conversely, a remarkable difference between surface station and average node energy per bit can be noticed in Scenario 3, where the phenomenon of traffic concentration at the surface station prevails as far as the total amount of dissipated energy in the network is concerned.

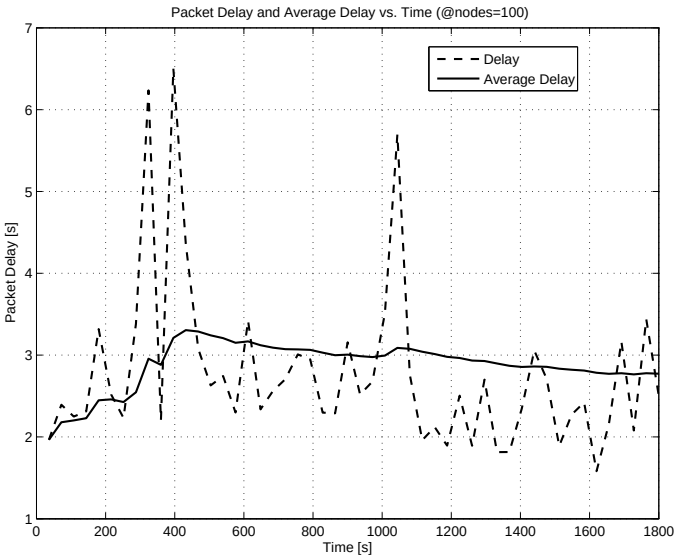

Figure 36: *Scenario 2: Delay-insensitive routing.* Packet delay and average delay vs. time for source rate equal to $300\,\mathrm{bps}$

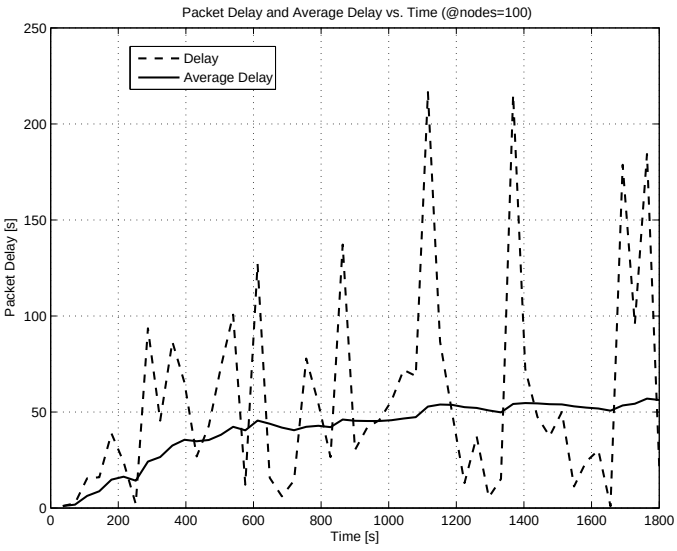

Figure 37: *Scenario 2: Delay-insensitive routing.* Packet delay and average delay vs. time for source rate equal to $600\,\mathrm{bps}$

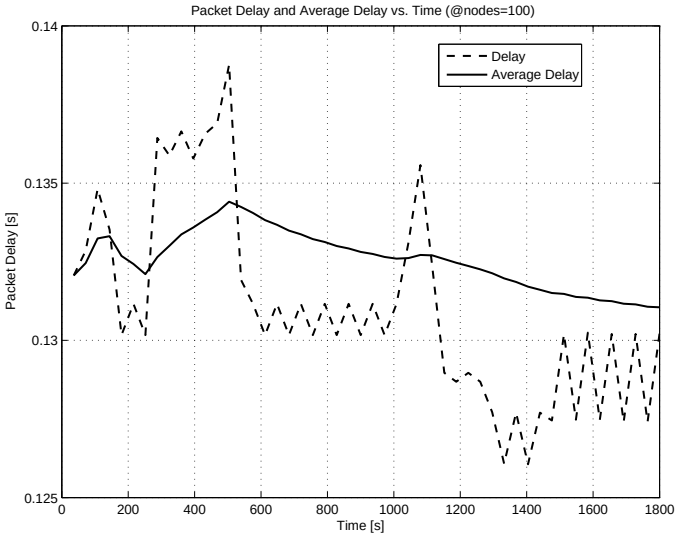

Figure 38: *Scenario 3: Delay-sensitive routing.* Packet delay and average delay vs. time for source rate equal to $150\,\mathrm{bps}$

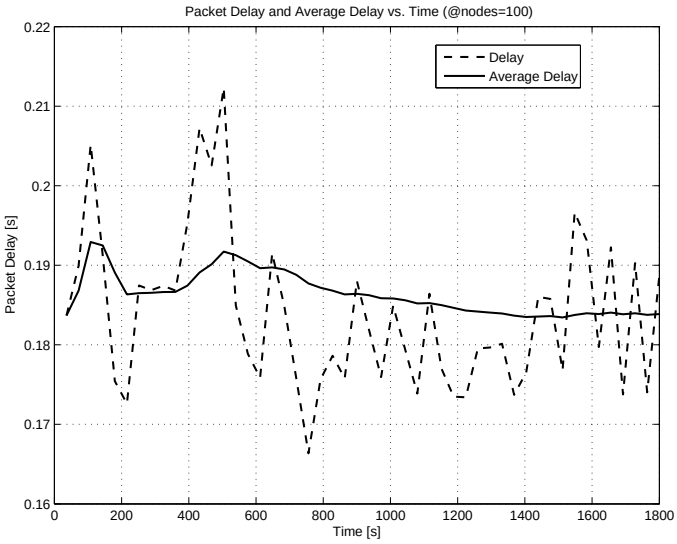

Figure 39: *Scenario 3: Delay-sensitive routing.* Packet delay and average delay vs. time for source rate equal to $300\,\mathrm{bps}$

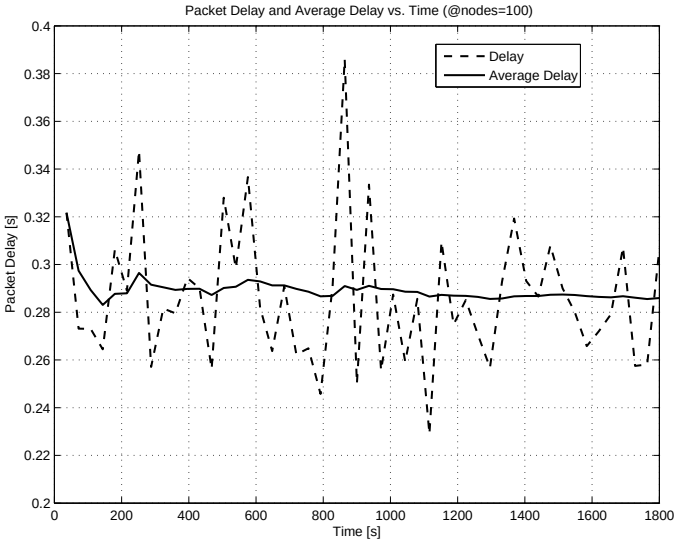

Figure 40: *Scenario 3: Delay-sensitive routing.* Packet delay and average delay vs. time for source rate equal to $600\,\mathrm{bps}$

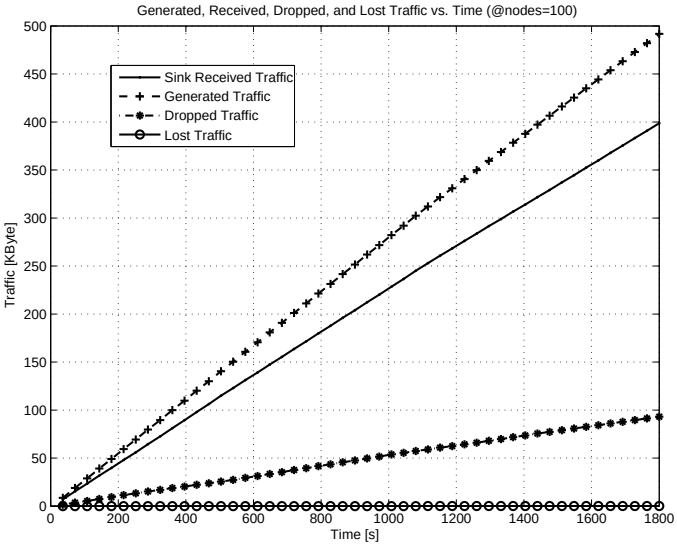

Figure 41: *Scenario 3: Delay-sensitive routing.* Generated, received, dropped, and lost traffic vs. time for source rate equal to $150\,\mathrm{bps}$

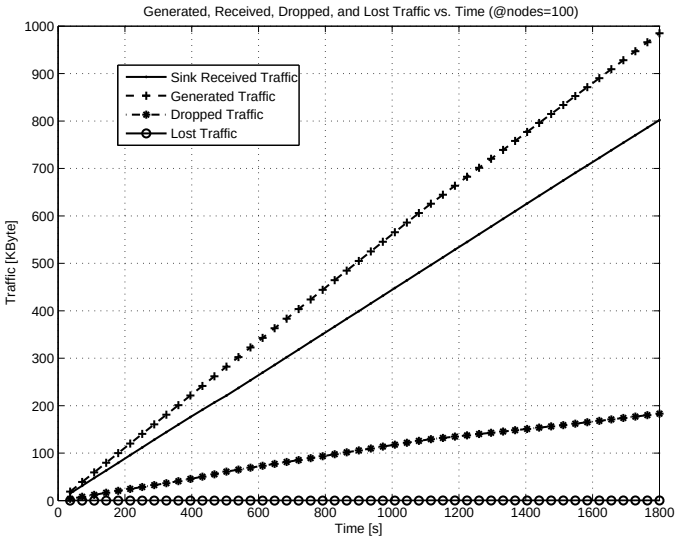

Figure 42: *Scenario 3: Delay-sensitive routing.* Generated, received, dropped, and lost traffic vs. time for source rate equal to $300\,\mathrm{bps}$

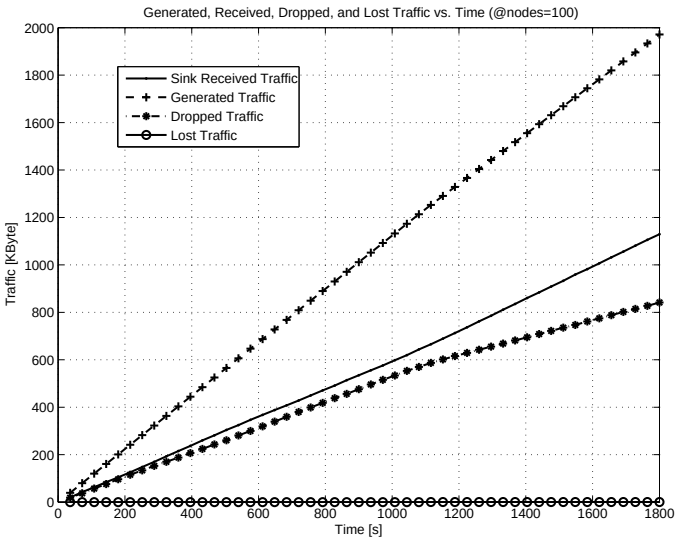

Figure 43: *Scenario 3: Delay-sensitive routing.* Generated, received, dropped, and lost traffic vs. time for source rate equal to $600\,\mathrm{bps}$

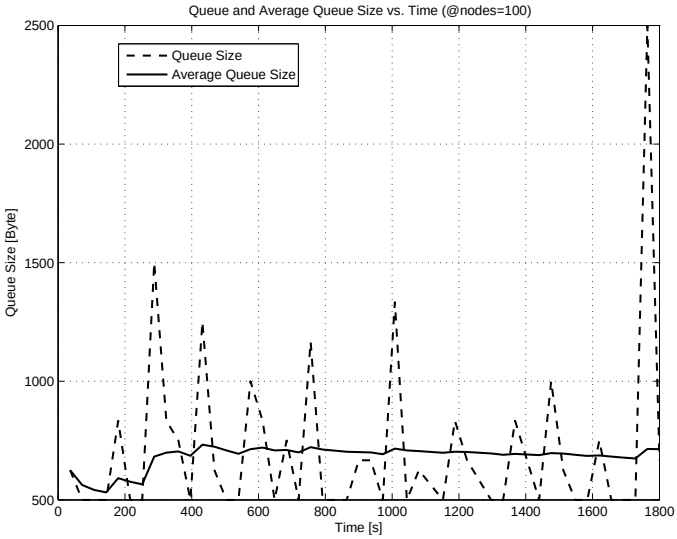

Figure 44: *Scenarios 2 and 3.* Queue and average queue size vs. time; delay-insensitive, source rate equal to $300\,\mathrm{bps}$

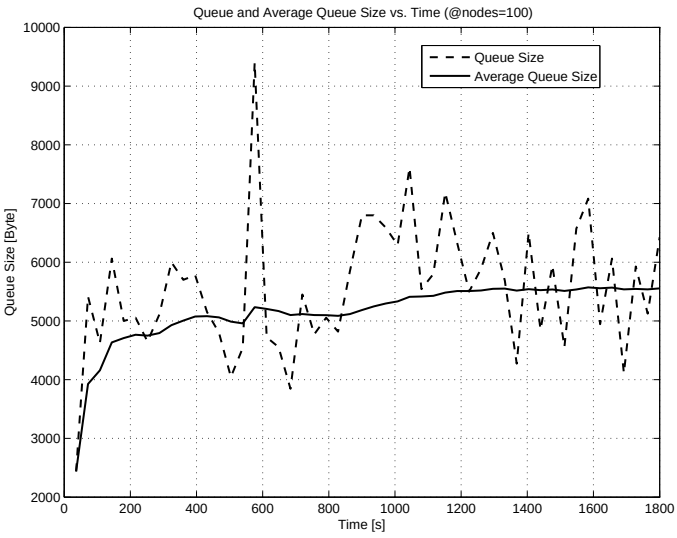

Figure 45: *Scenarios 2 and 3.* Queue and average queue size vs. time; delay-insensitive, source rate equal to $600\,\mathrm{bps}$

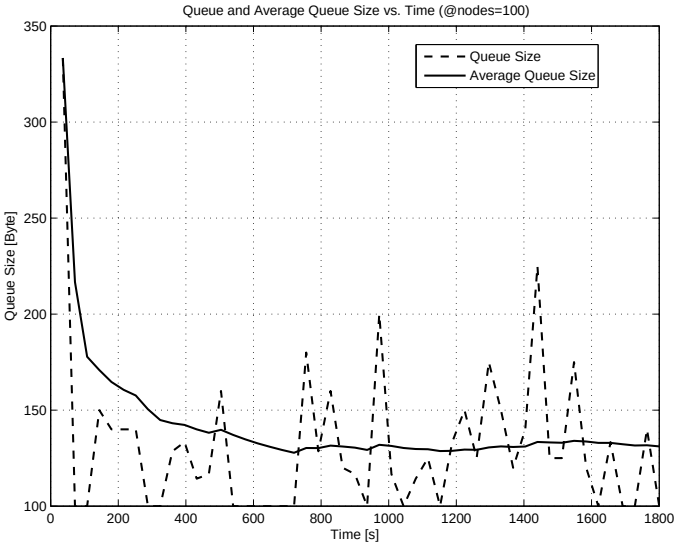

Figure 46: *Scenarios 2 and 3.* Queue and average queue size vs. time; delay-sensitive, source rate equal to $600\,\mathrm{bps}$

CHAPTER V

A RESILIENT ROUTING ALGORITHM FOR LONG-TERM UNDERWATER MONITORING MISSIONS

5.1 Preliminaries

The reliability requirements of long-term critical underwater missions, and the small scale of underwater sensor networks, suggest to devise routing solutions based on some form of centralized planning of the network topology and data paths, in order to optimally exploit the scarce network resources. Hence, the proposed solution relies on a *virtual circuit* routing technique, where multihop connections are established *a priori* between each source and sink, and each packet associated with a particular connection follows the same path. This requires centralized coordination and leads to a less flexible architecture, but allows exploiting powerful optimization tools on a centralized manager (e.g., the surface station) to achieve optimal performance at the network layer with minimum signaling overhead. The remainder of this chapter is organized as follows. In Section 5.2, we propose our resilient routing algorithm, while in Section 5.3 we show the performance results.

5.2 Basics of the Resilient Routing Algorithm

The proposed routing solution follows a *two-phase* approach. In the *first phase*, the network manager determines optimal *node-disjoint primary* and *backup* multihop data paths such that the energy consumption of the nodes is minimized. This is needed because, unlike in terrestrial sensor networks where sensors can be redundantly deployed, the underwater environment requires minimizing the number of sensors. Hence, protection is necessary to avoid network connectivity being disrupted by node or link failures. In the *second phase*, an on-line distributed solution guarantees survivability of the network, by locally repairing

paths in case of disconnections or failures, or by switching the data traffic on the backup paths in case of severe failures. The emphasis on survivability is motivated by the fact that underwater long-term monitoring missions can be extremely expensive. Hence, it is crucial that the deployed network be highly reliable, so as to avoid failure of missions due to failure of single or multiple devices. The protection scheme proposed can be classified as a dedicated backup scheme with 1:1 path protection, with node-disjoint paths. Link protection schemes are not suitable for the underwater environment as they are too bandwidth consuming [73].

The first phase of the algorithm is described in Section 5.2.1, while the second phase is presented in Section 5.2.2.

5.2.1 First Phase: Centralized Routing Problem

We formulate the problem of determining optimal primary and backup data paths for UW-ASNs as an *Integer Linear Program* (ILP) [4], where:

- e_{ij} is a binary variable representing a link that equals 1 iff nodes i and j are within each other's transmission range, while c_{ij} is the cost of the link between nodes i and j, i.e., the energy needed to transmit one bit;

- $f_{ij}^{1,s}$ and $f_{ij}^{2,s}$ are binary variables that equal 1 iff link (i, j) is in the *primary* or in the *backup* data path from the source s to the surface station, respectively;

- u_i is the capacity of node i (number of concurrent flows, ingoing and outgoing, that it can handle), while l_{ij} is the capacity of link (i, j) (number of concurrent flows that can be transmitted on the link).

The problem can be cast as follows.

$\mathbf{P_{Rout}}$: Optimal Node-disjoint Routing Problem

$$
\begin{aligned}
Given: &\quad \mathcal{G},\ \mathcal{S},\ e_{ij},\ c_{ij},\ w_1,\ w_2,\ u_i,\ l_{ij} \\
Find: &\quad f_{ij}^{1,s*},\ f_{ij}^{2,s*} \\
Minimize: &\quad C^T = \textstyle\sum_{s\in\mathcal{S}} \sum_{(i,j)\in\mathcal{E}} c_{ij} \cdot (w_1 f_{ij}^{1,s} + w_2 f_{ij}^{2,s}) \\
Subject\ to: &
\end{aligned}
$$

$$\sum_{j\in\mathcal{V}} (f_{sj}^{x,s} - f_{js}^{x,s}) = 1, \forall s \in \mathcal{S},\ x = 1,2; \tag{49}$$

$$\sum_{j\in\mathcal{V}} (f_{Nj}^{x,s} - f_{jN}^{x,s}) = -1, \forall s \in \mathcal{S},\ x = 1,2; \tag{50}$$

$$\sum_{j\in\mathcal{V}} (f_{ij}^{x,s} - f_{ji}^{x,s}) = 0, \forall s \in \mathcal{S}, \forall i \in \mathcal{V},\ i \neq s\ and\ i \neq N,\ x = 1,2; \tag{51}$$

$$f_{ij}^{x,s} \leq e_{ij}, \forall s \in \mathcal{S}, \forall i \in \mathcal{V}, \forall j \in \mathcal{V},\ x = 1,2; \tag{52}$$

$$\sum_{s\in S} (f_{ij}^{1,s} + f_{ij}^{2,s}) \leq l_{ij}, \forall i \in \mathcal{V}, \forall j \in \mathcal{V}; \tag{53}$$

$$\sum_{s\in S} \left[\sum_{j\in V} (f_{ji}^{1,s} + f_{ji}^{2,s}) + \sum_{j\in\mathcal{V}} (f_{ij}^{1,s} + f_{ij}^{2,s}) \right] \leq u_i, \forall i \in \mathcal{V}; \tag{54}$$

$$f_{ji}^{1,s} + \sum_{n\in\mathcal{V}} f_{ni}^{2,s} \leq 1, \forall s \in \mathcal{S}, \forall i \in \mathcal{V}\ s.t.\ i \neq N, \forall j \in \mathcal{V}. \tag{55}$$

The objective function of problem $\mathbf{P_{Rout}}$ aims at minimizing the overall energy consumption as a sum of the energy consumptions of all links that compose the primary and backup data paths. Two different weights w_1 and w_2 are assigned to the primary and backup data paths, respectively, with $w_1 + w_2 = 1$. By increasing w_2 we are increasing the weight of the backup paths in the optimal solution, i.e., we are trying to obtain energy efficient backup paths. This may worsen the energy consumption of the primary data paths, and should be done only in scenarios where we expect nodes to fail often, as will be discussed in Section 5.3. In general, we will have $w_2 << w_1$. Constraints (49), (50), and (51) express conservation of flows [4], i.e., each source generates a flow that has to reach the sink. In particular, constraint (49) imposes that a source node generates a flow, while non-source nodes do not generate any flow, for primary and backup data path, respectively. Constraint (50) requires

that flows generated by each source be collected by the sink. Constraint (51) guarantees that the balance between incoming and outgoing flows be null for non-source and non-sink nodes. Constraint (52) forces data paths to be created on links between adjacent nodes. Constraint (53) ensures that the sum of all flows (primary and backup) transported on a link do not exceed the link capacity, while constraint (54) imposes that the sum of all flows (incoming and outgoing, primary and backup) handled by a sensor node do not exceed the node capacity. Constraint (55) requires the primary and backup paths to be node disjoint. It can be shown that problem $\mathbf{P_{Rout}}$ is at least as complex as the Geometric Connected Dominating Set problem, which is proven to be NP-complete [32]. However, it is still possible to solve the routing problem for networks up to 100 nodes (UW-ASN case).

5.2.2 Second Phase: Localized Network Restoration

In the second phase of the proposed resilient routing algorithm, an on-line distributed solution guarantees survivability of the network, by locally repairing paths in case of disconnections or failures. Let us consider the set of connections $\mathcal{G}_i$ for which node i is either a *source* or a *relay* node. We refer to each element in $\mathcal{G}_i$ as g_i^s, i.e., a connection generated by source s and passing through node i. Hence, node i is a *source* for the connection g_i^i, while it is a *relay* for each other connection in $\mathcal{G}_i$, if any. The connections in this second group, i.e., $\mathcal{G}_i \setminus g_i^i$, are referred to as *relayed* connections for i, while g_i^i is referred to as *native* connection for i. The restoration of a network connection at node i is performed in different ways for native and relayed connections, as discussed in the following.

5.2.2.1 Restoration of a Native Connection

We refer to Fig. 47(a) and consider a node i as the source of a native connection g_i^i. Let us assume that j is the next hop of i on its primary path towards the sink. The restoration process is based on a link quality metric q_{ij} that is collaboratively estimated by the two corresponding nodes at each side of link (i, j), i.e., node i counts how many ACK timeouts

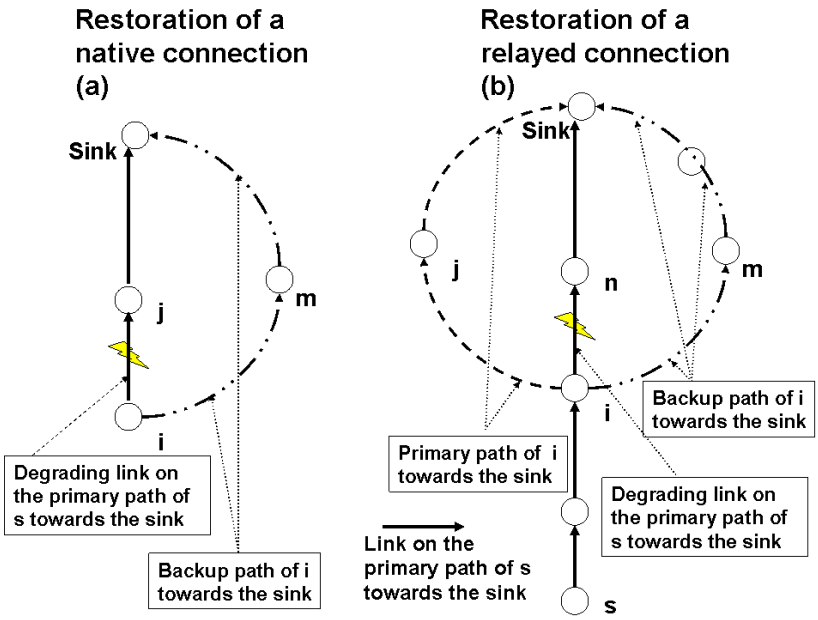

Figure 47: Restoration of a native (a) and relayed connection (b)

expire given a certain number of transmitted packets towards j. Based on this link quality, which accounts for both packets corruptions due to channel impairments and receive failures due to collisions, i performs the following operations.

- If $q_{ij} < q^{low}$, the link is considered to be in good standing and no action is taken.

- If $q_{ij} > q^{high}$, or if no acknowledgement is received from j, the link is considered to be impaired altogether. Then, i starts sending the data that it generates to its next hop m on the backup data path. According to $\mathbf{P_{Rout}}$, m is guaranteed to have node capacity reserved for the backup path of i towards the source, and capacity is guaranteed to have been reserved on the backup link (i, m), and on every link on the backup path of i towards the surface station.

- If $q^{low} \leq q_{ij} \leq q^{high}$, the link is considered to be in an intermediate state. Hence, i assumes that the quality of link (i, j) on the primary path is degrading. Therefore, i starts transmitting duplicated packets on the backup path, and, thus, starts computing estimates q_{im} of the quality of link (i, m). If $q^{low} \leq q_{im} \leq q^{high}$, i keeps transmitting all packets on both the primary and backup paths to increase the end-to-end reliability. Conversely, if the

quality of the backup link is good, i.e., $q_{im} < q^{low}$, node i tears down the connection on the primary path to save energy. Finally, if $q_{im} > q^{high}$, node i tears down the connection on the backup path.

As a final remark, if the quality metrics of the links on the primary and backup data paths are both below q^{low}, i.e., $q_{ij} < q^{low}$ and $q_{im} < q^{low}$, node i stops transmitting for a time $T_{blackout}$. After that, it probes the primary and backup links to check if their quality has improved. If not, i sends the data to a random neighbor in the positive advance set.

5.2.2.2 Restoration of Relayed Connections

Let us consider a relayed connection $g_i^s \in \mathcal{G}_i$, generated by a source s and relayed by node i. By referring to Fig. 47(b), let us assume that node n is the next hop of node i on the primary data path for the relayed connection g_i^s. As in the previous case, nodes j and m are the next-hop nodes of i on the primary and backup data paths towards the sink, respectively, while node i monitors the quality of link (i, n). However, if the quality of (i, n) degrades, node i itself cannot switch the connection on the backup path of s. In fact, i is not a relay node for the backup path of s towards the sink, since primary and backup paths are node disjoint. Hence, node i could either inform source s of the relayed connection to switch to its reserved backup path, or try to locally find an alternate path. Since informing source s would involve signaling from i back to the source, incurring in high energy consumption and delay, we propose a localized solution that tries to take advantage of possibly available local paths and uses the capacity reserved at source s only in the worst case, when no capacity is locally available. Hence, i tries to accommodate the relayed connection g_i^s on its own primary or backup data paths, since they are likely to be on energy efficient paths towards the sink. However, neither the node capacity of next hops j and m, nor the capacity of links (i, j) and (i, m) are guaranteed to be sufficient to accommodate the relayed connection. This happens because $\mathbf{P_{Rout}}$, implemented at the surface station, finds backup paths on an end-to-end basis (path protection). In other words, the primary path is

Table 6: Source Block Probability (SBP) vs. Observation Time

Obs. Time [Days]	**20**	**40**	**60**	**80**	**100**
SBP ($\lambda = 1\,\mathrm{year}^{-1}$)	0.05	0.18	0.33	0.47	0.55
SBP ($\lambda = 1/2\,\mathrm{year}^{-1}$)	0.02	0.05	0.12	0.18	0.26
SBP ($\lambda = 1/3\,\mathrm{year}^{-1}$)	0.01	0.03	0.07	0.10	0.15

protected by a node-disjoint backup path, but not every single link of the primary path is protected by its own backup path (link protection). Hence, each connection is guaranteed to have backup capacity reserved only on a path that starts from its source node. Therefore, i tries to route the failing connection on its primary or backup data paths, but it may fail due to lack of capacity. Thus, according to the available node and link capacities on links (i, j) and (i, m), their link qualities q_{ij} and q_{im}, and the link quality q_{in} of the original link (i, n), i decides whether to use one or both of its primary and backup data paths, according to the rules in Section 5.2.2.1. Note that n could coincide with either i or j, which would restrict the choice to only two data paths. If at any step in the end-to-end path towards the sink no node or link capacity is available, an error message is sent back. Each intermediate node tries to find an alternate path on its own primary and/or backup paths, as explained above. In the worst case, the source of the relayed connection is reached by the error message, which triggers a switch to the backup path. Connections that are using the capacity reserved for other connections are treated as best effort and can be preempted by those connections the capacity is reserved for.

5.3 Performance Evaluation

The optimization problem $\mathbf{P_{Rout}}$ presented in Section 5.2.1 was implemented in AMPL [29], and solved with CPLEX [2]. In Figs. 48-50, we compared its performance with a simpler solution, where two node-disjoint shortest weighted paths are calculated with an energy metric. We considered 50 sensors randomly deployed in a 3D volume of $500\mathrm{x}500\mathrm{x}50\,\mathrm{m}^3$, which may represent a small harbor, and we set the bandwidth to $50\,\mathrm{kbps}$ and the maximum transmission power to $5\,\mathrm{W}$.

In particular, Fig. 48 shows the expected energy consumption of the network by weighting the cost of the primary and backup paths with the probability of using each of them. We adopted a Poissonian model with failure rate $\lambda = 1/2\,\mathrm{year}^{-1}$ to capture the reliability of each sensor node (in average one node failure every two years). The expected energy consumption increases with the observation time, and decreases with increasing w_2. This happens because by increasing w_2 the objective function of $\mathbf{P_{Rout}}$ weights more the backup paths. Hence, when failures occur, the connections are switched to backup paths characterized by lower energy consumption, which ultimately results in decreased energy consumption. This phenomenon becomes more evident with increasing observation time. Table 6 shows the source block probability (SBP) with increasing observation time, when different failure rates are considered. The source block probability is defined as the probability that a source is able to transmit neither on the primary nor on the backup data path, since both have at least one failed node. While the source block probability increases with increasing observation time and failure rate λ, it only slightly depends on the weight w_2, which allows selecting w_2 based on energy considerations, irrespective of the required reliability. Figure 49 shows a comparison of the average number of hops of source-to-sink connections on primary and backup paths. Primary paths are shown to be longer (higher number of hops), and more energy efficient. Figure 50 compares our solution to primary and backup node-disjoint shortest weighted paths calculated with a hop-distance metric. While the number of hops of the paths calculated by our solution is doubled, the energy consumption is lower than with a shortest-hop metric. The cross-over points in Figs. 49 and 50 occur when $w_2 = w_1 = 0.5$, i.e., when the primary and backup paths are equally weighted to compensate for high failure rates.

As far as the restoration phase in Section 5.2.2 is concerned, we implemented the whole protocol stack of a sensor node to simulate the underwater transmission loss, the transmission and propagation delays, the channel fading, and the physical layer characteristics of underwater receivers. The packet size was set to $500\,\mathrm{Byte}$, and the initial node energy to

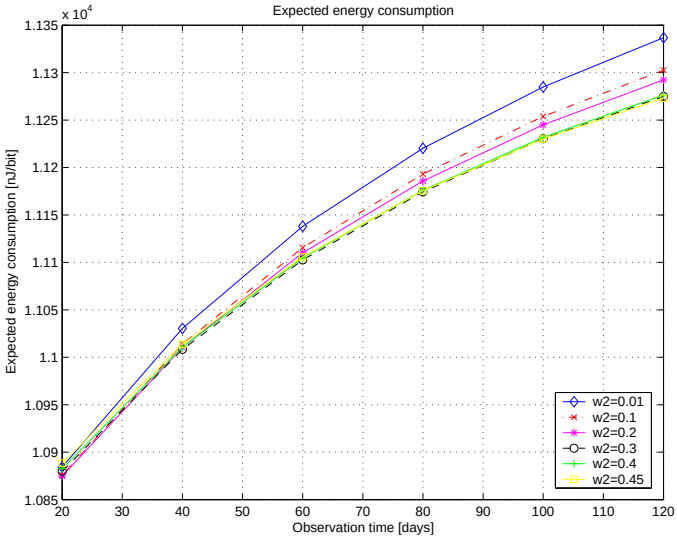

Figure 48: Expected energy consumption for primary and backup paths

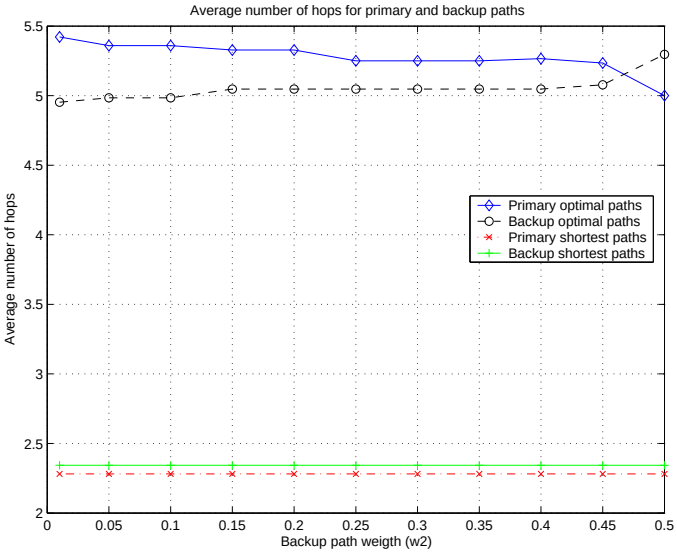

Figure 49: Average number of hops for primary and backup paths (optimal and shortest path)

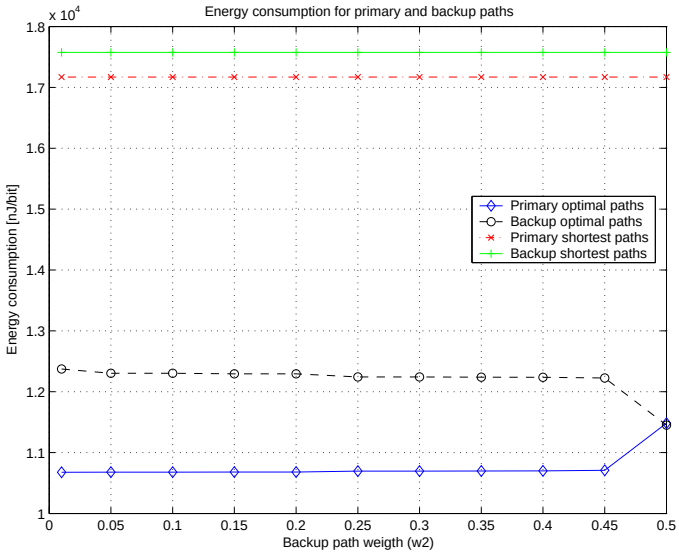

Figure 50: Energy consumption for primary and backup path (optimal and minimum-hop path)

$1000\,\mathrm{J}$. All deployed sensors are desynchronized sources, with packet inter-arrival time equal to $60\,\mathrm{s}$, which allows us to simulate a *low-intensity monitoring traffic* from the entire volume. As far as the MAC is concerned, we adapted the behavior of IEEE 802.11, although we do not advocate this access scheme for this environment. Firstly, we removed the RTS/CTS handshaking, as it yields high delays in a low-bandwidth high-propagation delay environment. Secondly, we tuned all the parameters of IEEE 802.11 according to the physical layer characteristics. For example, while the *slot time* is set to $20\ \mu s$ for 802.11 DSSS (Direct Sequence Spread Spectrum), we found that a value of $0.18\,\mathrm{s}$ is needed to allow devices a few hundred meters apart to share the underwater medium. We also set the values of the contention windows CW_{min} and CW_{max} [10] to 8 and 64, respectively, whereas in 802.11 DSSS they are set to 32 and 1024.

Figures 51-53 and 54-56 show the overall performance of the proposed algorithm, when sensor-sink primary and backup paths are set according to the first phase of our algorithm (Section 5.2.1), and sensor failures are locally handled by the restoration algorithm (Section 5.2.2). In particular, Fig. 51 reports the generated, received, dropped (due to queue

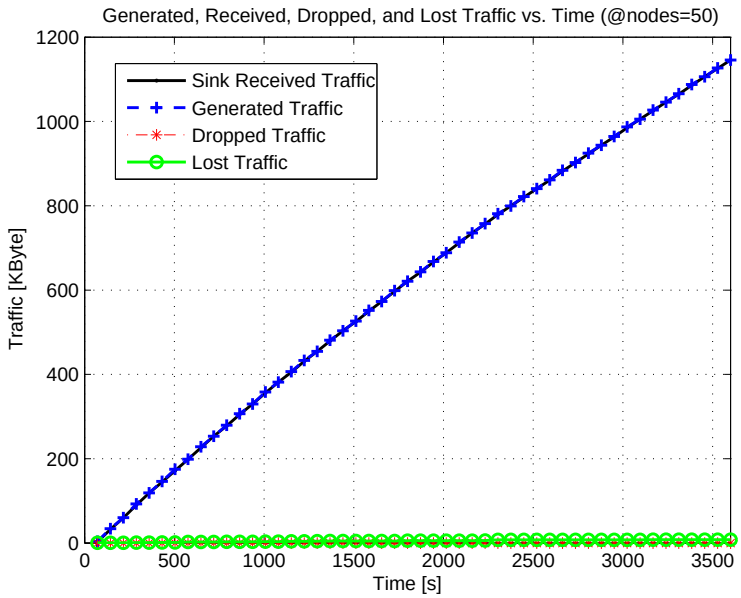

Figure 51: Generated, received, dropped, and lost traffic vs. time (50 nodes)

overflows), and lost traffic (due to sensor failures), while Fig. 52 shows the time evolution of the energy per received bit used by the surface station and by an average node. Figure 53 depicts delay and average delay of packets reaching the surface station. The effect of the fast fading Rayleigh channel (coherence time set to $1\,\mathrm{s}$), which models the heavy multipath UW channel, is captured in Fig. 54, which compares the number of corrupted packets because of channel impairments to the number of packet collisions and duplications (caused by lost ACKs). Finally, Fig. 55 depicts the average queue time evolution, while Fig. 56 quantifies the energy increase caused by the routing reconfigurations that are triggered by the algorithm restoration phase in order to face sensor failures occurring at unpredictable instants (vertical lines).

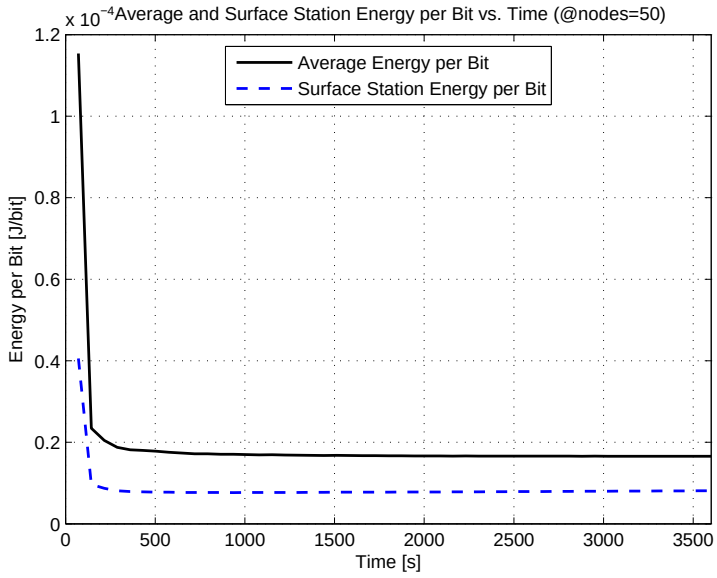

Figure 52: Average and surface station used energy per received bit vs. time (50 nodes)

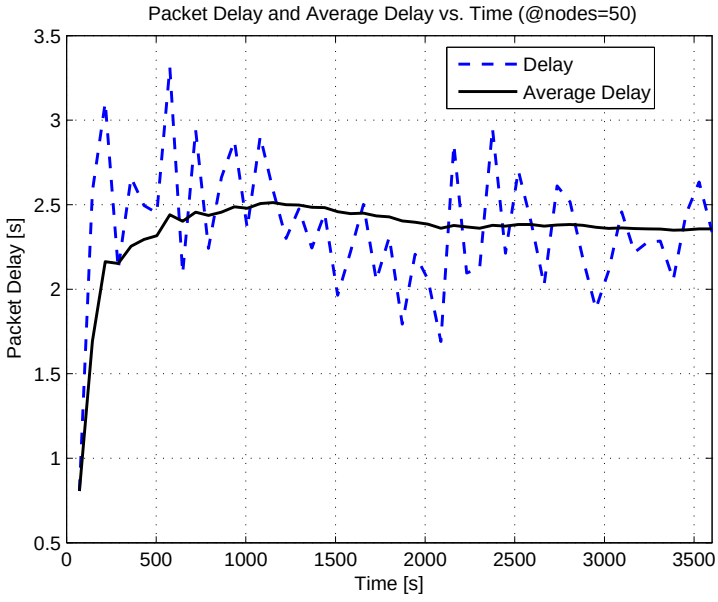

Figure 53: Packet delay and average delay vs. time (50 nodes)

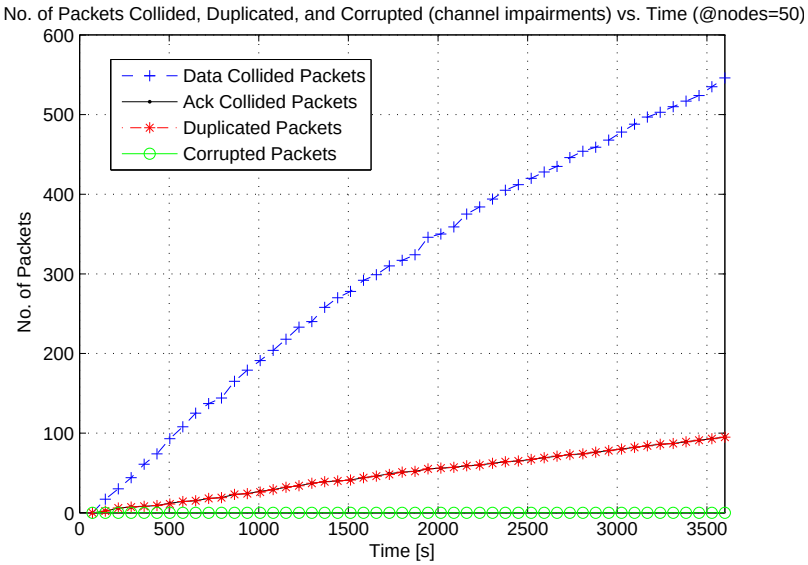

Figure 54: Number of packets collided, duplicated, and corrupted (due to channel impairments) vs. time (50 nodes)

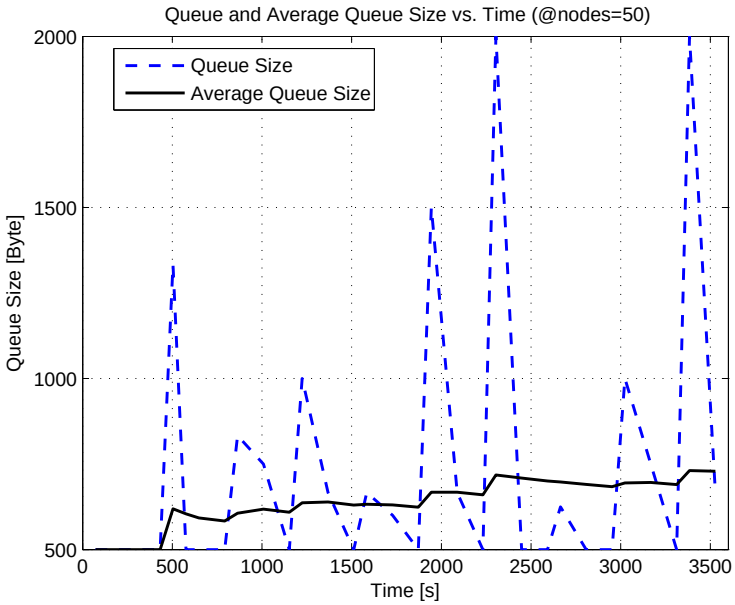

Figure 55: Queue and average queue size vs. time (50 nodes)

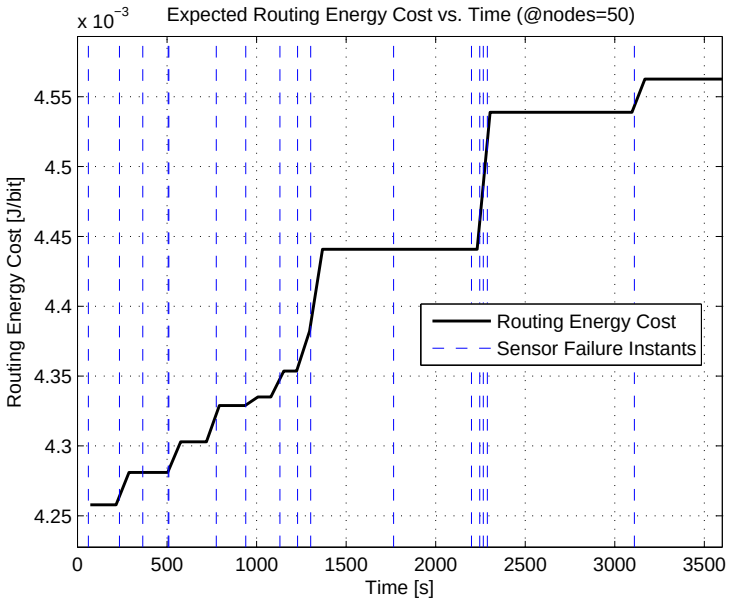

Figure 56: Expected routing energy increase due to sensor failure vs. time (50 nodes)

CHAPTER VI

A CDMA MEDIUM ACCESS CONTROL PROTOCOL FOR UNDERWATER ACOUSTIC SENSOR NETWORKS

6.1 Preliminaries

A major challenge for the deployment of UW-ASNs is the development of a Medium Access Control (MAC) protocol tailored for the underwater environment. In particular, an underwater MAC protocol should provide *high network throughput*, and *low channel access delay* and *energy consumption*, in face of the harsh characteristics of the underwater propagation medium, while guaranteeing *fairness* among competing nodes.

Code Division Multiple Access (CDMA) is the most promising physical layer and multiple access technique for UW-ASNs since i) it is robust to frequency-selective fading, ii) compensates for the effect of multipath by exploiting Rake filters [80] at the receiver, and iii) allows receivers to distinguish among signals simultaneously transmitted by multiple devices. As a result, CDMA increases channel reuse and reduces packet retransmissions, which results in decreased energy consumption and increased network throughput.

For these reasons, in this chapter we introduce UW-MAC, a transmitter-based CDMA MAC protocol for UW-ASNs that incorporates a novel closed-loop distributed algorithm to set the optimal transmit power and code length to minimize the *near-far effect*[1][61]. UW-MAC leverages a *multi-user detector* on resource-rich devices such as surface stations and underwater gateways, and a *single-user detector* on low-end sensors. UW-MAC aims at achieving three objectives, i.e., guarantee i) high network throughput, ii) low channel

[1]The *near-far effect* occurs when the signal received by a receiver from a sender near the receiver is stronger than the signal received from another sender located further. In this case, the remote sender will be dominated by the close sender. To overcome this problem power control strategies need to be implemented so that signals arrive at the receiver with approximately the same mean power.

access delay, and iii) low energy consumption. We prove that UW-MAC manages to simultaneously achieve the three objectives in deep water communications, which are not severely affected by multipath. In shallow water communications[2], which may be heavily affected by multipath, it dynamically finds the optimal trade-off among these objectives.

We also formulate the distributed power and code self-assignment problem to minimize the near-far effect, and propose a low-complexity yet optimal solution. UW-MAC uses locally generated chaotic codes to spread transmitted signals on the available bandwidth, which guarantees a flexible and granular bit rate, secure protection against eavesdropping, transmitter-receiver self-synchronization, and good auto- and cross-correlation properties [14]. To the best of our knowledge, UW-MAC is the first protocol that leverages CDMA properties to achieve multiple access in the bandwidth-limited underwater channel, while existing papers [31][44] considered CDMA schemes merely from a physical layer perspective.

The main features that characterize UW-MAC are: i) it provides a *unique and flexible solution* for different architectures such as static two- and three-dimensional in deep and shallow water; ii) it is *fully distributed*, since spreading codes and transmit power are distributively selected by each sender without relying on a centralized entity; iii) it is *intrinsically secure*, since it uses chaotic codes; iv) it *fairly shares* the bandwidth among active devices; and v) it *efficiently supports multicast transmissions*, since spreading codes are decided at the transmitter side.

The remainder of this chapter is organized as follows. In Section 6.2, we discuss the suitability of the existing ad hoc and sensor MAC protocols for the underwater environment. In Section 6.3, we introduce UW-MAC, while in Section 6.4 we formulate the distributed power and code self-assignment problem. Finally, in Section 6.5, we compare through simulation UW-MAC with existing MAC schemes for sensor networks tuned for

[2]In oceanic literature, *shallow water* refers to water with depth lower than $100\,\mathrm{m}$, while *deep water* is used for deeper oceans.

the underwater environment.

6.2 Related Work

There has been intensive research on MAC protocols for ad hoc [51] and wireless terrestrial sensor networks [50] in the last decade. However, due to the different nature of the underwater environment and applications, existing terrestrial MAC solutions are unsuitable for this environment. In fact, channel access control in UW-ASNs poses additional challenges due to the peculiarities of the underwater channel, in particular limited bandwidth, very high and variable propagation delays, high bit error rates, temporary losses of connectivity, channel asymmetry, and heavy multipath and fading phenomena. For a thorough discussion on the reasons why several multiple access techniques widely employed in terrestrial sensor networks such as TDMA, FDMA, and CSMA, are not suitable for the underwater environment, we refer the reader to [7]. Here, we mainly concentrate on previous work on CDMA, since this is the most promising physical layer and multiple access technique for UW-ASNs. In fact, CDMA is i) robust to frequency-selective fading, ii) compensates for the effect of multipath by exploiting Rake filters [80] at the receiver, and iii) allows receivers to distinguish among signals simultaneously transmitted by multiple devices. For these reasons, CDMA increases channel reuse and reduces packet retransmissions, which results in decreased energy consumption and increased network throughput.

In [31], two spread-spectrum physical layer techniques, namely Direct Sequence Spread Spectrum (DSSS) and Frequency Hopping Spread Spectrum (FHSS), are compared for shallow water communications. While in DSSS data is spread to minimize the mutual interference, in FHSS different simultaneous communications use different hopping sequences and transmit on different frequency bands. Interestingly, [31] shows that in the underwater environment FHSS leads to a higher bit error rate than DSSS. Another attractive access technique combines DSSS CDMA with multi-carrier transmissions [44], which may offer higher spectral efficiency than its single-carrier counterpart. This way, high data rate can be

supported by increasing the duration of each symbol, which reduces Inter Symbol Interference (ISI). However, multi-carrier transmissions may not be suitable for low-end sensors because of their high complexity. Therefore, we focus on single-carrier CDMA to keep the complexity of resource-limited sensor transceivers low. Remarkably, the above papers [31][44] merely consider CDMA from a physical layer perspective, i.e., they analyze the suitability of different forms of CDMA-based transmission techniques with respect to the challenges raised by the underwater channel. Instead, our contribution is to develop a dynamic multiple access protocol for UW-ASNs that efficiently shares the scarce underwater channel bandwidth by fully leveraging the CDMA medium access properties.

In [76], a solution for underwater networks with AUVs was devised. The scheme is based on organizing the network in multiple clusters, each composed of adjacent vehicles. Interference among different clusters is minimized by assigning orthogonal spreading codes to different clusters. Inside each cluster, TDMA is used with long band guards to overcome the effect of the propagation delay. Since vehicles in the same cluster are assumed to be close to one another, the negative effect of the very high underwater propagation delay is limited. The proposed solution, however, assumes a clustered network architecture and proximity among nodes within the same cluster, while we seek a more general and flexible solution suitable for different network sizes and architectures.

In [60], Slotted FAMA, a protocol based on a channel access discipline called Floor Acquisition Multiple Access (FAMA) is proposed. It combines both carrier sensing (CS) and a dialogue between the source and receiver prior to data transmission. During the initial dialogue, control packets are exchanged between the source node and the intended destination node to avoid multiple transmissions at the same time. Time slotting eliminates the asynchronous nature of the protocol and the need for long control packets, thus providing energy savings. However, guard times should be inserted in the time slot to account for any system clock drift. In addition, because of the high underwater acoustic propagation delay, the handshaking mechanism may lead to low system throughput, and the CS scheme

may sense the channel idle while a transmission is still taking place, thus causing packet collisions.

In [35], the impact of the large propagation delay on the throughput of selected classical MAC protocols and their variants is analyzed, and PCAP, Propagation-delay-tolerant Collision Avoidance Protocol, is introduced. Its objective is to fix the time spent on setting up links for data frames, and to avoid collisions by scheduling the activity of sensors. Although PCAP offers higher throughput than widely used conventional protocols for wireless networks, it does not provide a flexible solution for applications with heterogeneous requirements.

A distributed CSMA-based energy-efficient MAC protocol for the underwater environment was recently proposed in [75]. Its objective is to save energy based on sleep periods with low duty cycles. The solution is tied to the assumption that nodes follow sleep periods, and is aimed at efficiently organizing the sleep schedules. Conversely, we are interested in optimizing the utilization of the shared medium to maximize throughput and reduce the energy consumption. Moreover, while our proposed MAC protocol may be enhanced with a sleep schedule algorithm for dense deployment scenarios, we decided not to incorporate it in the basic protocol to make it suitable for a variety of traffic, architecture, and deployment scenarios.

6.3 UW-MAC: A Distributed CDMA MAC for UW-ASNs

6.3.1 Basics

UW-MAC is a transmitter-based Direct Sequence CDMA (DS-CDMA) scheme for UW-ASNs that implements a novel *closed-loop distributed algorithm* to set the optimal transmit power and code length to minimize the near-far effect. UW-MAC leverages a *multi-user detector* on resource-rich devices such as uw-gateways and surface stations, and a *single-user detector* on low-end sensor nodes. In DS-CDMA communication systems, the information-bearing signal is directly multiplied by a spreading code with a larger bandwidth than the

data. The receiver despreads the transmitted spread spectrum signal using a locally generated code sequence. To perform the despreading operation, the receiver must know the code sequence used to spread the signal. Moreover, the received signal and the locally generated code must be synchronized. This synchronization must be accomplished at the beginning of the reception and maintained until the whole signal has been received. In a DS-CDMA scheme the major problem encountered is the Multiuser Access Interference (MAI), which is caused by simultaneous transmissions from different users. In fact, the system efficiency is limited by the total amount of interference and not by the background noise exclusively [17]. Therefore, low cross-correlation between the desired and the interfering users is important to reduce the MAI. Moreover, adequate auto-correlation properties are required for reliable initial synchronization. In fact, large sidelobes of the autocorrelation function can easily lead to erroneous code synchronization decisions. In addition, good autocorrelation properties of the spreading code result in a better resolution of the multipath components of a spread spectrum signal. Unfortunately, cross-correlation and autocorrelation properties cannot be optimized simultaneously.

Single-user detection (SUD) devices use low-cost conventional Rake receivers [80] to detect one user without regard to the existence of other users, which are treated as noise. Although these receivers leverage multipath diversity, there is no sharing of multi-user information or joint signal processing. Conversely, multi-user detection (MUD) devices simultaneously despread signals from several users. Consequently, the two problems of *channel equalization* and *signal separation* are jointly solved to increase the signal-to-interference-plus-noise ratio (SINR) and achieve good performance. MUD techniques have been studied extensively and a number of optimal and suboptimal algorithms have been proposed [52]. These techniques, however, usually require channel estimation and knowledge of all the active user spreading codes, and have considerable computational cost. While this may be feasible for the surface station, and in general for resource-rich devices such as uw-gateways and AUVs, it contrasts with the desire to keep low-end sensors simple and power

efficient. For these reasons, MUD techniques may be suitable for resource-rich devices such as uw-gateways and surface stations, but not for low-end underwater sensors. Thus, UW-MAC relies on low-complexity single-user detectors on low-end underwater sensor nodes.

6.3.2 Protocol Description

Our proposed distributed closed-loop solution aims at setting the optimal combination of transmit power and code length at the transmitter side relying on local periodic broadcasts of MAI values from active nodes, as shown in Fig. 57. Here, node i needs to transmit a data packet to j, without impairing ongoing communications from h to k and from t to n. Since the system efficiency is limited by the amount of total interference, it is crucial for i to optimize its transmission, in terms of transmit power and code length, to limit the near-far problem. The power and code self-assignment problem is formally introduced in Section 6.4, where a distributed low-complexity yet optimal solution is proposed.

In UW-MAC, nodes *randomly access* the channel transmitting a short header called the *Extended Header (EH)*. The EH, of size L_{EH} bits, is sent using a *common chaotic code* c_{EH} known by all devices at the maximum rate (minimum code length). Sender i transmits to its next hop j, located d_{ij} meters apart, the short header EH. The EH contains information about the final destination, i.e., the surface station, the chosen next hop, i.e., node j, and the parameters that i will use to generate the *chaotic spreading code* for the actual data packet, of size L_D bits, that j will receive from i. Immediately after the transmission of the EH, i transmits the data packet on the channel, which is characterized by a raw chip rate r [cps] and sound velocity $\overline{q} \approx 1500\,\mathrm{m/s}$, using the optimal transmit power P_{ij}^{*} [W] and code length c_{ij}^{*} set by the power and code self-assignment algorithm. If no collision occurs during the reception of the EH, i.e., if i is the only node transmitting an EH in the neighborhood of node j, j will be able to synchronize to the signal from i, despread the EH using the common code, and acquire the carried information. At this point, if the EH

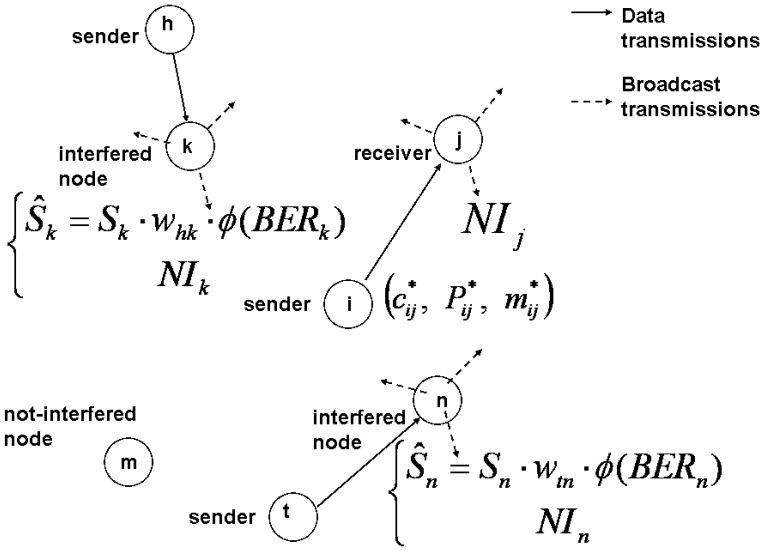

Figure 57: Data and broadcast message transmissions

is successfully decoded, receiver j will be able to locally generate the chaotic code that used to send its data packet, and set its decoder according to this chaotic code in such a way as to decode the data packet. Once j has correctly received the data packet from i, it acknowledges it by sending an ACK packet, of size L_A bits, to j using code c_A. In case i does not receive the ACK before a timeout T_{out} expires, it will keep transmitting the packet until a maximum transmission number N_{max}^T is reached. The timeout must be tuned considering the long propagation and transmission delays, i.e., $T_{out} \geq c_{EH} \cdot L_{EH}/r + c_{ij} \cdot L_D/r + 2d_{ij}/\overline{q} + c_A \cdot L_A/r$. Algorithm 2 reports the pseudo-code executed by sender i.

Note that if sender i does not have updated information about the MAI in j, it increases the code length every time a timeout expires to improve the probability that the packet is successfully decoded, i.e., $c_{ij}^{N_{ij}^T} = \min\left[c_{ij}^{N_{ij}^T-1} \cdot 2^{\beta}, c_{max}\right]$, where $1 \leq N_{ij}^T \leq N_{max}^T$ and $\beta \in \mathbb{R}^+$. As will be shown in Section 6.5, this mechanism guarantees stability and decreases transients, although it temporarily decreases the transmission data rate.

Algorithm 2 UW-MAC pseudo-code executed by sender i

Send an EH packet to node j using common code c_{EH}
Execute *Power and Code Self-assignment Algorithm* $\Rightarrow (c_{ij}^*, P_{ij}^*, m_{ij}^*)$
Generate chaotic code c_{ij}^* and spread the data packet
Transmit the data packet using power P_{ij}^* and margin m_{ij}^*

6.4 Power and Code Self-assignment Problem

Hereafter, we formulate the distributed power and code self-assignment problem, and propose a low-complexity yet optimal closed-loop solution. An open-loop power control algorithm that does not rely on feedback from the receiver would rely on the symmetric link assumption, which does not hold in the underwater environment.

6.4.1 Deep Water Channels

We consider a deep water acoustic channel, which is not severely affected by multipath, where the transmission loss TL_{ij} that a narrow-band acoustic signal centered at frequency $f\,[\mathrm{kHz}]$ experiences between nodes i and j at distance $d\,[\mathrm{m}]$ is described by the Urick propagation model [90], $TL_{ij} = d_{ij}^2 \cdot 10^{[\alpha(f)\cdot d_{ij}+A]/10}$, where $\alpha(f)\,[\mathrm{dB/m}]$ represents the *medium absorption coefficient*, and $A \in [0,5]\,\mathrm{dB}$ is the so-called *transmission anomaly*, which accounts for the degradation of the acoustic intensity caused by multiple path propagation, refraction, diffraction, and scattering of sound.

Each node i needs to i) limit the near-far effect when it transmits to j and ii) avoid impairing ongoing communications. These constraints are mathematically expressed by the following equations,

$$\begin{cases} \frac{N^0+I_j}{\frac{P_{ij}}{TL_{ij}}} \leq w_{ij} \cdot \Phi(BER_j) \\ \frac{N^0+I_k+\frac{P_{ij}}{TL_{ik}}}{S_k} \leq w_{t_k k} \cdot \Phi(BER_k),\ \forall k \in \mathcal{K}_i. \end{cases} \tag{56}$$

In (56), $N^0\,[\mathrm{W}]$ is the average noise power, I_j and I_k $[\mathrm{W}]$ are the MAI at nodes j and $k \in \mathcal{K}_i$, with $\mathcal{K}_i$ being the set of nodes whose ongoing communications may be affected by node i's transmit power. Then, w_{ij} and $w_{t_k k}$ are the bandwidth spreading factors of

the ongoing transmissions from i to j and from t_k to k, respectively, where t_k is the node transmitting to k. Furthermore, P_{ij} [W] represents the power transmitted by i to j when an ideal channel (without multipath, i.e., $A = 0\,\mathrm{dB}$) is assumed, i.e., when no power margin is considered to face the fading dips. Finally, TL_{ij} and TL_{ik} are the transmission losses from i to j and from i to $k \in \mathcal{K}_i$, respectively, while S_k [W] is the power of the signal that receiver k is decoding, and $\Phi()$ is the MAI threshold, which depends on the target bit error rate (BER) at the receiver node (see [61]). We will denote the noise and MAI power of a generic node n as $NI_n = N^0 + I_n$, and the normalized received spread signal, i.e., the signal power after despreading, as $\hat{S}_n = S_n \cdot w_{t_n n} \cdot \Phi(BER_n)$.

The first constraint in (56) states that the SINR^{-1} at receiver j needs to be below a certain threshold, i.e., the power P_{ij} transmitted by i needs to be sufficiently high to allow receiver j to successfully decode the signal, given its current noise and MAI power level (NI_j). The second constraint in (56) states that the SINR^{-1} at receivers $k \in \mathcal{K}_i$ must not be above a threshold, i.e., the power P_{ij} transmitted by i must not impair the ongoing communications toward nodes $k \in \mathcal{K}_i$, given their normalized received user spread signals $(\hat{S}_k)$, and noise and MAI level (NI_k). By combining the constraints in (56), we obtain the following compact expression,

$$\frac{NI_j \cdot TL_{ij}}{w_{ij} \cdot \Phi(BER_j)} \leq P_{ij} \leq \min_{k \in \mathcal{K}_i} \left[(\hat{S}_k - NI_k) \cdot TL_{ik} \right]. \tag{57}$$

Consequently, to set the transmit power P_{ij} and spreading factor w_{ij}, node i needs to leverage information on the MAI and normalized receiving spread signal of neighboring nodes. This information is broadcast periodically by active nodes, as depicted in Fig. 57. In particular, to limit such broadcasts, a generic node n transmits only significant values of NI_n and $\hat{S}_n$, i.e., out of predefined tolerance ranges.

To save energy, node i will select a transmit power P_{ij} and a code length c_{ij} in such a way as to satisfy the set of constraints in (57) and to minimize the energy per bit $E^b_{ij}(P_{ij}, c_{ij}) = (P_{tx} + P_{ij}) \cdot c_{ij}/r$ [J/bit]. Here, P_{tx} [W] is a *distance-independent* component accounting for the power needed by the transmitting circuitry, and r [cps] the *constant* underwater chip

rate, which is proportional to the available acoustic spectrum B [Hz] and to the modulation spectrum efficiency η_B, i.e., $r = \eta_B \cdot B$. Since E_{ij}^b decreases as transmit power and code length decrease, and since the relation between the spreading factor w_{ij} and the code length c_{ij} depends on the family of codes, i.e., $w_{ij} = \mathcal{W}^{\mathcal{C}}(c_{ij})$, the optimal solution is $c_{ij}^* = c_{min}$ and $P_{ij}^* = NI_j \cdot TL_{ij}/[\alpha \cdot c_{min} \cdot \Phi(BER_i)]$, where we assumed the spreading factor to be proportional to the code length, i.e., $w_{ij} = \alpha \cdot c_{ij}$. Note that this solution achieves the three objectives of minimizing the energy per bit E_{ij}^b that i needs to successfully communicate with j in the minimum possible time, i.e., minimize the energy consumption while transmitting at the highest possible data rate, i.e., r/c_{min}.

6.4.2 Shallow Water Channels

We assume now that the channel is heavily affected by multipath (*saturated condition*, see [70]) as it is often the case in shallow water [7]. In this environment, the signal fading can be modeled by a Rayleigh r.v., which accounts for a *worst-case scenario*, and the transmission loss between i and j is $TL_{ij} \cdot \rho^2$, where $TL_{ij} = d_{ij} \cdot 10^{[\alpha(f) \cdot d_{ij} + A]/10}$, with $A \in [5, 10]$ dB, and ρ has a unit-mean Rayleigh cumulative distribution $D_\rho(\rho) = 1 - \exp(-\pi\rho^2/4)$. Let us define the *signal transmission margin* for link (i, j) as m_{ij}, where $P_{ij}^* \cdot m_{ij}^2$ [W] is the actual transmit power, while P_{ij}^* [W] represents the optimal transmission power in an ideal channel, as introduced in Section 6.4.1, i.e., the transmit power before applying the margin to face the fading dips. The packet error rate PER_{ij} experienced on link (i, j) when sender i transmits power $P_{ij}^* \cdot m_{ij}^2$ can be defined as the probability that the received power at node j be smaller than that required in an ideal channel where no multipath is experienced, i.e.,

$$PER_{ij} = \Pr\left\{\frac{P_{ij}^* \cdot m_{ij}^2}{TL_{ij} \cdot \rho^2} < \frac{{P_{ij}}^*}{TL_{ij}}\right\} = \Pr\left\{\rho \geq m_{ij}\right\} = 1 - D_\rho(m_{ij}) = \exp\Big(-\frac{\pi m_{ij}^2}{4}\Big). \tag{58}$$

Hence, the average number of transmissions of a packet such that receiver j correctly decodes it when it is sent with signal transmission margin m_{ij} is $N_{ij}^T(m_{ij}) = [1 - PER_{ij}]^{-1} = D_\rho(m_{ij})^{-1}$. This relation assumes independent errors among adjacent packets, which holds

when the channel coherence time is shorter than the retransmission timeout, i.e., the time before retransmitting an unacknowledged packet. We can now cast the power and code self-assignment optimization problem in a Rayleigh channel.

P: **Power and Code Self-assignment Optimization Problem**

$$
\begin{aligned}
Given: \quad & P^{max}, r, TL_{ij}, NI_j, BER_j; \hat{S}_k, NI_k, \forall k \in \mathcal{K}_i \\
Find: \quad & c_{ij}^* \in [c_{min}, c_{max}], \; P_{ij}^* \in \mathbb{R}^+, \; m_{ij}^* \in \mathbb{R}^+ \\
Min.: \quad & E_{ij}^b(c_{ij}, P_{ij}, m_{ij}) = \frac{(P_{tx}+P_{ij}\cdot m_{ij}^2)\cdot c_{ij}}{r} \cdot N_{ij}^T(m_{ij}) \\
Subject\ to: \quad &
\end{aligned}
$$

$$
N_{ij}^T(m_{ij}) = D_\rho(m_{ij})^{-1} = \left[1 - \exp\Big(-\frac{\pi m_{ij}^2}{4}\Big)\right]^{-1}; \tag{59}
$$

$$
P_{ij}^{min}(c_{ij}) \leq P_{ij} \leq \min\left[P_{ij}^{max}, P^{max}\right]; \tag{60}
$$

$$
P_{ij}^{min}(c_{ij}) \leq P_{ij} \cdot m_{ij}^2 \leq \min\left[P_{ij}^{max}, P^{max}\right]; \tag{61}
$$

where

$$
P_{ij}^{min}(c_{ij}) = \frac{NI_j \cdot TL_{ij}}{\alpha \cdot c_{ij} \cdot \Phi(BER_j)} = \frac{\Gamma_{ij}}{c_{ij}}, \tag{62}
$$

$$
\Gamma_{ij} = \frac{NI_j \cdot TL_{ij}}{\alpha \cdot \Phi(BER_j)}, \tag{63}
$$

$$
P_{ij}^{max} = \min_{k \in \mathcal{K}_i}\left[(\hat{S}_k - NI_k) \cdot TL_{ik}\right]. \tag{64}
$$

Note that, in constraints (60) and (61), the transmit power *lower bound*, P_{ij}^{min}, is a *function* that depends on the chosen code length c_{ij}, which is a solution variable of $\mathbf{P}$, whereas the transmit power *upper bound*, $\min\left[P_{ij}^{max}, P^{max}\right]$, is a *constant* only depending on the node maximum transmit power (P^{max}) and on the broadcast MAI (NI_k) and normalized received spread signal $(\hat{S}_k)$.

While $\mathbf{P}$ may seem a fairly complex optimization problem, it admits a low-complexity yet optimal closed-form solution. To find it, we rely on a property of the objective function, i.e., the minimum energy per bit E_{ij}^b monotonically decreases as P_{ij} and the code length c_{ij} decrease. $\mathbf{P}$ *may* admit a feasible solution if in (60) $P_{ij}^{min}(c_{ij}) \leq \min\left[P_{ij}^{max}, P^{max}\right]$ holds,

i.e., if $c_{ij} \geq \frac{\Gamma_{ij}}{\min[P_{ij}^{max}, P^{max}]}$. Consequently, to minimize the objective function, we want the optimal code length[3] c_{ij}^* to be

$$c_{ij}^* = \max\left[\min\left[\frac{\gamma \cdot \Gamma_{ij}}{\min[P_{ij}^{max}, P^{max}]}, c_{max}\right], c_{min}\right], \tag{65}$$

where γ is a margin on the code length aimed at absorbing information inaccuracy. By substituting (65) into (62), given (60), we obtain the optimal transmit power *before* applying the margin to the channel, P_{ij}^*, as

$$P_{ij}^* = \min\left[\frac{\Gamma_{ij}}{c_{ij}^*}, P^{max}\right]. \tag{66}$$

Finally, by substituting (65) and (66) into the objective function, we obtain the energy per bit as a function of the margin only,

$$E_{ij}^b(m_{ij}) = \frac{P_{tx} \cdot c_{ij}^* + \Gamma_{ij} \cdot m_{ij}^2}{r \cdot \left[1 - \exp\left(-\frac{\pi m_{ij}^2}{4}\right)\right]}, \tag{67}$$

which can then be minimized to obtain the optimal margin m_{ij}^* as numeric solution of the following equation

$$\frac{dE_{ij}^b}{dm_{ij}} = 0; \;\; \Rightarrow \;\; \frac{{m_{ij}^*}^2}{4} + \frac{\pi P_{tx} c_{ij}^*}{4\Gamma_{ij}} + 1 = \exp\left(\frac{\pi {m_{ij}^*}^2}{4}\right). \tag{68}$$

Note that $\mathbf{P}$ is feasible iff the optimal solution $(c_{ij}^*, P_{ij}^*, m_{ij}^*)$ meets constraint (61), i.e., iff $P_{ij}^* \cdot {m_{ij}^*}^2 \leq \min[P_{ij}^{max}, P^{max}]$. Otherwise, an energy-efficient suboptimal solution, $(c_{ij}^+, P_{ij}^+, m_{ij}^+)$, would be $c_i^+ = c_{max}$ and $P_{ij}^+ \cdot {m_{ij}^+}^2 = \min[P_{ij}^{max}, P^{max}]$.

The computational complexity of the proposed optimal closed-form solution is very low since the most computation-intense operation is finding the solution to (68). Many numerical algorithms such as the *Newton descending approximation* can be effectively used. Moreover, a transmitting node does not have to adjust its transmit power and code length every time it needs to communicate, but only if any of the inputs of $\mathbf{P}$ has consistently changed. Not only does this make the computational burden on low-end sensors easily

[3]Note that, by using *chaotic codes* as opposed to *pseudo-random sequences*, a much higher granularity in the choice of the code length can be achieved; code lengths, in fact, do not need to be a power of 2.

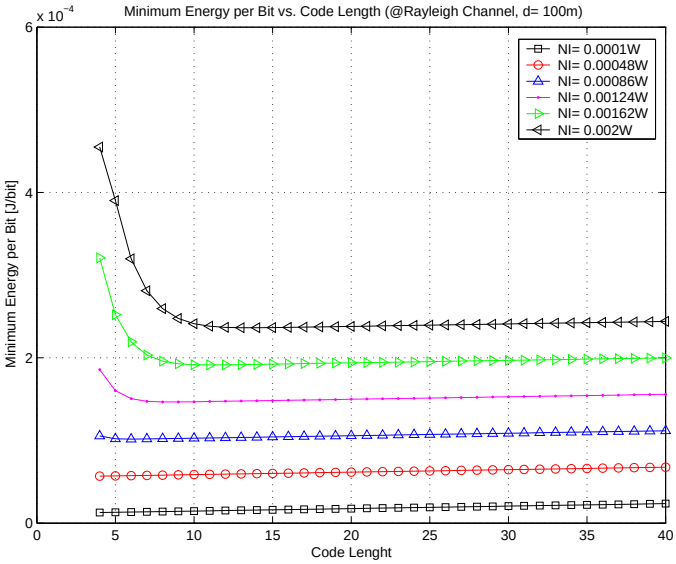

Figure 58: Minimum energy per bit vs. code length (Rayleigh Channel)

affordable, but it also helps reach system stability while limiting the signaling overhead, as will be shown in Section 6.5.

Differently from the deep water case, the energy per bit in a Rayleigh channel sky-rockets when an adequate power margin is not used, because of the high number of packet retransmissions, as accounted by (59). Moreover, a trade-off between the optimal transmit power and code length occurs, which suggests that it is not always possible to *jointly* achieve the highest data rate and the lowest energy consumption, as it is possible in a channel that is not affected by multipath.

This non-trivial result is confirmed by Fig. 58, where the minimum energy per bit in a Rayleigh channel under different MAI power levels (NI_j) at receiver j is reported, when the code length c_{ij} ranges from $c_{min} = 4$ to $c_{max} = 40$. As previously anticipated, when the MAI at the receiver side is higher than a certain threshold $(NI_j \geq 1.24\,\mathrm{mW})$ it is not possible anymore to select the highest data rate, i.e., the shortest code, to achieve the minimum energy per bit. Conversely, with low MAI at the receiver, this twofold objective can still be achieved. In fact, the lowest three monotonic curves in Fig. 58 show that the minimum energy per bit is achieved when the code length is minimum $(c = c_{min})$, i.e.,

when the transmit rate is maximum. Conversely, the upper curves have minima that are not associated with the lowest code length, which shows the need to trade off between energy consumption and transmission rate.

6.5 Performance Evaluation

In this section, we discuss performance results of UW-MAC, presented in Section 6.3, for three different UW-ASN architectures described in [7], the *2D deep water*, the *3D shallow water*, and the *3D with AUVs*. In addition, we evaluate the added benefit in terms of energy consumption, channel access delay, and network throughput of multi-user detectors over single-user detectors, introduced in Section 6.3, in a wide variety of conditions and scenarios to capture relevant underwater setups. To accomplish this, we evaluate two versions of our proposed MAC solution. In particular, we refer to *UW-MACsgl* as the case where all nodes implement a single-user detector, and to *UW-MACmlt* as the case where resource-rich devices such as uw-gateways and surface stations implement a multi-user detector, while low-end sensor nodes implement a single-user detector.

We implemented the entire protocol stack of a sensor node to simulate the characteristics of the underwater environment. In particular, we modeled the underwater transmission loss, the transmission and propagation delays, and the physical layer characteristics of underwater receivers. We decided to implement neither Slotted FAMA [60] nor the MAC protocol proposed in [75] since their objectives differ from those of our CDMA MAC solution, as described in Section 6.2, and a fair comparison is not possible. Rather, we compare the two versions of UW-MAC, UW-MACsgl and UW-MACmlt, with four existing random access MAC protocols, which we optimized to the underwater environment, i.e., CSMA, CSMA with power control (CSMApw), IEEE 802.11, and ALOHA. In particular, in IEEE 802.11 the value of the slot time in the backoff mechanism has to account for the propagation delay at the physical layer. Hence, while it is set to $20\,\mu\mathrm{s}$ for 802.11 DSSS, a value of $0.18\,\mathrm{s}$ is needed to allow devices a few hundred meters apart to share the underwater

medium. This implies that the delay introduced by the backoff contention mechanism is several orders of magnitude higher than in terrestrial channels, which in turn leads to very low channel utilization efficiencies. In addition, we set the values of the contention windows CW_{min} and CW_{max} to 8 and 64, respectively, whereas in 802.11 DSSS they are set to 32 and 1024, and the binary backoff coefficient to 1.5, whereas it is usually set to 2 in terrestrial implementations.

In all the simulation scenarios, we considered a common set of parameters, which is reported in the following, whereas specific parameters for each architecture are reported in the appropriate section. We set the chip rate r to $100\,\mathrm{kcps}$, the minimum code length c_{min} to 4 and the maximum c_{max} to 40, the maximum transmission power P^{max} to $10\,\mathrm{W}$, the data packet size to $250\,\mathrm{Byte}$, the control and header packet size to $10\,\mathrm{Byte}$, the initial node energy to $1000\,\mathrm{J}$, the queue size to $10\,\mathrm{kByte}$, the available acoustic spectrum to $50\,\mathrm{kHz}$, and the transmission anomalies caused by multipath in deep and shallow water to $0\,\mathrm{dB}$ and $5\,\mathrm{dB}$, respectively. Moreover, all deployed sensors are sources, with packet inter-arrival time equal to $20\,\mathrm{s}$, which allows us to simulate a *low-intensity background monitoring traffic* from the entire volume toward the surface station, which is centered on the surface of the underwater volume. Finally, we adopted the geographical routing algorithm tailored for UW-ASNs, which we proposed in [66], according to which each node selects its next hop with the objective of minimizing the energy consumption. Simulation results presented in the next sections are averaged on several experiments to obtain small 95% confidence relative intervals, which are showed in the figures.

6.5.1 Two-dimensional Deep Water UW-ASNs

We considered a variable number of sensors (from 10 to 50) randomly deployed on the bottom of a deep water volume of $500\mathrm{x}500\mathrm{x}500\,\mathrm{m}^3$. The underwater gateways are randomly deployed on the bottom as well, and their number is varied in such a way as to be 20%

of the total number of deployed sensors. The antenna gain at the transmitting and receiving side of a vertical link is set to $10\,\mathrm{dB}$, according to data sheets of available long-haul hydrophones (underwater microphones).

Figures 59 and 60 depict the average packet delay and energy per received bit in the simulation transient state when 30 sensors are deployed. The proposed UW-MAC protocol versions outperform the competing MAC schemes in terms of both delay (one order of magnitude) and energy consumption ($25\mu\,\mathrm{J/bit}$ vs. $45\mu\,\mathrm{J/bit}$ and over), although the extremely harsh scenario leads to delays in the order of seconds and high energy per bit for all the MAC schemes. Figures 61 and 62-64 show the overall performance of the competing MAC protocols when the number of deployed sensors and uw-gateways increases. Figure 61 shows that both UW-MACsgl and Uw-MACmlt have a much smaller average packet delay than the competing schemes. In particular, it is pointed out that the RTS/CTS handshaking of 802.11 yields high delays in the low-bandwidth high-delay underwater environment. As far as the energy per successfully received bit is concerned, we note that our MAC solutions are the most energy efficient (Fig. 62). Surface sinks, however, are resource-rich devices since they are in general endowed with higher capacity batteries. Moreover, batteries on surface stations can be recharged through renewable energy sources, whereas the energy of underwater sensors is limited and usually batteries cannot be easily recharged, also because solar energy cannot be exploited.

The highest successfully received number of packets is associated with our UW-MACmlt (Fig. 63), which takes advantage of its multi-user receiving capabilities. All the schemes relying on carrier sense (CSMA, CSMApw, and 802.11) perform poorly since this mechanism prevents collisions with the current transmissions only at the transmitter side. To prevent collisions at the receiver side it would be necessary to add a guard time between transmissions dimensioned according to the maximum propagation delay in the network, which would make the protocols dramatically inefficient in the underwater environment.

Consequently, the *hidden terminal* and the *exposed terminal* problems [4] are the main causes for the low performance of MAC schemes relying on carrier sense. Figure 64 quantifies the dramatic decrease in terms of data packet collisions of our proposed UW-MAC schemes, which is motivated by the very low collision probability of the small EH randomly accessing the channel. Conversely, ALOHA experiences a high number of packet collisions since it directly accesses the medium whenever there is data to be transmitted. In the underwater environment, ALOHA is often affected by low efficiency, mainly because of the low acoustic propagation speed. Moreover, the need for retransmissions increases the power consumption of sensors, as confirmed in Fig. 62, which ultimately reduces the network lifetime.

As a final remark, the use of contention-based techniques that rely on handshaking mechanisms such as RTS/CTS in shared medium access (e.g., MACA [45], IEEE 802.11) is impractical in underwater, for the following reasons: i) large delays in the propagation of RTS/CTS control packets lead to low channel utilization efficiency and throughput; ii) because of the high underwater acoustic propagation delay, when carrier sense is used, it is more likely that the channel will be sensed idle while a transmission is taking place, since the signal may not have reached the receiver yet; iii) the variability of delay in handshaking packets makes it impractical to accurately predict the start and finish time of the transmissions of other nodes.

6.5.2 Three-dimensional Shallow Water UW-ASNs

We considered a variable number of sensors (from 10 to 50) randomly deployed in the 3D shallow water with volume of $500\text{x}500\text{x}50\,\mathrm{m}^3$, which may represent a small harbor. We modeled the multipath phenomenon by considering a worst-case scenario consisting of a saturated fast fading Rayleigh channel with coherence time equal to $1\,\mathrm{s}$. As compared to

[4] The *hidden terminal problem* arises when the channel is sensed free by the sender although the receiver is already receiving another packet from another node, while the *exposed terminal problem* is encountered when the channel is sensed busy by the sender although the receiver is free to receive.

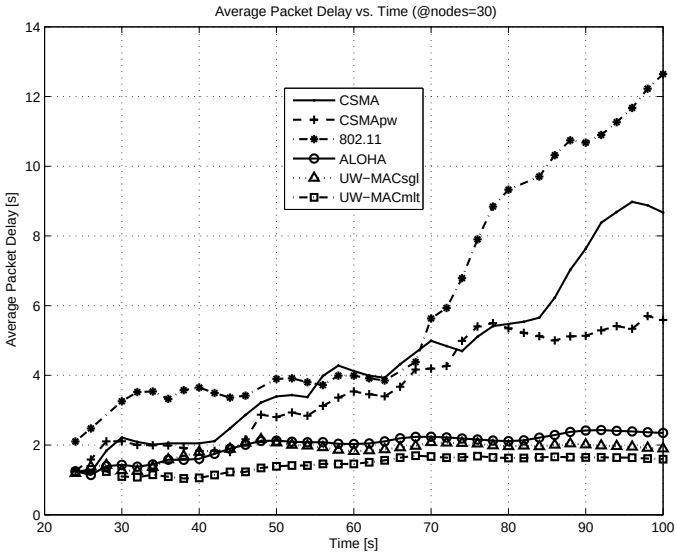

Figure 59: *2D Deep Water UW-ASNs.* Average packet delay vs. simulation time (30 sensors, 6 uw-gateways)

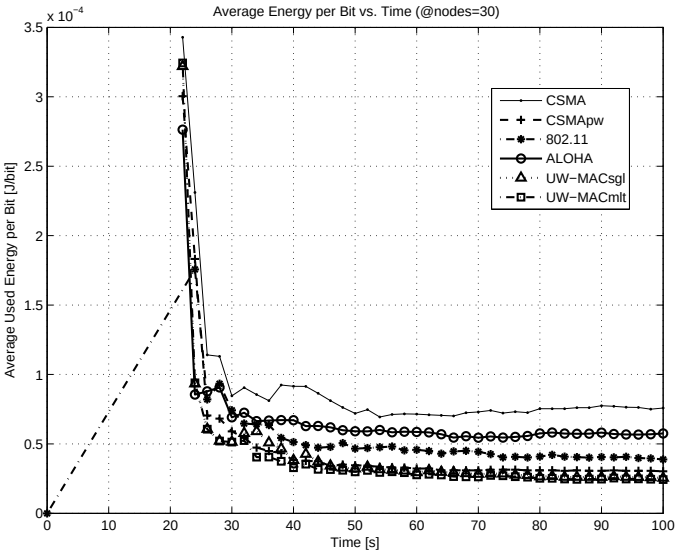

Figure 60: *2D Deep Water UW-ASNs.* Average energy per received bit vs. simulation time (30 sensors, 6 uw-gateways)

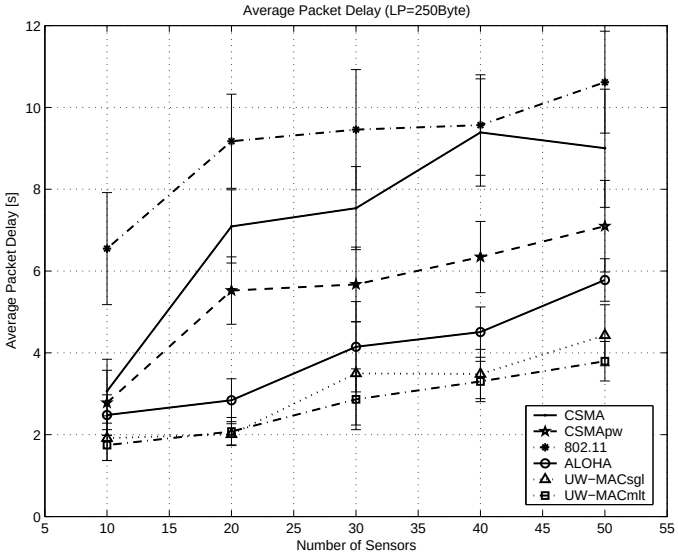

Figure 61: *2D Deep Water UW-ASNs.* Average packet delay vs. number of sensors

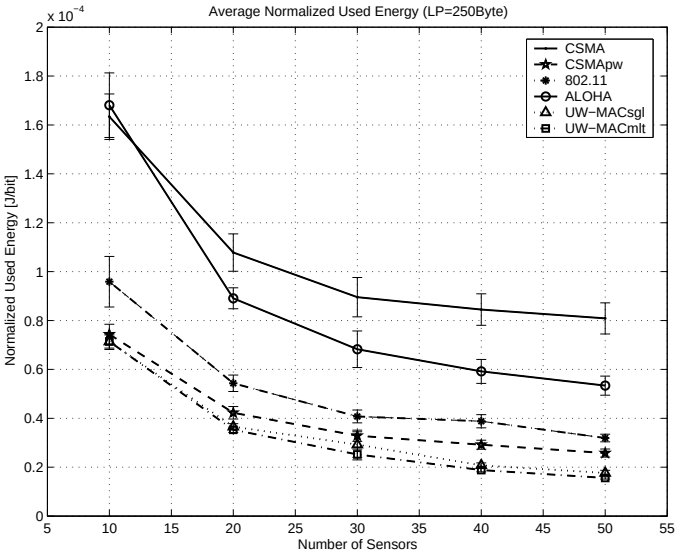

Figure 62: *2D Deep Water UW-ASNs.* Average normalized used energy vs. number of sensors

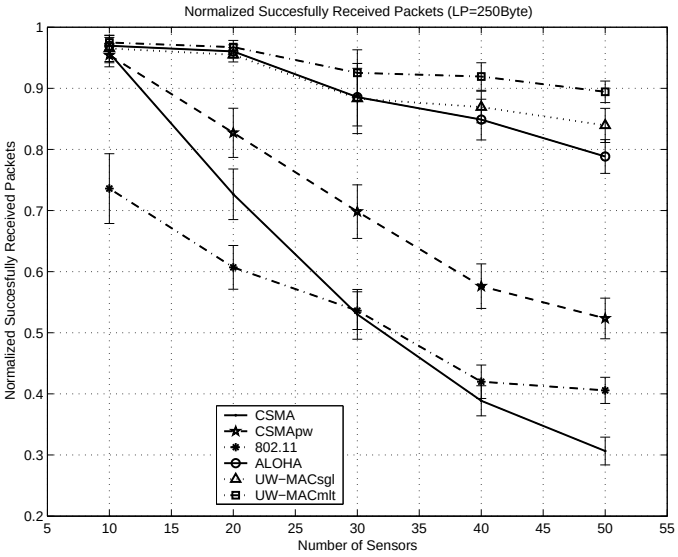

Figure 63: *2D Deep Water UW-ASNs.* Normalized successfully received packets vs. number of sensors

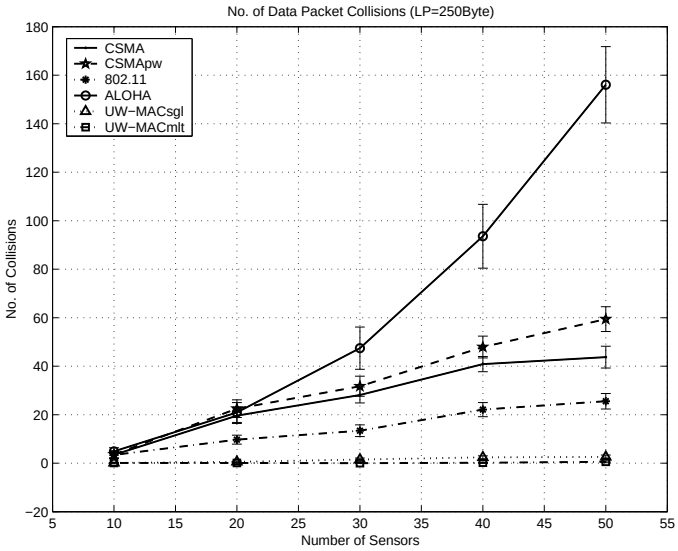

Figure 64: *2D Deep Water UW-ASNs.* Number of data packet collisions vs. number of sensors

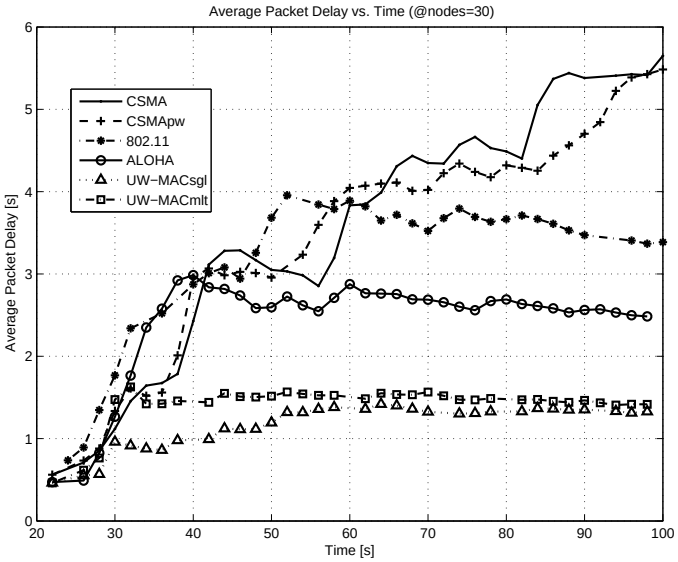

Figure 65: *3D Shallow Water UW-ASNs.* Average packet delay vs. simulation time (30 sensors)

the 2D deep water scenario, in this shallow water scenario the overall performance of our solution is even better with respect to the competing MAC schemes mainly because of the higher channel reuse achieved. When the number of sensors increases, the implemented routing algorithm [66] has a higher flexibility in the choice of data paths, which rely more on multi-hop communications, thus increasing their average number of hops. While at the routing layer this decreases the expected end-to-end energy to forward packets, higher interference is generated at the MAC layer. Interestingly, both versions of our UW-MAC solution show very good robustness to this effect, while their competing MAC schemes are negatively affected, as shown throughout the reported figures (Figs. 65-70). This phenomenon is particularly evident in Fig. 69, where the normalized received packet metric drops below 0.45 in all the random-access MAC schemes when 50 sensors are deployed, while UW-MACsgl, and even more UW-MACmlt, have very high performance (UW-MACsgl over 0.80 and UW-MACmlt close to 0.95 with 50 sensors).

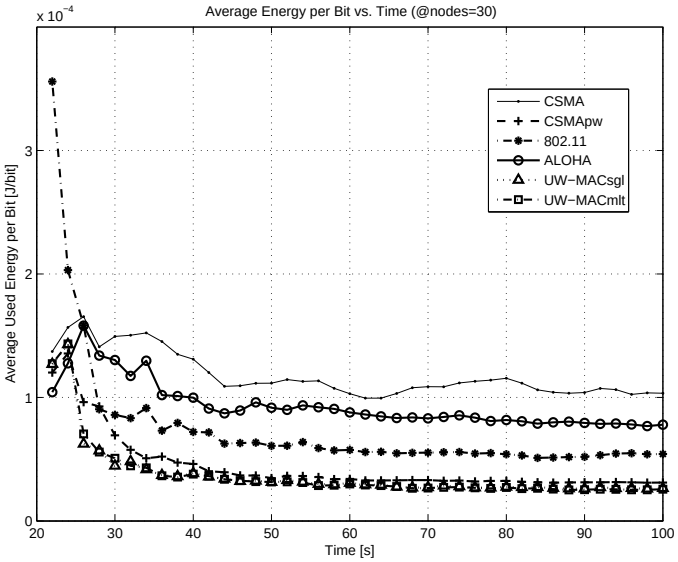

Figure 66: *3D Shallow Water UW-ASNs.* Average energy per received bit vs. simulation time (30 sensors)

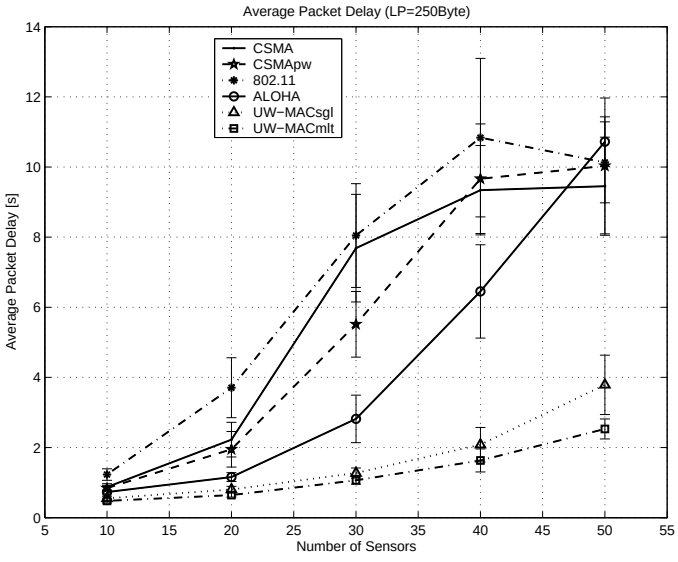

Figure 67: *3D Shallow Water UW-ASNs.* Average packet delay vs. number of sensors

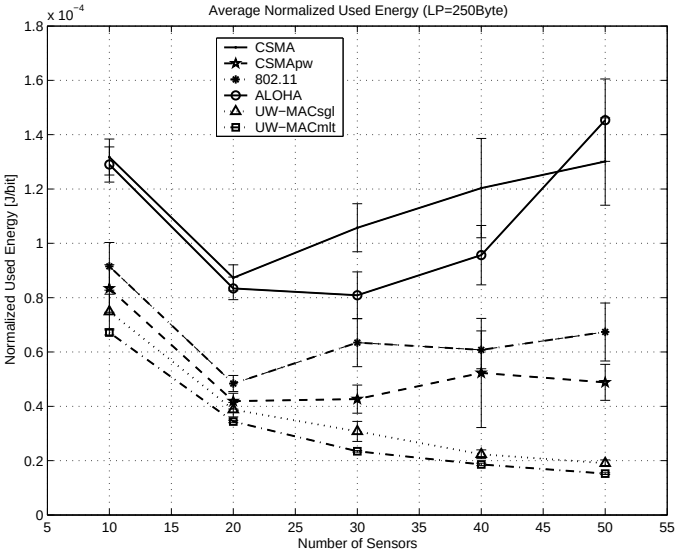

Figure 68: *3D Shallow Water UW-ASNs.* Average normalized used energy vs. number of sensors

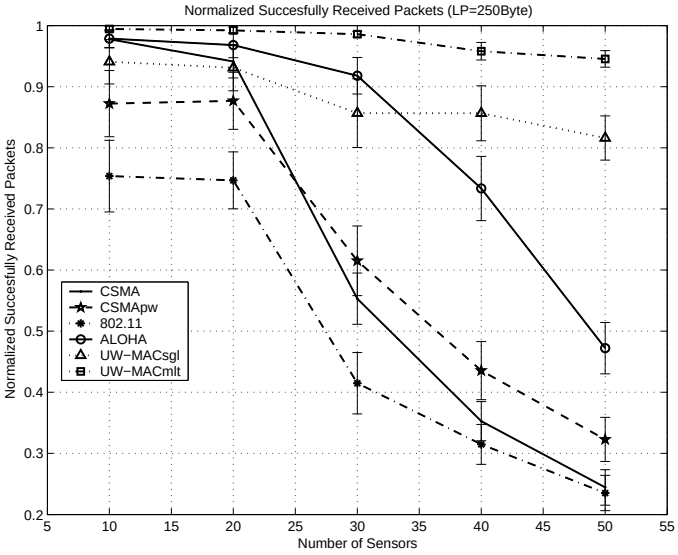

Figure 69: *3D Shallow Water UW-ASNs.* Normalized successfully received packets vs. number of sensors

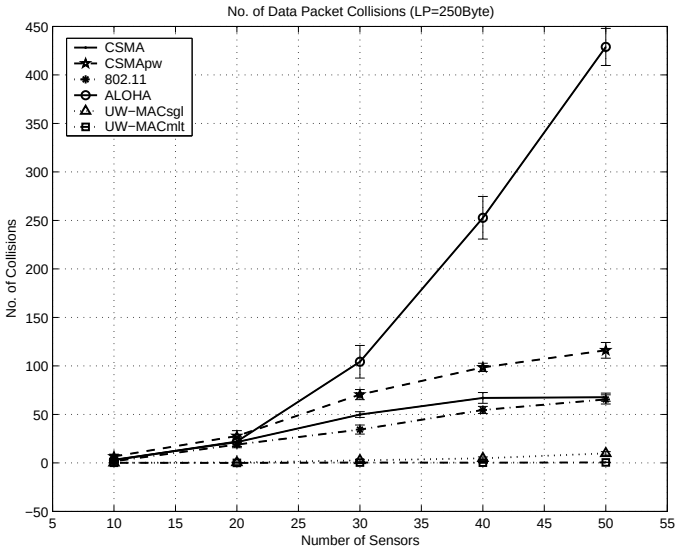

Figure 70: *3D Shallow Water UW-ASNs.* Number of data packet collisions vs. number of sensors

6.5.3 Three-dimensional UW-ASNs with Mobile AUVs

We considered a variable number of sensors (from 5 to 50) randomly deployed in the 3D shallow water with volume of $500\text{x}500\text{x}50\,\mathrm{m}^3$, and 3 AUVs moving in the entire volume according to the Random Waypoint mobility model. We set the velocity to $3\,\mathrm{m/s}$ and no pause between consecutive movements to simulate a worst-case mobility scenario. In all MAC schemes, AUVs broadcast location update messages when their position has changed by more than $20\,\mathrm{m}$. Figures 71-76 report the overall performance in this simulation setting, and show the robustness of our MAC solutions against inaccurate node position and interference information mainly caused by mobility, traffic unpredictability, and packet loss due to channel impairment. In particular, Figs. 74 and 75 show the dramatic improvements of UW-MAC over other MAC solutions, both in terms of energy ($15\mu\,\mathrm{J/bit}$ vs. $30-40\mu\,\mathrm{J/bit}$ and over) and normalized received packets ($0.7-0.9$ vs. 0.3 for more than 35 sensors).

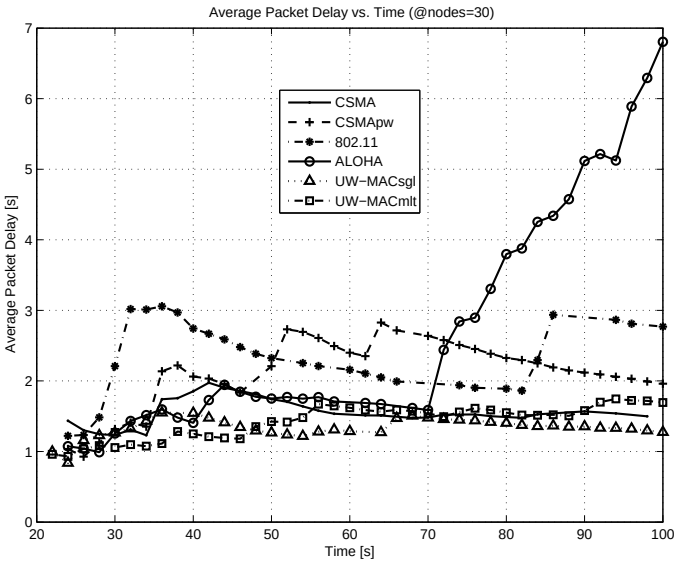

Figure 71: *3D UW-ASNs with mobile AUVs.* Average packet delay vs. simulation time (30 sensors)

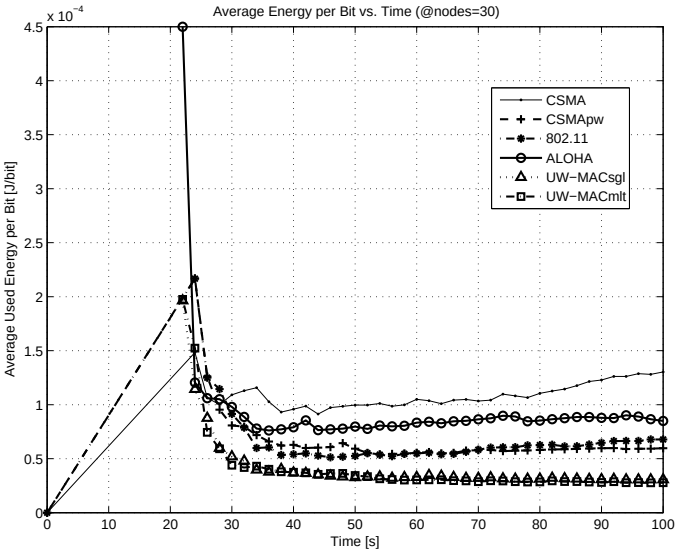

Figure 72: *3D UW-ASNs with mobile AUVs.* Average energy per received bit vs. simulation time (30 sensors)

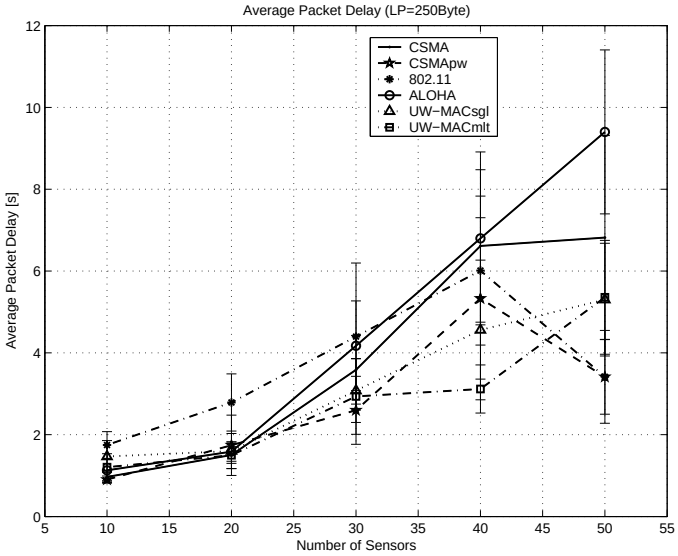

Figure 73: *3D UW-ASNs with mobile AUVs.* Average packet delay vs. number of sensors

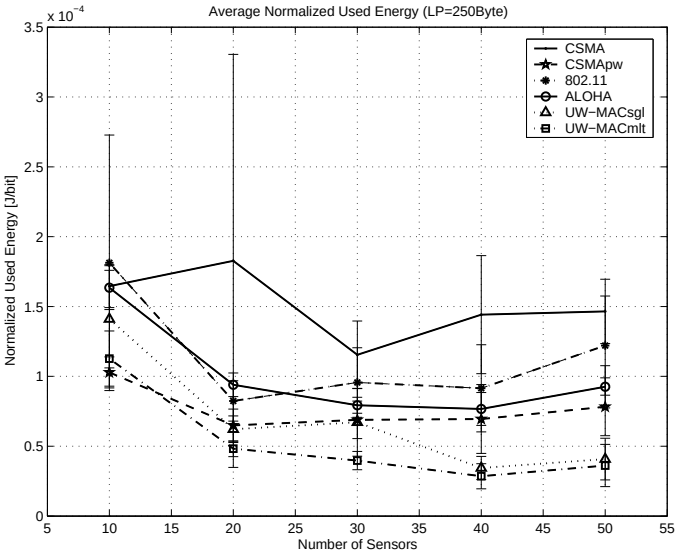

Figure 74: *3D UW-ASNs with mobile AUVs.* Average normalized used energy vs. number of sensors

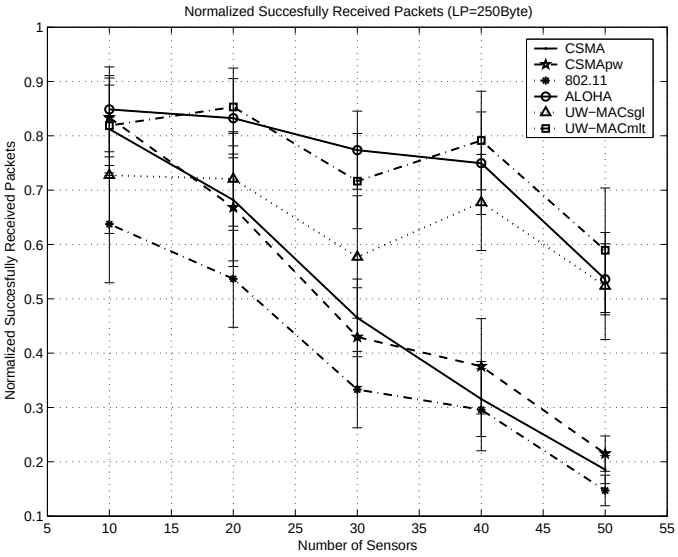

Figure 75: *3D UW-ASNs with mobile AUVs.* Normalized successfully received packets vs. number of sensors

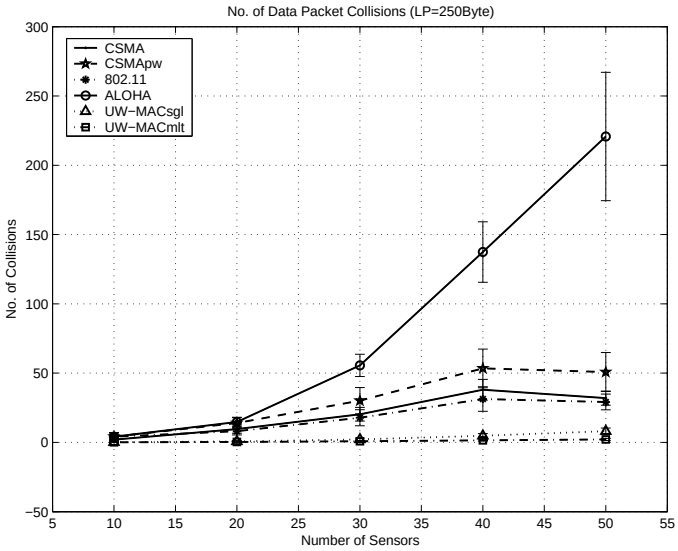

Figure 76: *3D UW-ASNs with mobile AUVs.* Number of data packet collisions vs. number of sensors

CHAPTER VII

CROSS-LAYER COMMUNICATION FOR MULTIMEDIA APPLICATIONS IN UNDERWATER ACOUSTIC SENSOR NETWORKS

7.1 Preliminaries

A significant surge in research on underwater sensor networks in the last few years, partly inspired by our position paper on this topic [7], has resulted in increased interest in the networking community for this leading-edge technology. Several architectures, protocols, and solutions for underwater networking have been proposed [67][60][65][66][91].

Moreover, the new recently started ACM International Workshop on UnderWater Networks (WUWNet) has been rated in 2006 as the most successful workshop co-located with the prestigious ACM Conference on Mobile Computing and Networking (MobiCom). This growing interest can be largely attributed to new applications enabled by underwater networks of small devices capable of harvesting information from the physical environment, performing simple processing on the extracted data and transmitting it to remote locations. As of today, existing studies on underwater networks are mostly focused on enabling the measurement of scalar physical phenomena like temperature, water content, or presence of contaminants in water. In general, most of the applications have very low bandwidth demands, and are usually delay tolerant.

Another recent trend in the terrestrial sensor networks domain, driven by the availability of inexpensive hardware such as CMOS cameras and microphones that are able to ubiquitously capture multimedia content from the environment, is to integrate multimedia communications in the sensor network paradigm, thus giving rise to the so-called Wireless

Multimedia Sensor Networks (WMSNs) [6]. These are networks of wirelessly interconnected devices that allow retrieving video and audio streams, still images, and scalar sensor data.

Underwater multimedia sensor networks will not only enhance existing sensor network applications, such as tracking and environmental monitoring, but they will also enable several new applications such as: underwater multimedia surveillance, advanced coastal surveillance, environmental monitoring, undersea explorations, disaster prevention, assisted navigation.

Many of the above applications require the sensor network paradigm to be re-thought in view of the need for mechanisms to deliver multimedia content with a certain level of quality of service (QoS). Since the need to minimize the energy consumption and to efficiently utilize the channel has driven most of the research in underwater sensor networks so far, mechanisms to efficiently deliver application-level QoS, and to map these requirements to network-layer metrics such as latency and packet error rate, have not been primary concerns in mainstream research on underwater sensor networks. Conversely, algorithms, protocols, and techniques to deliver multimedia content over large-scale networks have been the focus of intensive research in the last twenty years, especially in ATM wired and wireless networks. Later, many of the results derived for ATM networks have been re-adapted, and architectures such as Diffserv and Intserv for Internet QoS delivery have been developed. However, there are several main peculiarities of sensor networks and of the underwater environment in particular that make QoS delivery of multimedia content an even more challenging, and largely unexplored, task such as: characteristics of the underwater channel, resource constraints, variable channel capacity, cross-layer coupling of functionalities.

We envision that underwater sensor networks will need to provide support and differentiated service for several different classes of applications. In particular, they will need to provide differentiated service between delay-sensitive and delay-tolerant applications, and

loss-sensitive and loss-tolerant applications. Therefore, the main traffic classes that need to be supported are:

- **Delay-tolerant Applications:**
  - *Loss-tolerant, Multimedia Streams.* This class includes multimedia streams that, being intended for storage or subsequent offline processing, do not need to be delivered within strict delay bounds.
  - *Loss-tolerant, Data.* This may include environmental data from scalar sensor networks, or non time-critical snapshot multimedia content, with low or moderate bandwidth demand.
  - *Loss-sensitive, Data.* This may include data from critical monitoring processes, with low or moderate bandwidth demand, that require some form of offline post processing.
- **Delay-sensitive Applications:**
  - *Loss-tolerant, Multimedia Streams.* This class includes video and audio streams, or multi-level streams composed of video/audio and other scalar data (e.g., temperature readings), as well as metadata associated with the stream, that need to reach a human or automated operator in real-time, i.e., within strict delay bounds, and that are however relatively loss tolerant (e.g., video streams can be within a certain level of distortion). Traffic in this class usually has relatively high bandwidth demand.
  - *Loss-tolerant, Data.* This class may include monitoring data from densely deployed scalar sensors such as light sensors whose monitored phenomenon is characterized by spatial correlation, or loss-tolerant snapshot multimedia data (e.g., images of a phenomenon taken from several multiple viewpoints at the same time). Hence, sensor data has to be received timely but the application is

moderately loss-tolerant. The bandwidth demand is usually between low and moderate.

– *Loss-sensitive, Data.* This may include data from time-critical monitoring processes such as distributed control applications. The bandwidth demand varies between low and moderate.

This chapter is organized as follows. Section 7.2 proposes a general methodology to design a cross-layer protocol suite to enable efficient communications in a sensor network. Section 7.3 specializes this framework for underwater multi-hop sensor networks and proposes a cross-layer solution for delay-tolerant UW-ASN applications, while Section 7.4 deals with challenges for delay-sensitive applications. Section 7.5 discusses the protocol operation and proposes possible mechanisms to improve its efficiency in the case of mobile AUVs.

7.2 Cross-layer Resource Allocation Framework

As discussed in the previous section, several protocols have been developed for underwater acoustic communication at different layers of the protocol stack. However, existing protocols do not consider cross-layer interactions, which play a crucial role in the design of wireless networks.

The attention of researchers in recent years focused on developing protocols for each individual layer. We have developed MAC [67] and routing protocols [65][66] considering the effect of the underwater channel on these protocols. Based on the experience that we gained in this research domain over the last 4 years, we came to the conclusion that a cross-layer design approach would be the most suited solution for underwater sensor networks.

Several approaches to cross-layer design are possible.

- *Pairwise interactions* [19][49]. Resource allocation problems are treated by considering simple interactions between two communication layers. A typical example is

the interaction between the congestion control and power control mechanisms [19]. In [49], the joint power control and scheduling problem is addressed. However, this approach does not take into account the tight coupling among functionalities handled at all layers of the protocol stack typical of multi-hop underwater networks.

- *Heuristic approaches* [53]. Resource allocation problems following this approach consider interactions between several communication functionalities at different layers. However, since it is not easy to model and control the interactions between functionalities, solutions in these category rely on heuristic approaches, thus leading to suboptimal performance.

- *Resource allocation frameworks* [72][55]. These approaches integrate different communication functionalities into a coherent mathematical framework and provide a unified foundation for the cross-layer design and control in multi-hop wireless networks. Usually, solutions developed try to reach optimality based on an objective function that is application dependent and provide guidelines and tools to develop mathematically sound distributed solutions.

Recent studies [55] have demonstrated the need to integrate various protocol layers into a coherent framework, to help provide a unified foundation for the analysis of disparate problems and algorithms in wireless networking. Lately, there has been an increasing interest in research activities that build on recently developed nonlinear (often convex, and sometimes nonconvex) optimization theory to deal with the design of wireless communication systems [55]. Our objective is to develop a framework that accurately models every aspect of the layered network architecture, resulting in theoretical and practical impacts beyond the previously established results. Our previous experience in modeling functionalities of the communication stack of underwater networks led us to develop an adaptive coherent framework that can adapt to different application requirements and seek optimality in any possible situation. Still, we will seek to develop low-complexity distributed

solutions that can be implemented on low-end sensors.

7.2.1 Related Work

Resource allocation in multi-hop ad hoc wireless networks has been extensively studied in the last years, typically with the objectives of maximizing the network lifetime [18], minimizing the energy consumption [58], and maximizing the network capacity [72]. Several papers in the literature focus on the joint power control and MAC problem, and/or power control and routing issues, although most of them studies the interactions among different layers under restricted assumptions, forming a literature that is too large to be exhaustively reviewed here. Rather, we report a set of significative examples. In [25], the problem of scheduling maximum number of links in the same time slot is studied. The objective of the paper is to develop a power control based multiple access algorithm for contention-based wireless ad hoc networks, so that the network maximum per-hop throughput is achieved. To this end, the transmit powers are set to their minimum required levels such that all transmissions achieve a target signal-to-interference-plus-noise ratio (SINR). In [21], the problem of joint routing, link scheduling, and power control to support high data rates for broadband wireless multi-hop networks is analyzed. In particular, the work focuses on the minimization of the total average transmission power in the wireless multi-hop network, subject to given constraints regarding the minimum average data rate per link, as well as peak transmission power constraints per node. In [49], the joint power control and scheduling problem is addressed under the assumption that the session paths are already given. The main contribution in [49] is the formulation of a QoS framework that is able to capture both the different definitions of QoS from network layer to physical layer and the general requirements of the individual sessions. By exploiting this framework, [49] showed the need of close interactions between these layers.

7.2.2 Precautionary Guidelines in Cross-layer Design

In this section, we describe possible risks raising when a cross-layer approach is followed, and propose precautionary guidelines and principles for cross-layer design.

The increased interactions and dependencies across layers turn into an interesting optimization opportunity that may be worth exploiting. Following this intuition, many cross-layer design papers that explore a much richer interaction between parameters across layers have been proposed in the recent past. While, however, as an immediate outcome most of these cross-layer suggestions may yield a performance improvement in terms of throughput or delay, this result is often obtained by decreasing the *architecture modularity*, and by loosing the logical separation between designers and developers. This abstraction decoupling is needed to allow the former to understand the overall system, and the latter to realize a more efficient production. For these reasons, when a cross-layer solution is proposed, the system performance gain needs to be weighed against the possible longer-term downfalls raised by a diminished degree of modularity.

In [47], the authors reexamine holistically the issue of cross-layer design and its architectural ramifications. They contend that a good architectural design leads to *proliferation* and *longevity* of a technology, and illustrate this with some historical examples, e.g., John von Neumann's architecture for computer systems, at the origin of the separation of software and hardware; the layered OSI architecture for networking, base of the current Internet architecture success; Shannon's architecture for communication systems, motivating the nonobvious separation of source and channel coding; last but not least, the plant controller feedback paradigm in control systems, providing universal principles common to human engineered systems as well as biological systems.

Although the concerns and cautionary advice expressed in [47] about cross-layer design are sound and well motivated, the layered-architecture, which turned to be a successful design choice for wired networks, may need to be carefully rethought for energy-constrained WSNs, where the concept itself of 'link' is labile, and many different effective transmission

schemes and communication paradigms are conceivable.

This is also the conclusion drawn in [89], where the pros and cons of cross-layer design approach are evaluated. In [89], cross-layer design to improve reliability and optimize performance is advocated, although the design needs to be cautiously developed to provide long-term survivability of cross-layer architectures. In the following, we present some concerns and precautionary considerations, which need to be considered when a cross-layer design architecture is proposed, and suggest some possible research directions.

- *Modularity.* In the classical layered design approach, a system architecture is broken down into *modular components*, and the *interactions* and *dependencies* between these components are systematically specified. This design philosophy allows to break complex problems into easier subproblems, which can then be solved in *isolation*, without considering all the details pertaining the overall system. This approach guarantees the inter-operability of subsystems in the overall system once each subsystem is tested and standardized, leading to quick proliferation of technology and mass production. Conversely, a cross-layer design approach may loose the decoupling between design and development process, which may impair both the design and the implementation development and slow the innovation down.

- *System enhancement.* Design improvements and innovations may become difficult in a cross-layer design, since it will be hard to assess how a new modification will interact with the already existing solutions. Furthermore, a cross-layer architecture would be hard to upkeep, and the maintaining costs would be high. In the worst cases, rather than modifying just one subsystem, the entire system may need to be replaced. For these reasons, we advocate keeping some degree of modularity in the design of cross-layer solutions. This could be achieved by relying on functional entities - as opposed to layers in the classical design philosophy - that implement particular functions. This would also have the positive consequence of limiting the duplication

of functions that often characterizes a layered design. This functional redundancy is, in fact, one the cause for poor system performance.

- *Instability.* In cross-layer design, the effect of any single design choice may affect the whole system, leading to various negative consequences such as instability. This is a non trivial problem to solve, since it is well known from control theory that stability is a paramount issue. Moreover, the fact that some interactions are not easily foreseen makes cross-layer design choices even trickier. Hence, great care should be paid to prevent design choices from negatively affecting the overall system performance. To this purpose, there is a need to integrate and further develop control theory techniques to study stability properties of system designed following a cross-layer approach. Dependency graphs, which may be used to capture the dependency relation between parameters, could be valuable means to prove stability, although hard to implement in some cases.

- *Robustness.* Besides stability, there is also the issue of robustness. Robustness is the property of a system to be able to absorb parameter uncertainties and, in general, the degrading effect on the overall performance experienced by a system when unpredictable events occur such as transmission anomalies, channel impairments, loss of connectivity, etc. Techniques such as *timescale separation* and *performance tracking and verification* may need to be employed to separate interactions and verify on-the-fly the system performance. Moreover, an accompanying theoretical framework may be needed to fully support cross-layer design and study its robustness properties.

7.2.3 General Framework for Cross-layer Optimization

As previously discussed, our objective is to formulate cross-layer resource allocation problems in multi-hop wireless underwater networks as (possibly convex) optimization problems. While in this section we outline a general framework where different resource allocation problems will fit by specifying the form of particular functions, in Section 7.3 we

specialize the framework for the underwater environment.

The general framework for cross-layer optimization problem can be cast as follows:

$\mathbf{P}^{Opt}$: Cross-Layer Problem for Optimal Resource Allocation

$$Given: \qquad P_s^e,\ d_{ij}(),\ l_{ij}(),\ B^s \tag{69}$$

$$Find: \qquad \mathbf{r},\ \mathbf{F},\ \mathbf{p} \tag{70}$$

$$Maximize: \quad \sum_{s\in\mathcal{S}} \mathcal{U}_s(r_s) + \ sum_{j\in\mathcal{N}} \mathcal{V}_j(p_j) \tag{71}$$

$$Subject\ to:$$

$$\sum_{s\in\mathcal{S}} f_{ij}^s \cdot r_s \leq l_{ij}(\mathbf{P}^e, \mathbf{p}); \tag{72}$$

$$\sum_{(i,j)\in\mathcal{E}} f_{ij}^s \cdot d_{ij}(\mathbf{r}, l_{ij}(\mathbf{P}^e, \mathbf{p})) \leq B_s; \tag{73}$$

$$\mathbf{F} \in \mathcal{F}_{feas}(\mathbf{r}), \mathbf{r} \in \mathcal{R}_{feas}, \mathbf{p} \in \mathcal{P}_{feas}. \tag{74}$$

The following notations are introduced in the above problem:

- $\mathbf{r} = [r_1, r_2, .., r_s, .., r_{|\mathcal{S}|}]$ is the vector whose generic element r_s represents the bit rate assigned to source $s \in \mathcal{S}$; $\mathbf{p} = [p_1, p_2, .., p_j, .., p_{|\mathcal{N}|}]$ is the transmission power vector, where the generic element p_j is the transmission power assigned to node $j \in \mathcal{N}$; $\mathbf{F} = [f_{ij}^s]$ is a binary matrix that represents the routing decisions, where the generic element f_{ij}^s equals 1 iff link (i, j) is part of the end-to-end path associated with source s; $\mathbf{P}^e = [P_1^e, P_2^e, .., P_j^e, .., P_{|\mathcal{N}|}^e]$ is a vector whose generic element P_j^e represents the decoding error probability desired by node $j \in \mathcal{N}$;

- $d_{ij}()$ is the delay expression associated to link (i, j), that models the specific physical and MAC layer, and their interaction with the routing and congestion control functions; $l_{ij}()$ is the capacity expression associated to link (i, j), that depends on the physical layer characteristics; B^s is the delay bound associated to source s;

- $\mathcal{U}_s$ and $\mathcal{V}_j$ are utility functions in the objective function, which model the desired optimality characteristics of the network, according to the application requirements.

The above formulation jointly models problems at different layers in a cross-layer fashion. The optimization variables, whose values have to be jointly determined, are associated to different resources at different layers of the protocol stack. The *transport problem* consists of deciding the bit rate vector **r** to be assigned to the set of sources in the network. The *routing problem* consists of determining the routing matrix **F** according to which the sources route their data flows. The *physical problem* consists of selecting the optimal transmission power vector **p** that the set of sources should use. The above variables have to be jointly selected in order to maximize the objective function in (71). In particular, (71) maximizes the sum of the utilities of each source $s \in \mathcal{S}$ and of each node $j \in \mathcal{N}$, according to the utility functions $\mathcal{U}_s$ and $\mathcal{V}_j$, respectively. While the former increases with increasing bit rates granted at each sources, the latter increases with decreasing power assigned to each node. Note that the heterogeneous characteristics of underwater sources and nodes in the network can be captured by the simultaneous use of different utility functions. Constraint (72) imposes that the resource utilized on each link be lower than the link capacity, which depends on the desired decoding error probability vector and on the used transmission powers. Constraint (73) forces the end-to-end delay of each source to be bounded by the maximum tolerated delay. The delay on each link can be expressed as a function of the assigned vector rate and link capacity. The constraints in (74) impose limitations on the routing decisions, the available bit rates, and the selectable transmission powers, respectively, considering the MAC and physical constraints. Specifically, in the underwater routing decision an end-to-end path is considered feasible if it is composed only of links connecting adjacent nodes. Moreover, concurrent transmissions are considered feasible if the generated interference is within certain bounds.

In the next section, we explain how we intend to specialize the above framework for underwater multi-hop acoustic networks. In particular, we do so by:

- *Identifying adequate utility functions.* We identify utility functions that: i) represent

the desired global design objectives; ii) exhibit properties, e.g., convexity, that allow finding a unique global optimum with efficient methods such as the primal-dual interior point algorithm [12].

- *Specifying details of the physical layer.* We integrate in the framework underwater physical layer characteristics, such as error control and the characteristics of the underwater channel, that mainly impact the overall resource allocation problem.

7.3 Cross-layer Routing/MAC/PHY Solution for Delay-tolerant Applications

The proposed algorithm is a distributed routing/MAC/PHY solution for different traffic classes, and allow each node to *jointly* select its best next hop, the optimal transmitted power, the code length, and the forward error correction (FEC) rate for each packet, with the objective of minimizing the energy consumption, while taking the condition of the underwater physical channel and the application requirements into account. The proposed solution relies on a geographical routing paradigm. Geographical routing protocols are very promising for their scalability feature and limited required signaling.

In the following, we assume that the channel is heavily affected by multipath (*saturated condition*, see [70]) as it is often the case in shallow water [7]. In this environment, the signal fading can be modeled by a Rayleigh r.v., which accounts for a worst-case scenario, and the transmission loss between i and j is $TL_{ij} \cdot \rho^2$, where $TL_{ij} = d_{ij} \cdot 10^{[\alpha(f) \cdot d_{ij} + A]/10}$, with $A \in [5, 10]\,\mathrm{dB}$, and ρ has a unit-mean Rayleigh cumulative distribution $D_\rho(\rho) = 1 - \exp(-\pi\rho^2/4)$. Let us define the *signal transmission margin* for link (i, j) as m_{ij}, where $P^*_{ij} \cdot m^2_{ij}\,[\mathrm{W}]$ is the actual transmit power, while $P^*_{ij}\,[\mathrm{W}]$ represents the optimal transmission power in an ideal channel, i.e., the transmit power before applying the margin to face the fading dips. The packet error rate PER_{ij} experienced on link (i, j) when sender i transmits power $P^*_{ij} \cdot m^2_{ij}$ can be defined as the probability that the received power at node j be smaller

than that required in an ideal channel where no multipath is experienced, i.e.,

$$PER_{ij} = \Pr\left\{\frac{P_{ij}^{*} \cdot m_{ij}^2}{TL_{ij} \cdot \rho^2} \leq \frac{P_{ij}{}^{*}}{TL_{ij}}\right\} = \Pr\left\{\rho \geq m_{ij}\right\} = 1 - D_{\rho}(m_{ij}) = \exp\Big(-\frac{\pi m_{ij}^2}{4}\Big). \tag{75}$$

Hence, the average number of transmissions of a packet such that receiver j correctly decodes it when it is sent with signal transmission margin m_{ij} is $N_{ij}^{T}(m_{ij}) = [1 - PER_{ij}]^{-1} = D_{\rho}(m_{ij})^{-1}$. This relation assumes independent errors among adjacent packets, which holds when the channel coherence time is shorter than the retransmission timeout, i.e., the time before retransmitting an unacknowledged packet. Note that, while for loss-sensitive applications a packet is locally retransmitted until it is correctly decoded at the receiver (and the average number of transmissions is $N_{ij}^{T}(m_{ij})$), for loss-tolerant applications packets may be protected unequally, depending on the importance of the data they are carrying for correct perceptual reconstruction.

The main features that characterize our cross-layer solution are: i) it provides a *unique and flexible solution* for different architecture such as *static* 2D deep water and 3D shallow water, and scenarios with *mobile* AUVs; ii) it is *fully distributed*, since spreading codes, transmit power, and next hop are distributively selected by each sender without relying on a centralized entity; iii) it is *intrinsically secure*, since it uses chaotic codes; iv) it *fairly shares* available resources among active devices; v) it *efficiently supports multicast transmissions*, since spreading codes are decided at the transmitter side; and vi) it is *robust* against inaccurate node position and interference information caused by mobility, traffic unpredictability, currents, and control packet loss caused by channel impairment.

According to our distributed routing/MAC/PHY algorithm, node i will select j^* as its best next hop iff

$$j^* = argmin_{j \in \mathcal{S}_i \cap \mathcal{P}_i^N} E_i^{(j)^*}, \tag{76}$$

where $E_i^{(j)^*}$ represents the minimum energy required to successfully transmit a payload bit from node i to the sink, taking the condition of the underwater channel and the interference state at j into account, when i selects j as next hop. Moreover, in (76), $\mathcal{S}_i$ is the *neighbor*

set of node i, while $\mathcal{P}_i^N$ is the *positive advance set*, composed of nodes closer to sink N than node i, i.e., $j \in \mathcal{P}_i^N$ iff $d_{jN} < d_{iN}$

This link metric, objective function (77) in $\mathbf{P}_{\mathbf{layer}}^{\mathbf{cross}}$, takes into account the number of packet transmissions ($\hat{N}_{ij}^T$) associated with link (i,j), given the optimal packet size (L_P^*), and the optimal combination of FEC $(L_{Pij}^F{}^*)$ and transmitted power (P_{ij}^*). Moreover, it accounts for the average hop-path length $(\hat{N}_{ij}^{Hop})$ from node i to the sink when j is selected as next hop, by assuming that the following hops will guarantee the same advance towards the surface station (sink). While this approach to estimate the number of remaining hops towards the surface station is simple, several advantages can be pointed out, as described in [88], such as: i) it does not incur any signaling overhead since it is locally computed and does not require end-to-end information exchange; ii) its accuracy increases as the density increases; iii) its accuracy increases as the distance between the surface station and the current node decreases. For these reasons, we decided to use this method rather than trying to estimate the exact number of hops towards the destination.

We can now cast the cross-layer Routing/MAC/PHY optimization problem in a Rayleigh channel.

$\mathbf{P}_{\mathbf{layer}}^{\mathbf{cross}}$: Cross-layer Routing/MAC/PHY Optimization Problem

$$
\begin{aligned}
Given: \quad & i,\, \mathcal{S}_i,\, \mathcal{P}_i^N,\, L_P^*,\, L_P^H,\, E_{elec}^b,\, r,\, \hat{N}_{0j},\, P_i^{max},\, TL_{ij},\, NI_j,\, BER_j,\, \hat{S}_k,\, NI_k, \forall k \in \mathcal{K}_i \\
Find: \quad & j^* \in \mathcal{S}_i \cap \mathcal{P}_i^N,\; P_{ij^*}^* \leq P_i^{max},\; c_{ij}^* \in [c_{min}, c_{max}],\; m_{ij}^* \in \mathbb{R}^+ \\
Minimize: \quad & E_i^{(j)} = E_{ij}^b \cdot \tfrac{L_P^*}{L_P^* - L_P^H - L_{Pij}^F} \cdot \hat{N}_{ij}^T(m_{ij}) \cdot \hat{N}_{ij}^{Hop} \qquad (77) \\
Subject\ to: \quad &
\end{aligned}
$$

$$
E_{ij}^b = 2 \cdot E_{elec}^b + \frac{P_{ij} \cdot m_{ij}^2}{r/c_{ij}}; \qquad (78)
$$

$$
L_{Pij}^F = \Psi^{\mathcal{F}^{-1}}\left(L_P^*, PER_{ij}, \Phi^{\mathcal{M}}\left(\frac{P_{ij}}{\hat{N}_{0j} \cdot (r/c_{ij}) \cdot TL_{ij}}\right)\right); \qquad (79)
$$

$$
\hat{N}_{ij}^{Hop} = \max\left(\frac{d_{iN}}{< d_{ij} >_{iN}}, 1\right); \qquad (80)
$$

$$N_{ij}^{T}(m_{ij}) = D_{\rho}(m_{ij})^{-1} = \left[1 - \exp\Big(-\frac{\pi m_{ij}^2}{4}\Big)\right]^{-1}; \tag{81}$$

$$P_{ij}^{min}(c_{ij}) \leq P_{ij} \leq \min\left[P_{ij}^{max}, P_{i}^{max}\right]; \tag{82}$$

$$P_{ij}^{min}(c_{ij}) \leq P_{ij} \cdot m_{ij}^2 \leq \min\left[P_{ij}^{max}, P_{i}^{max}\right]; \tag{83}$$

where

$$P_{ij}^{min}(c_{ij}) = \frac{NI_j \cdot TL_{ij}}{\alpha \cdot c_{ij} \cdot \Phi(BER_j)} = \frac{\Gamma_{ij}}{c_{ij}}, \tag{84}$$

$$\Gamma_{ij} = \frac{NI_j \cdot TL_{ij}}{\alpha \cdot \Phi(BER_j)}, \tag{85}$$

$$P_{ij}^{max} = \min_{k \in \mathcal{K}_i}\left[(\hat{S}_k - NI_k) \cdot TL_{ik}\right]. \tag{86}$$

We introduce the following notations that are used in the cross-layer protocol suite optimization problem:

- $L_P^* = L_P^H + L_{P\,ij}^F + L_{P\,ij}^N\ [bit]$ is the ***fixed*** optimal packet size, solution of an ***off-line*** optimization problem presented in [66], where L_P^H is the ***fixed*** header size of a packet, while $L_{P\,ij}^F$ is the ***variable*** FEC redundancy that is included in each packet transmitted from node i to j; thus, $L_{P\,ij}^N = L_P^* - L_P^H - L_{P\,ij}^F$ is the ***variable*** payload size of each packet transmitted in a train on link (i, j).

- $E_{elec}^b = E_{elec}^{trans} = E_{elec}^{rec}\,[\mathrm{J/bit}]$ is the ***distance-independent*** energy to transit one bit, where E_{elec}^{trans} is the energy per bit needed by transmitter electronics (PLLs, VCOs, bias currents, etc.) and digital processing, and E_{elec}^{rec} represents the energy per bit utilized by receiver electronics. Note that E_{elec}^{trans} does not represent the overall energy to transmit a bit, but only the distance-independent portion of it.

- $E_{ij}^b = 2 \cdot E_{elec}^b + \frac{P_{ij} \cdot m_{ij}^2}{r/c_{ij}}\ [\mathrm{J/bit}]$ accounts for the energy to transmit one bit from node i to node j, when the transmitted power and the bit rate are $P_{ij}\ [\mathrm{W}]$ and $r/c_{ij}\ [\mathrm{bps}]$, respectively. The second term represents the ***distance-dependent*** portion of the energy necessary to transmit a bit.

- $P_i^{max}\ [\mathrm{W}]$ is the maximum transmitting power for node i.

- $\Phi^{\mathcal{M}}\left(\frac{\overline{P}_{ij}}{\overline{N}_{0j}(r/c_{ij})\cdot TL_{ij}}\right)$ represents the average bit error rate on link (i,j); it is a function of the ratio between the average energy of the received bit $\overline{P}_{ij}/((r/c_{ij})\cdot TL_{ij})$ and the expected noise $\overline{N_{0j}}$ at the receiver, and it depends on the modulation scheme $\mathcal{M}$; in general, the noise has a thermal, an ambient, and a man-made component; studies of shallow water noise measurements [34] suggest considering an average value of $70\,\mathrm{dB}_{\mu\mathrm{Pa}}$ for the ambient noise.

- $\psi^{\mathcal{F}}\left(L_P, L_P^F, BER\right)$ represents the average packet error rate $(\overline{PER})$, given the packet size L_P, the FEC redundancy L_P^F, and the average bit error rate $(\overline{BER})$, and it depends on the adopted FEC technique $\mathcal{F}$.

- PER_{max}^{e2e} is the application maximum allowed end-to-end packet error rate, while N_{max}^{Hop} is the maximum expected number of hops, function of the network diameter [74].

- $TL_{ij}\,[\mathrm{dB}]$ is the transmission loss from i to j, which is computed according to the Urick model [90].

- $\hat{N}_{ij}^{T}$ is the average number of transmissions of a packet sent by node i such that the packet is correctly decoded at receiver j.

- $\hat{N}_{ij}^{Hop} = \max\left(\frac{d_{iN}}{<d_{ij}>_{iN}}, 1\right)$ is the estimated number of hops from node i to the surface station (sink) N when j is selected as next hop, where d_{ij} is the distance between i and j, and $< d_{ij} >_{iN}$ (which we refer to as *advance*) is the projection of d_{ij} onto the line connecting node i with the sink.

- $BER_{ij} = \phi^{\mathcal{M}}(E_{rec}^{b}/\hat{N}_{0j})$ represents the bit error rate on link (i,j); it is a function of the ratio between the energy of the received bit, $E_{rec}^{b} = P_{ij}^{TX}/(r\cdot TL_{ij})$, and the expected noise at node j, $\hat{N}_{0j}$, and it depends on the adopted modulation scheme $\mathcal{M}$.

- $L_{Pij}^{F} = \psi^{\mathcal{F}^{-1}}\left(L_P^*, PER_{ij}, BER_{ij}\right)$ returns the needed FEC redundancy, given the

optimal packet size L_P^*, the packet error rate and bit error rate on link (i, j), and it depends on the adopted FEC technique $\mathcal{F}$.

Each node i needs to i) limit the near-far effect when it transmits to j and ii) avoid impairing ongoing communications, which is expressed by the following

$$\begin{cases} \frac{N^0+I_j}{\frac{P_{ij}}{TL_{ij}}} \leq w_{ij} \cdot \Phi(BER_j) \\ \frac{N^0+I_k+\frac{P_{ij}}{TL_{ik}}}{S_k} \leq w_{t_k k} \cdot \Phi(BER_k),\ \forall k \in \mathcal{K}_i. \end{cases} \tag{87}$$

In (87), $N^0\,[\mathrm{W}]$ is the average noise power, I_j and I_k $[\mathrm{W}]$ are the MAI at nodes j and $k \in \mathcal{K}_i$, with $\mathcal{K}_i$ being the set of nodes whose ongoing communications may be affected by node i's transmit power. In addition, w_{ij} and $w_{t_k k}$ are the bandwidth spreading factors of the ongoing transmissions from i to j and from t_k to k, respectively, where t_k is the node from which k is receiving data. Furthermore, $P_{ij}\,[\mathrm{W}]$ represents the power transmitted by i to j when an ideal channel (without multipath, i.e., $A = 0\,\mathrm{dB}$) is assumed, i.e., when no power margin is considered to face the fading dips. Finally, TL_{ij} and TL_{ik} are the transmission losses from i to j and from i to $k \in \mathcal{K}_i$, respectively, while $S_k\,[\mathrm{W}]$ is the user signal power that receiver k is decoding, and $\Phi()$ is the MAI threshold, which depends on the target bit error rate (BER) at the receiver node (see [61]). We will denote the noise and MAI power of a generic node n as $NI_n = N^0 + I_n$, and the normalized received spread signal, i.e., the signal power after despreading, as $\hat{S}_n = S_n \cdot w_{t_n n} \cdot \Phi(BER_n)$.

The first constraint in (87) states that the SINR^{-1} at receiver j needs to be below a certain threshold, i.e., the power P_{ij} transmitted by i needs to be sufficiently high to allow receiver j to successfully decode it, given its current noise and MAI power level (NI_j). The second constraint in (87) states that the SINR^{-1} at receivers $k \in \mathcal{K}_i$ must not be above a threshold, i.e., the power P_{ij} transmitted by i must not impair the ongoing communications toward nodes $k \in \mathcal{K}_i$. By combining the constraints in (87), we obtain

$$\frac{NI_j \cdot TL_{ij}}{w_{ij} \cdot \Phi(BER_j)} \leq P_{ij} \leq \min_{k \in \mathcal{K}_i} \left[(\hat{S}_k - NI_k) \cdot TL_{ik}\right]. \tag{88}$$

Consequently, to set its transmit power P_{ij} and spreading factor w_{ij}, node i needs to leverage information on the MAI and normalized receiving spread signal of neighboring nodes. This information is broadcast periodically by active nodes. In particular, to limit such broadcasts, a generic node n transmits only significant values of NI_n and $\hat{S}_n$, i.e., out of predefined tolerance ranges. Constraints (88) are incorporated in the cross-layer routing/MAC/PHY optimization problem $\mathbf{P}_{\mathbf{layer}}^{\mathbf{cross}}$ in (82) and (83).

The choice of a fixed packet size for UW-ASNs is motivated by the need for system simplicity and ease of sensor buffer management. In fact, a design proposing per-hop optimal packet size, e.g., solving an optimization problem for any link distance and using the resulting *distance-dependent* optimal packet size in the routing algorithm, would encounter several implementation problems, such as the need for segmentation and re-assembly functionalities that incur tremendous overhead, which are unlikely affordable by low-end sensors. In [66], the packet size is optimized given the distance distribution between neighboring nodes, which determines the average transmission loss, and ultimately the bit error rate, computed as a function $\Phi^{\mathcal{M}}()$ of the modulation scheme $\mathcal{M}$ and the average signal-to-noise ratio at the receiver.

The link metric ${E_i^{(j)}}^*$ in (76) stands for the optimal energy per payload bit when i transmits a packet train to j using the optimal combination of power P_{ij}^* and FEC redundancy ${L_{Pij}^F}^*$ to achieve link reliability, jointly found by solving problem $\mathbf{P}_{\mathbf{layer}}^{\mathbf{cross}}$. This interpretation allows node i to optimally decouple $\mathbf{P}_{\mathbf{layer}}^{\mathbf{cross}}$ into two *sub-problems*: first, minimize the link metric $E_i^{(j)}$ for each of its feasible next-hop neighbors; second, pick as best next hop that node j^* associated with the minimal link metric. This means that the generic node i does not have to solve a complicated optimization problem to find its best route towards a sink. Rather, it only needs to sequentially solve the two aforementioned low-complexity subproblems, each characterized by a complexity $O(|\mathcal{S}_i \cap \mathcal{P}_i^N)|$, i.e., proportional to the number of its neighboring nodes with positive advance towards the sink. Moreover, this operation does not need to be performed each time a sensor has to route a packet, but only

when the channel conditions have consistently changed. To summarize, the proposed routing/MAC solution allows node i to select as next hop that node j^* among its neighbors that satisfies the following requirements: i) it is closer to the surface station than i, and ii) it minimizes the link metric ${E_i^{(j)}}^*$.

7.4 Cross-layer Routing/MAC/PHY Solution for Delay-sensitive Applications

Similarly to the cross-layer protocol solution tailored for delay-tolerant applications, a communication protocol for delay-sensitive applications should allow each node to distributively select the optimal next hop, transmitting power, code length, and FEC packet rate, with the objective of minimizing the energy consumption. However, a protocol solution tailored for delay-sensitive applications should also include new constraints to statistically meet the delay-sensitive requirements, such as:

1. The end-to-end packet error rate should be lower than an application-dependent threshold PER_{max}^{e2e}, which is reflected in the following:

$$1 - \left(1 - PER_{ij}\right)^{\lceil \hat{N}_{ij}^{Hop} + N_{HC}^{(m)} \rceil} \leq PER_{max}^{e2e}; \tag{89}$$

2. The probability that the end-to-end packet delay be over a delay bound B_{max}, should be lower than an application-dependent parameter γ:

$$\frac{\tilde{d_{ij}}}{q_{ij}} + \delta \cdot \sigma_{ij}^{q} \leq \min_{m=1,..,M} \left(\frac{\Delta B_i^{(m)}}{\hat{N}_{ij}^{Hop}} \right) - \hat{Q}_{ij} - \frac{L_P^*}{r}. \tag{90}$$

where

- PER_{max}^{e2e} and B_{max} $[s]$ are the application-dependent end-to-end packet error rate threshold and delay bound, respectively;
- $\Delta B_i^{(m)} = B_{max} - \left(t_{i,now}^{(m)} - t_0^{(m)}\right)$ $[s]$ is the time-to-live of packet m arriving at node i, where $t_{i,now}^{(m)}$ is the arriving time of m at i, and $t_0^{(m)}$ is the time m was generated, which is time-stamped in the packet header by its source;

- $N_{HC}^{(m)}$ is the hop count, which reports the number of hops of packet m from the source to the current node;

- $T_{ij} = \frac{L_P^*}{r} + T_{ij}^q \ [s]$ accounts for the packet transmission delay and the propagation delay associated with link (i, j); we will consider a Gaussian distribution for T_{ij}, i.e., $T_{ij} \backsim \mathcal{N}\left(\frac{L_P^*}{r} + \overline{T_{ij}^q}, {\sigma_{ij}^q}^2\right)$;

- $\overline{Q}_i \ [s]$ and $\overline{Q}_j \ [s]$ are the average queueing delays of node i (at the time the node computes its train next hop), and node j, which is a neighbor node of i;

- $\hat{Q}_{ij} \ [s]$ is the network queueing delay estimated by node i when j is selected as next hop, computed according to the information carried by incoming packets and broadcast by neighboring nodes.

As a design guideline to meet these requirements, differently from the cross-layer protocol for delay-tolerant applications, a protocol tailored for delay-sensitive applications may not retransmit corrupted or lost packets at the link layer. Rather, it should discard corrupted packets. Moreover, it should time-stamp packets when they are generated by a source so that it could discard expired packets. To save energy, while statistically limiting the end-to-end packet delay, an *earliest deadline first* scheduling may be successfully developed to dynamically assign higher priority to packets closer to their deadline.

An open problem in the design of a cross-layer solution for delay-sensitive applications is how to dynamically adjust the packet error rate that will be experienced by a packet on a link to respect the application end-to-end packet error rate requirement (PER_{max}^{e2e}), given the estimated number of hops to reach the sink if a specific node is selected as next hop. Also, the objective function of the optimization problem should be adjusted since no selective packet retransmission would be performed.

Other important open problems in the design of a cross-layer solution for efficient communication for delay-sensitive UW-ASN applications are:

- **Unreliability of the Underwater Channel.** Streaming of multimedia data over an underwater sensor network is particularly challenging because of the QoS requirements of a video/audio stream, the bandwidth constraints, and the unreliability of the underwater medium. For example, for good quality video perception a frame loss rate lower than 10^{-2} is required. This constitutes a hard task since the underwater channel is highly unreliable, mostly caused by multipath fading and noise at the physical layer, and by collisions or co-channel interference at the MAC layer. Automatic repeat request (ARQ), mechanisms use bandwidth efficiently at the cost of additional latency. Hence, while carefully designed selective repeat schemes may be of some interest, naive use of ARQ techniques is clearly infeasible for applications requiring quasi real-time delivery of multimedia content in underwater networks.

- **Unequal Error Protection.** An important characteristic of multimedia content is *unequal importance*, i.e., not all packets have the same importance for correct perceptual reconstruction of the multimedia content. Moreover, in case of *loss-tolerant* multimedia data, even if some errors are introduced, the original information may still be reconstructed with tolerable distortion. Therefore, an idea that has been used effectively consists of applying different degrees of FEC to different parts of the video stream, depending on their relative importance (*unequal protection*). For example, this idea can be applied to layered coded streams to provide graceful degradation in the observed image quality in presence of error losses, thus avoiding so-called "cliff" effects [36].

- **Joint Source and Channel Coding.** In general, delivering error-resilient multimedia content and minimizing energy consumption are contradicting objectives. For this reason, and because of the time-varying characteristics of the underwater channel, several joint source and channel coding schemes have been developed, e.g., [24],

which try to reduce the energy consumption of the whole process. Some recent papers [56][96] even try to jointly reduce the energy consumption of the whole process of multimedia content delivery, i.e., jointly optimize source coding, channel coding, and transmission power control. In these schemes, the image coding and transmission strategies are adaptively adjusted to match current channel conditions by exploiting the peculiar characteristics of multimedia data, such as unequal importance of different frames or layers. However, most of these efforts have originated from the multimedia or coding communities. Thus, not only these papers do not consider the unique characteristics of the underwater channel, but they are not even reminiscent of other important networking aspects of content delivery over a multi-hop wireless networks of memory-, processing- and battery-constrained devices.

- **Multimedia In-network Processing.** Processing of multimedia content has mostly been approached as a problem isolated from the network-design problem, with a few exceptions such as joint source-channel coding [24] and channel-adaptive streaming [33]. Hence, research that addressed the content delivery aspects has typically not considered the characteristics of the source content and has primarily studied cross-layer interactions among lower layers of the protocol stack. However, the processing and delivery of multimedia content are not independent and their interaction has a major impact on the levels of QoS that can be delivered. Hence, the QoS required at the application level will be delivered by means of a combination of both cross-layer optimization of the communication process, and in-network processing of raw data streams that describe the phenomenon of interest from multiple views, with different media, and on multiple resolutions.

7.5 Protocol Operation of the Cross-layer Solution

Our proposed cross-layer solution aims at setting the optimal combination of next hop, transmit power, and code length at the transmitter side relying on local periodic broadcasts

of MAI values from active nodes. Here, node i needs to transmit a data packet to j, without impairing ongoing communications from h to k and from t to n. Since the system efficiency is limited by the amount of total interference, it is crucial for i to optimize its transmission, in terms of transmit power and code length, to limit the near-far problem.

Once the optimization problem has been solved at sender i, and the optimal next hop, transmitting power, and code length have been found, node i randomly access the channel transmitting a short header called *Extended Header (EH)*. The EH, of size L_{EH} bits, is sent using a *common chaotic code* c_{EH} known by all devices at the maximum rate (minimum code length). Sender i transmits to its next hop j, located d_{ij} meters apart, the short header EH. The EH contains information about the final destination, i.e., the surface station, the chosen next hop, i.e., node j, and the parameters that i will use to generate the *chaotic spreading code* for the actual data packet, of size L_D bits, that j will receive from i. Immediately after the transmission of the EH, i transmits the data packet on the channel, which is characterized by a raw chip rate r [cps] and expected sound velocity $\overline{q} \approx 1500\,\mathrm{m/s}$, using the optimal transmit power P_{ij}^{*} [W] and code length c_{ij}^{*} set by the power and code self-assignment algorithm. If no collision occurs during the reception of the EH, i.e., if i is the only node transmitting an EH in the neighborhood of node j, j will be able to synchronize to the signal from i, despread the EH using the common code, and acquire the carried information. At this point, if the EH is successfully decoded, receiver j will be able to locally generate the chaotic code that i used to send its data packet, and set its decoder according to this chaotic code in such a way as to decode the data packet. Once j has correctly received the data packet from i, it acknowledges it by sending an ACK packet, of size L_A bits, to j using code c_A. In case i does not receive the ACK before a timeout T_{out} expires, it will keep transmitting the packet until a maximum transmission number N_{max}^{T} is reached. The timeout must be tuned considering the long propagation and transmission delays, i.e., $T_{out} \geq c_{EH} \cdot L_{EH}/r + c_{ij} \cdot L_D/r + 2d_{ij}/\overline{q} + c_A \cdot L_A/r$.

Note that if sender i does not have updated information about the MAI in j, it increases

the code length every time a timeout expires to improve the probability that the packet is successfully decoded, i.e., $c_{ij}^{N_{ij}^T} = \min[c_{ij}^{N_{ij}^T-1} \cdot 2^{\beta}, c_{max}]$, where $1 \leq N_{ij}^T \leq N_{max}^T$ and $\beta \in \mathbb{R}^+$.

To enhance the protocol performance and limit the signaling overhead in the case of mobile AUVs, we will introduce a hybrid location management scheme to handle the mobility of AUVs with minimal energy expenditure for the sensors. The proposed solution will overcome the drawbacks of previously proposed localization services [54][22] for wireless networks. In general, the objective of these mechanisms, which can be classified as rendezvous-based protocols [22], is to potentially allow each single device in the network to retrieve the location of any other node, based on queries and replies. Clearly, query-based mechanisms can introduce delays that may not be acceptable in delay-sensitive applications. Moreover, the extensive message exchange and complex server structures, often hierarchical, associated with these protocols, should be avoided in UW-ASNs.

The idea of our hybrid location management scheme is that AUVs broadcast updates limiting their scope based on Voronoi diagrams extended for three-dimensional networks, while underwater sensors predict the movements of AUVs based on Kalman filtering of previously received updates. This scheme is aimed at reducing the energy consumption on underwater sensors and the acoustic channel utilization by avoiding location updates. We will develop a proactive location management approach based on update messages sent by mobile AUVs to sensors. In the spatial domain, broadcasts can be limited based on 3D Voronoi diagrams. At the same time, AUV movement may be to some extent predictable. Hence, in the temporal domain, location updates can be limited to *AUV positions that cannot be predicted* at the sensor side. Location updates are triggered at the AUVs when the actual position of the AUV is "far" from what can be predicted at the sensors based on past measurements. Therefore, AUVs that move following predictable trajectories will need to update their position much less frequently than AUVs that follow temporally uncorrelated trajectories.

CHAPTER VIII

CONCLUSION

In this thesis, we explored fundamental key aspects of underwater acoustic communications, proposed communication architectures for underwater acoustic sensor networks, and developed efficient sensor communication protocols tailored for the underwater environment. The ultimate objective of this work is to encourage research efforts to lay down fundamental bases for the development of new advanced communication techniques for efficient underwater communication and networking for enhanced ocean monitoring and exploration applications. The thesis was organized in eight chapters.

In Chapter 1, we briefly described the background of this work, and presented the organization of the thesis.

In Chapter 2, we presented an overview of the state of the art in underwater acoustic sensor network. We described the challenges posed by the peculiarities of the underwater channel with particular reference to monitoring applications for the ocean environment. We discussed characteristics of the underwater channel and outlined future research directions for the development of efficient and reliable underwater acoustic sensor networks.

In Chapter 3, deployment strategies for two-dimensional and three-dimensional architectures for underwater sensor networks were proposed, and deployment analysis was provided. The objectives were to determine the minimum number of sensors to be deployed to achieve the application-dependent target sensing and communication coverage; provide guidelines on how to choose the deployment surface area, given a target region; study the robustness of the sensor network to node failures, and provide an estimate of the number of required redundant sensors.

In Chapter 4, the problem of data gathering in a 3D underwater sensor network was

investigated, by considering the interactions between the routing functions and the characteristics of the underwater acoustic channel. A model characterizing the acoustic channel utilization efficiency was developed to investigate fundamental characteristics of the underwater environment, and to set the optimal packet size for underwater communications given the application requirements. Two distributed routing algorithms were also introduced, for delay-insensitive and delay-sensitive applications, respectively, with the objective of minimizing the energy consumption taking the varying condition of the underwater channel and the different application requirements into account. The proposed routing solutions were shown to achieve the performance targets of the underwater environment by means of simulation.

In Chapter 5, a resilient routing solution tailored for long-term critical monitoring missions was proposed. Its effectiveness in providing energy-efficient data paths and its robustness to sensor failures were evaluated by means of simulation.

In Chapter 6, UW-MAC, a distributed MAC protocol for underwater acoustic sensor networks, was proposed. It is a transmitter-based CDMA scheme that incorporates a closed-loop distributed algorithm to set the optimal transmit power and code length. It is proven that UW-MAC manages to simultaneously achieve high network throughput, limited channel access delay, and low energy consumption in deep water communications, which are not severely affected by multipath. In shallow water communications, which are heavily affected by multipath, UW-MAC dynamically finds the optimal trade-off among these objectives. Experiments showed that UW-MAC outperforms competing MAC protocols under all considered network architecture scenarios and simulation settings.

In Chapter 7, a cross-layer resource allocation problem was formulated in multi-hop wireless underwater networks as an optimization problem. While we first outlined a general framework where different resource allocation problems will fit by specifying the form of particular functions, then we specialized the framework for the underwater environment.

We strongly advocated the use of a cross-layer approach to jointly optimize the main networking functionalities in order to design communication suites that are adaptable to the variability of the characteristics of the underwater channel and optimally exploit the extremely scarce resources.

REFERENCES

[1] The J-Sim Simulator, http://www.j-sim.org/.

[2] CPLEX solver, http://www.cplex.com.

[3] ABOLHASAN, M., WYSOCKI, T., and DUTKIEWICZ, E., "A Review of Routing Protocols for Mobile Ad Hoc Networks," *Ad Hoc Networks (Elsevier)*, vol. 2, pp. 1–22, Jan. 2004.

[4] AHUJA, R., MAGNANTI, T., and ORLIN, J., *Network Flows: Theory, Algorithms, and Applications*. Prentice Hall, Feb. 1993.

[5] AKKAYA, K. and YOUNIS, M., "A Survey on Routing Protocols for Wireless Sensor Networks," *Ad Hoc Networks (Elsevier)*, vol. 3, pp. 325–349, May 2005.

[6] AKYILDIZ, I. F., MELODIA, T., and CHOWDURY, K. R., "A Survey on Wireless Multimedia Sensor Networks," *Computer Networks (Elsevier)*, vol. 51, pp. 921–960, Mar. 2007.

[7] AKYILDIZ, I. F., POMPILI, D., and MELODIA, T., "Underwater Acoustic Sensor Networks: Research Challenges," *Ad Hoc Networks (Elsevier)*, vol. 3, pp. 257–279, May 2005.

[8] AKYILDIZ, I., SU, W., SANKARASUBRAMANIAM, Y., and CAYIRCI, E., "Wireless Sensor Networks: A Survey," *Computer Networks (Elsevier)*, vol. 38, pp. 393–422, Mar. 2002.

[9] BARU, C., MOORE, R., RAJASEKAR, A., and WAN, M., "The SDSC Storage Resource Broker," in *Proc. of Conference of the Centre for Advanced Studies on Collaborative Research*, (Toronto, Ontario, Canada), Dec. 1998.

[10] BIANCHI, G., "Performance Analysis of the IEEE 802.11 DCF," *IEEE Journal of Selected Areas in Communications*, vol. 18, pp. 535–547, Mar. 2000.

[11] BOSE, P., MORIN, P., STOJMENOVIC, I., and URRUTIA, J., "Routing with Guaranteed Delivery in Ad Hoc Wireless Networks," *ACM-Kluver Wireless Networks (Springer)*, vol. 7, pp. 609–616, Nov. 2001.

[12] BOYD, S. and VANDENBERGHE, L., *Convex Optimization*. Cambridge University Press, Mar. 2004.

[13] BREKHOVSKIKH, L. and LYSANOV, Y., *Fundamentals of Oceans Acoustics*. New York: Springer, 2001.

[14] BROOMHEAD, D., HUKE, J., and MULDOON, M., "Codes for Spread Spectrum Applications Generated Using Chaotic Dynamical System," *Dynamics and Stability of Systems*, vol. 14, pp. 95–105, Mar. 1999.

[15] CATIPOVIC, J., "Performance Limitations in Underwater Acoustic Telemetry," *IEEE Journal of Oceanic Engineering*, vol. 15, pp. 205–216, July 1990.

[16] CAYIRCI, E., TEZCAN, H., DOGAN, Y., and COSKUN, V., "Wireless Sensor Networks for Underwater Surveillance Systems," *Ad Hoc Networks (Elsevier)*, vol. 4, no. 4, pp. 431–446, 2006.

[17] CHANG, C.-S. and CHEN, K.-C., "Medium Access Protocol Design for Delay-guaranteed Multicode CDMA Multimedia Networks," *IEEE Transactions on Wireless Communications*, vol. 2, pp. 1159–1167, Nov. 2003.

[18] CHANG, J. H. and TASSIULAS, L., "Energy conserving routing in wireless ad-hoc networks," in *Proc. of IEEE Conference on Computer Communications (INFOCOM)*, (Tel-Aviv, Israel), pp. 22–31, Mar. 2000.

[19] CHIANG, M., "Balancing Transport and Physical Layers in Wireless Multihop Networks: Jointly Optimal Congestion Control and Power Control," *IEEE Journal on Selected Areas in Communications*, vol. 23, pp. 104 – 116, January 2005.

[20] CODIGA, D., RICE, J., and BAXLEY, P., "Networked Acoustic Modems for Real-Time Data Delivery from Distributed Subsurface Instruments in the Coastal Ocean: Initial System Development and Performance," *Journal of Atmospheric and Oceanic Technology*, vol. 21, no. 2, pp. 331–346, 2004.

[21] CRUZ, R. and SANTHANAM, A., "Optimal Routing, Link Scheduling and Power Control in Multi-hop Wireless Networks," in *Proc. of IEEE Conference on Computer Communications (INFOCOM)*, (San Francisco, USA), pp. 702–711, Mar. 2003.

[22] DAS, S. M., PUCHA, H., and HU, Y. C., "Performance Comparison of Scalable Location Services for Geographic Ad Hoc Routing," in *Proc. of IEEE Conference on Computer Communications (INFOCOM)*, (Miami, FL, USA), Mar. 2005.

[23] DAVIS, R., ERIKSEN, C., and JONES, C., "Autonomous Buoyancy-driven Underwater Gliders," in *The Technology and Applications of Autonomous Underwater Vehicles* (GRIFFITHS, G., ed.), Taylor and Francis, London, 2002.

[24] EISENBERG, Y., LUNA, C. E., PAPPAS, T. N., BERRY, R., and KATSAGGELOS, A. K., "Joint Source Coding and Transmission Power Management for Energy Efficient Wireless Video Communications," *IEEE Transactions on Cirtuits and Systems for Video Technology*, vol. 12, pp. 411–424, June 2002.

[25] ELBATT, T. and EPHREMIDES, A., "Joint Scheduling and Power Control for Wireless Ad-hoc Networks," in *Proc. of IEEE Conference on Computer Communications (INFOCOM)*, (New York, USA), June 2002.

[26] FALL, K., "A Delay-tolerant Network Architecture for Challenged Internets," in *Proc. of ACM Special Interest Group on Data Communications (SIGCOMM)*, (Karlsruhe, Germany), Aug. 2003.

[27] FIORELLI, E., LEONARD, N., BHATTA, P., PALEY, D., BACHMAYER, R., and FRATANTONI, D., "Multi-AUV Control and Adaptive Sampling in Monterey Bay," in *Proc. of IEEE Autonomous Underwater Vehicles: Workshop on Multiple AUV Operations (AUV04)*, (Sebasco, ME, USA), June.

[28] FISHER, F. and SIMMONS, V., "Sound Absorption in Sea Water," *Journal of Acoustical Society of America*, vol. 62, pp. 558–564, Sept. 1977.

[29] FOURER, R., GAY, D., and KERNIGHAN, B., *AMPL: A Modeling Language for Mathematical Programming*. Duxbury Press / Brooks/Cole Publishing Company, 2002.

[30] FREITAG, L. and STOJANOVIC, M., "Acoustic Communications for Regional Undersea Observatories," in *Proc. of Oceanology International*, (London, UK), Mar. 2002.

[31] FREITAG, L., STOJANOVIC, M., SINGH, S., and JOHNSON, M., "Analysis of Channel Effects on Direct-sequence and Frequency-hopped Spread-spectrum Acoustic Communication," *IEEE Journal of Oceanic Engineering*, vol. 26, pp. 586–593, Oct. 2001.

[32] GAREY, M. and JOHNSON, D., *Computer and Intractability*. W.H. Freeman and Co., 1979.

[33] GIROD, B., KALMAN, M., LIANG, Y., and ZHANG, R., "Advances in Channel-adaptive Video Streaming," *Wireless Communications and Mobile Computing*, vol. 2, pp. 549–552, Sept. 2002.

[34] GLEGG, S. A., PIRIE, R., and LAVIGNE, A., "A Study of Ambient Noise in Shallow Water," in *Florida Atlantic University Technical Report*, 2000.

[35] GUO, X., FRATER, M. R., and RYAN, M. J., "A Propagation-delay-tolerant Collision Avoidance Protocol for Underwater Acoustic Sensor Networks," in *Proc. of MTS/IEEE Conference and Exhibition for Ocean Engineering, Science and Technology (OCEANS)*, (Boston, MA), Sept. 2006.

[36] GURSES, E. and AKAN, O. B., "Multimedia Communication in Wireless Sensor Networks," *Annals of Telecommunications*, vol. 60, pp. 799–827, July-Aug. 2005.

[37] HINCHEY, M., "Development of a Small Autonomous Underwater Drifter," in *Proc. of IEEE Newfoundland Electrical and Computer Engineering Conference (NECEC)*, (Chicago, IL, USA), Nov. 2004.

[38] HOWE, B., MCGINNIS, T., and KIRKHAM, H., "Sensor Networks for Cabled Ocean Observatories," in *Geophysical Research Abstracts*, vol. 5, 2003.

[39] HSIN, C. and LIU, M., "Network Coverage using Low Duty Cycled Sensors: Random and Coordinated Sleep Algorithms," in *Proc. of IEEE/ACM Conference on Information Processing in Sensor Networks (IPSN)*, (Berkeley, California), pp. 433–442, Apr. 2004.

[40] JACQUET, P., MUHLETHALER, P., CLAUSEN, T., LAOUITI, A., QAYYUM, A., and VIENNOT, L., "Optimized Link State Routing Protocol for Ad Hoc Networks," in *Proc. of IEEE Multi Topic Conference (INMIC)*, (Pakistan), pp. 62–68, Dec. 2001.

[41] JALBERT, J., BLIDBERG, D., and AGEEV, M., "Some Design Considerations for a Solar Powered AUV: Energy Management and its Impact on Operational Characteristics," *Unmanned Systems*, vol. 15, pp. 26–31, Fall 1997.

[42] JOHNSON, D. B., MALTZ, D. A., and BROCH, J., "DSR: The Dynamic Source Routing Protocol for Multi-Hop Wireless Ad Hoc Networks," in *Ad Hoc Networking* (PERKINS, C. E., ed.), pp. 139–172, Addison-Wesley, 2001.

[43] JURDAK, R., LOPES, C., and BALDI, P., "Battery Lifetime Estimation and Optimization for Underwater Sensor Networks," *IEEE Sensor Network Operations*, Winter 2004.

[44] KALOFONOS, D., STOJANOVIC, M., and PROAKIS, J., "Performance of Adaptive MC-CDMA Detectors in Rapidly Fading Rayleigh Channels," *IEEE Transactions on Wireless Communications*, vol. 2, pp. 229–239, Mar. 2003.

[45] KARN, P., "MACA - A New Channel Access Method for Packet Radio," in *Proc. of ARRL Computer Networking Conference*, (Ontario, Canada), 1990.

[46] KARP, B. and KUNG, H., "GPSR: Greedy Perimeter Stateless Routing for Wireless Networks," in *Proc. of ACM Conference on Mobile Computing and Networking (MobiCom)*, (Boston, MA), pp. 243–254, Aug. 2000.

[47] KAWADIA, V. and KUMAR, P., "A Cautionary Perspective On Cross-Layer Design," *IEEE Wireless Communications Magazine*, vol. 12, pp. 3–11, Feb. 2005.

[48] KILFOYLE, D. and BAGGEROER, A., "The State of the Art in Underwater Acoustic Telemetry," *IEEE Journal of Oceanic Engineering*, vol. 25, pp. 4–27, Jan. 2000.

[49] KOZAT, U. C., KOUTSOPOULOS, I., and TASSIULAS, L., "A Framework for Cross-layer Design of Energy-efficient Communication with QoS Provisioning in Multi-hop Wireless Networks," in *Proc. of IEEE Conference on Computer Communications (INFOCOM)*, (Hong Kong S.A.R., PRC), Mar. 2004.

[50] KREDO II, K. and MOHAPATRA, P., "Medium Access Control in Wireless Sensor Networks," *Computer Networks (Elsevier)*, vol. 51, pp. 961–994, Mar. 2007.

[51] KUMAR, S., RAGHAVANB, V. S., and DENGC, J., "Medium Access Control Protocols for Ad Hoc Wireless Networks: A Survey," *Ad Hoc Networks (Elsevier)*, vol. 4, pp. 326–358, May 2006.

[52] KWANG, Y. H., SHARIF, B., ADAMS, A., and HINTON, O., "Implementation of Multiuser Detection Strategies for Coherent Underwater Acoustic Communication," *IEEE Journal of Oceanic Engineering*, vol. 27, pp. 17–27, Jan. 2002.

[53] LACHENMANN, A., MARRÓN, P. J., MINDER, D., and ROTHERMEL, K., "An analysis of cross-layer interactions in sensor network applications," in *Proc. of the Second International Conference on Intelligent Sensors, Sensor Networks & Information Processing (ISSNIP 2005)*, pp. 121–126, December 2005.

[54] LI, J., JANNOTTI, J., COUTO, D. D., KARGER, D., and MORRIS, R., "A scalable location service for geographic ad hoc routing," in *Proc. of ACM Intl. Conf. on Mobile Computing and Networking (MobiCom)*, (Boston, Massachussets), pp. 120–30, 2000.

[55] LIN, X., SHROFF, N. B., and SRIKANT, R., "A Tutorial on Cross-Layer Optimization in Wireless Networks," *IEEE Journal of Selected Areas in Communications*, vol. 24, pp. 1452–1463, Aug. 2006.

[56] LU, X., ERKIP, E., WANG, Y., and GOODMAN, D., "Power Efficient Multimedia Communication Over Wireless Channels," *IEEE Journal on Selected Areas of Communications*, vol. 21, pp. 1738–1751, December 2003.

[57] MELODIA, T., POMPILI, D., and AKYILDIZ, I., "Optimal Local Topology Knowledge for Energy Efficient Geographical Routing in Sensor Networks," in *Proc. of IEEE Conference on Computer Communications (INFOCOM)*, (Hong Kong S.A.R., PRC), Mar. 2004.

[58] MELODIA, T., POMPILI, D., and AKYILDIZ, I. F., "On the Interdependence of Distributed Topology Control and Geographical Routing in Ad Hoc and Sensor Networks," *IEEE Journal of Selected Areas in Communications*, vol. 23, pp. 520–532, Mar. 2005.

[59] MILLER, L., "Distribution of Link Distances in a Wireless Network," *Journal of Research of the National Institute of Standards and Technology*, vol. 106, pp. 401–412, Mar./Apr. 2001.

[60] MOLINS, M. and STOJANOVIC, M., "Slotted FAMA: a MAC Protocol for Underwater Acoustic Networks," in *Proc. of MTS/IEEE Conference and Exhibition for Ocean Engineering, Science and Technology (OCEANS)*, (Boston, MA), Sept. 2006.

[61] MUQATTASH, A., KRUNZ, M., and RYAN, W. E., "Solving the Near-far Problem in CDMA-based Ad Hoc Networks," *Ad Hoc Networks (Elsevier)*, vol. 1, pp. 435–453, Nov. 2003.

[62] OGREN, P., FIORELLI, E., and LEONARD, N. E., "Cooperative Control of Mobile Sensor Networks: Adaptive Gradient Climbing in a Distributed Environment," *IEEE Transactions on Automatic Control*, vol. 49, pp. 1292–1302, Aug. 2004.

[63] PERKINS, C., BELDING-ROYER, E., and DAS, S., "Ad Hoc On Demand Distance Vector (AODV) Routing." IETF RFC 3561.

[64] PERKINS, C. and BHAGWAT, P., "Highly Dynamic Destination Sequenced Distance Vector Routing (DSDV) for Mobile Computers," in *Proc. of ACM Special Interest Group on Data Communications (SIGCOMM)*, (London, UK), 1994.

[65] POMPILI, D., MELODIA, T., and AKYILDIZ, I. F., "A Resilient Routing Algorithm for Long-term Applications in Underwater Sensor Networks," in *Proc. of Mediterranean Ad Hoc Networking Workshop (Med-Hoc-Net)*, (Lipari, Italy), June 2006.

[66] POMPILI, D., MELODIA, T., and AKYILDIZ, I. F., "Routing Algorithms for Delay-insensitive and Delay-sensitive Applications in Underwater Sensor Networks," in *Proc. of ACM Conference on Mobile Computing and Networking (MobiCom)*, (Los Angeles, LA), Sept. 2006.

[67] POMPILI, D., MELODIA, T., and AKYILDIZ, I. F., "A Distributed CDMA Medium Access Control for Underwater Acoustic Sensor Networks," in *Proc. of Mediterranean Ad Hoc Networking Workshop (Med-Hoc-Net)*, (Corfu, Greece), June 2007.

[68] PROAKIS, J., *Digital Communications*. New York: McGraw-Hill, 1995.

[69] PROAKIS, J., RICE, J., SOZER, E., and STOJANOVIC, M., "Shallow Water Acoustic Networks," in *Encyclopedia of Telecommunications* (PROAKIS, J. G., ed.), John Wiley and Sons, 2003.

[70] PROAKIS, J., SOZER, E., RICE, J., and STOJANOVIC, M., "Shallow Water Acoustic Networks," *IEEE Communications Magazine*, pp. 114–119, Nov. 2001.

[71] QUAZI, A. and KONRAD, W., "Underwater Acoustic Communication," *IEEE Communications Magazine*, pp. 24–29, Mar. 1982.

[72] RADUNOVIC, B. and BOUDEC, J.-Y. L., "Rate Performance Objectives of Multihop Wireless Networks," *IEEE/ACM Transactions on Mobile Computing*, vol. 3, pp. 334–349, Oct. 2004.

[73] RAMAMURTHYT, S. and MUKHERJEE, B., "Survivable WDM Mesh Networks, Part I - Protection," in *Proc. of IEEE Conference on Computer Communications (INFOCOM)*, vol. 2, (New York, NY), pp. 744–751, Mar. 1999.

[74] RAVELOMANANA, V., "Extremal Properties of Three-dimensional Sensor Networks with Applications," *IEEE Transactions on Mobile Computing*, vol. 3, pp. 246–257, July/Sept. 2004.

[75] RODOPLU, V. and PARK, M. K., "An Energy-Efficient MAC Protocol for Underwater Wireless Acoustic Networks," in *Proc. of MTS/IEEE Conference and Exhibition for Ocean Engineering, Science and Technology (OCEANS)*, Sept. 2005.

[76] SALVA-GARAU, F. and STOJANOVIC, M., "Multi-cluster Protocol for Ad Hoc Mobile Underwater Acoustic Networks," in *Proc. of MTS/IEEE Conference and Exhibition for Ocean Engineering, Science and Technology (OCEANS)*, (San Francisco, CA), Sept. 2003.

[77] SERWAY, R. A. and JEWETT, J. W., *Physics for Scientists and Engineers*. Brooks/Cole, 2004.

[78] SHAKKOTTAI, S., SRIKANT, R., and SHROFF, N., "Unreliable Sensor Grids: Coverage, Connectivity, and Diameter," in *Proc. of IEEE Conference on Computer Communications (INFOCOM)*, vol. 2, (San Francisco, CA), pp. 1073–1083, Apr. 2003.

[79] SOREIDE, N., WOODY, C., and HOLT, S., "Overview of Ocean Based Buoys and Drifters: Present Applications and Future Needs," in *International Conference on Interactive Information and Processing Systems for Meteorology, Oceanography, and Hydrology (IIPS)*, Jan. 2004.

[80] SOZER, E., PROAKIS, J., STOJANOVIC, M., RICE, J., BENSON, A., and HATCH, M., "Direct Sequence Spread Spectrum Based Modem for Underwater Acoustic Communication and Channel Measurements," in *Proc. of MTS/IEEE Conference and Exhibition for Ocean Engineering, Science and Technology (OCEANS)*, Nov. 1999.

[81] SOZER, E., STOJANOVIC, M., and PROAKIS, J., "Underwater Acoustic Networks," *IEEE Journal of Oceanic Engineering*, vol. 25, pp. 72–83, Jan. 2000.

[82] STOJANOVIC, M., "Acoustic (Underwater) Communications," in *Encyclopedia of Telecommunications* (PROAKIS, J. G., ed.), John Wiley and Sons, 2003.

[83] STOJANOVIC, M., "Optimization of a Data Link Protocol for an Underwater Acoustic Channel," in *Proc. of MTS/IEEE Conference and Exhibition for Ocean Engineering, Science and Technology (OCEANS)*, (Brest, France), June 2005.

[84] STOJANOVIC, M., CATIPOVIC, J., and PROAKIS, J., "Phase Coherent Digital Communications for Underwater Acoustic Channels," *IEEE Journal of Oceanic Engineering*, vol. 19, pp. 100–111, Jan. 1994.

[85] STOJANOVIC, M., PROAKIS, J., and CATIPOVIC, J., "Analysis of the Impact of Channel Estimation Errors on the Performance of a Decision Feedback Equalizer in Multipath Fading Channels," *IEEE Transactions on Communications*, vol. 43, pp. 877–886, Feb./Mar./Apr. 1995.

[86] STOJANOVIC, M., PROAKIS, J., and CATIPOVIC, J., "Performance of High-rate Adaptive Equalization on a Shallow Water Acoustic Channel," *Journal of the Acoustical Society of America*, vol. 100, pp. 2213–2219, Oct. 1996.

[87] STOJANOVIC, M., "On The Relationship Between Capacity and Distance in an Underwater Acoustic Communication Channel," in *Proc. of ACM International Workshop on UnderWater Networks (WUWNet)*, (Los Angeles, CA), Sept. 2006.

[88] STOJMENOVIC, I., "Localized Network Layer Protocols in Wireless Sensor Networks Based on Optimizing Cost over Progress Ratio," *IEEE Networks*, vol. 20, pp. 21–27, Jan./Feb. 2006.

[89] TOUMPIS, S. and GOLDSMITH, A. J., "Performance, optimization, and cross-layer design of media access protocols for wireless ad hoc networks," in *Proc. of IEEE International Conference on Communications (ICC)*, (Seattle, Washington, USA), May 2003.

[90] URICK, R. J., *Principles of Underwater Sound*. McGraw-Hill, 1983.

[91] VASILESCU, I., KOTAY, K., RUS, D., DUNBABIN, M., and CORKE, P., "Data Collection, Storage, and Retrieval with an Underwater Sensor Network," in *ACM Conference on Embedded Networked Sensor Systems (SenSys)*, (San Diego, CA), Nov. 2005.

[92] XIE, G. and GIBSON, J., "A Network Layer Protocol for UANs to Address Propagation Delay Induced Performance Limitations," in *Proc. of MTS/IEEE Conference and Exhibition for Ocean Engineering, Science and Technology (OCEANS)*, vol. 4, (Honolulu, HI), pp. 2087–2094, Nov. 2001.

[93] XIE, P. and CUI, J.-H., "SDRT: A Reliable Data Transport Protocol for Underwater Sensor Networks." University of Connecticut, Technical Report UbiNet-TR06-03, Feb. 2006.

[94] XIE, P., CUI, J.-H., and LAO, L., "VBF: Vector-Based Forwarding Protocol for Underwater Sensor Networks," in *Proc. of Networking*, (Coimbra, Portugal), pp. 1216–1221, May 2006.

[95] YANG, X., ONG, K. G., DRESCHEL, W. R., ZENG, K., MUNGLE, C. S., and GRIMES, C. A., "Design of a Wireless Sensor Network for Long-term, In-situ Monitoring of an Aqueous Environment," *Sensors*, vol. 2, pp. 455–472, 2002.

[96] YU, W., SAHINOGLU, Z., and VETRO, A., "Energy-Efficient JPEG 2000 Image Transmission over Wireless Sensor Networks," in *Proc. of IEEE Global Communications Conference (GLOBECOM)*, (Dallas, TX, USA), pp. 2738–2743, January 2004.

[97] ZHANG, B., SUKHATME, G. S., and REQUICHA, A. A., "Adaptive Sampling for Marine Microorganism Monitoring," in *IEEE/RSJ International Conference on Intelligent Robots and Systems*, (Sendai, Japan), Sept. 2004.

[98] ZOU, Y. and CHAKRABARTY, K., "Sensor Deployment and Target Localization Based on Virtual Forces," in *Proc. of IEEE Conference on Computer Communications (INFOCOM)*, vol. 2, (San Francisco, CA), pp. 1293–1303, Apr. 2003.

LIST OF ACRONYMS

ACCP Acoustic Correlation Current Profilers

ACM Association for Computing Machinery

AODV Ad Hoc On Demand Distance Vector Routing

ARQ Automatic Repeat Request

AUV Autonomous Underwater Vehicle

BER Bit Error Rate

CDMA Code Division Multiple Access

CSMA Carrier Sense Multiple Access

CTS Clear To Send

DFE Decision Feedback Equalizer

DPSK Differential Phase Shift Keying

DSDV Destination Sequenced Distance Vector

DSR Dynamic Source Routing

DSSS Direct Sequence Spread Spectrum

EDF Earliest Deadline First

FAMA Floor Acquisition Multiple Access

FDMA Frequency Division Multiple Access

FEC Forward Error Correction

FHSS Frequency Hopping Spread Spectrum

FIFO First Input First Output

FSK Frequency Shift Keying

GFG Greedy Face Greedy Routing

GPS Global Positioning System

GPSR Greedy Perimeter Stateless Routing

IEEE Institute of Electrical and Electronics Engineers

ILP Integer Linear Programming

IP Internet Protocol

ISI Inter Symbol Interference

MAC Medium Access Control

MACA Multiple Access with Collision Avoidance

MAI Multiple Access Interference

MANET Mobile Ad Hoc Network

MUD Multi User Detection

OFDM Orthogonal Frequency Division Multiplexing

OLSR Optimized Link State Routing

PER Packet Error Rate

PLL Phase Locked Loop

PSK Phase Shift Keying

PTKF Partial Topology Knowledge Forwarding

QAM Quadrature Amplitude Modulation

QoS Quality of Service

RF Radio Frequency

RTS Request To Send

RTT Round Trip Time

SACK Selective Acknowledge

SDRA Segmented Data Reliable Transport

SDV Small Delivery Vehicle

SINR Signal-to-Interference-plus-Noise Ratio

SNR Signal-to-Noise Ratio

SUD Single User Detection

TCP Transmission Control Protocol

TDMA Time Division Multiple Access

UUV Unmanned Underwater Vehicle

UW-A UnderWater Acoustic

UW-ASN UnderWater Acoustic Sensor Network

UW-MAC UnderWater Medium Access Control

VITA

Dario Pompili graduated in Telecommunications Engineering (summa cum laude) from the University of Rome 'La Sapienza', Italy, in May 2001. Since June 2001, he had been working at the same university on the EU IST BRAHMS and SATIP6 projects as a Ph.D. student. In Spring 2003, he worked on sensor networks at the Broadband and Wireless Networking Laboratory, Georgia Institute of Technology, Atlanta, as a Visiting Researcher. In November 2004, he earned from the University of Rome 'La Sapienza' the Ph.D. Degree in System Engineering. Since 2004, he is pursuing the Ph.D. Degree in Electrical and Computer Engineering at the Georgia Institute of Technology under the guidance of Dr. I. F. Akyildiz. In 2005, he was awarded Georgia Institute of Technology BWN-Lab Researcher of the Year for *"outstanding contributions and professional achievements"*. Starting August 2007, he is an Assistant Professor in the Electrical and Computer Engineering Department at Rutgers, the State University of New Jersey. His main research interests are in wireless ad hoc and sensor networks, underwater acoustic sensor networks, and overlay networks. Over the last few years he has authored and co-authored 10 journal and 25 conference refereed publications, as well as 2 book chapters and 6 submitted papers. He is a member of the IEEE Communications Society and the ACM Communication Society.